DEVELOPMENT OF SUPERHYDROPHOBICITY IN SILANE TREATED DIATOMACEOUS EARTH AND POLYMER COATINGS

By

BHISHMA RAJ SEDAI

Bachelor of Science
Tri-Chandra Multiple Campus
Kathmandu, Nepal
2000

Master of Science
Tribhuvan University
Kirtipur, Nepal
2003

Submitted to the Faculty of the
Graduate College of the
Oklahoma State University
in partial fulfillment of
the requirements for
the Degree of
DOCTOR OF PHILOSOPHY
December, 2016

DEVELOPMENT OF SUPERHYDROPHOBICITY IN SILANE TREATED DIATOMACEOUS EARTH AND POLYMER COATINGS

Dissertation Approved:

Dr. Frank D. Blum

Dissertation Adviser

Dr. Jeffery L. White

Dr. Jimmie D. Weaver

Dr. Sadagopan Krishnan

Jacques H. H. Perk

ACKNOWLEDGEMENTS

I would like to express sincere gratitude to my advisor Prof. Frank D. Blum for his guidance, support, motivation, enthusiasm, and immense knowledge. I would also like to acknowledge Stewart Kennedy for providing materials and chemicals during my research.

I would like to thank Prof. Sandip P. Harimkar and Prof. Joseph F. Donoghue for allowing me to use their instruments. My special thanks to Mark Mcollum and Habib S. Alavi for their kind help during particle size analysis and profilometry experiments, respectively.

Additional thanks goes to my past and present lab mates: Abhijit Paul, Bal K. Khatiwada, Charmaine Munro, Tan Zhang, Madduma Arachchilage, Hamid Mortazavian, Helanka Parera and Ugo Arua for making nice environment in the lab and their valuable comments and discussions during my PhD research.

At last, I would like to thank my parents, brothers, wife (Jyotsna), son (Niket) and daughter (Nysha) for their support, encouragement, love, and motivation throughout my doctorate study.

Name: BHISHMA RAJ SEDAI

Date of Degree: DECEMBER, 2016

Title of Study: DEVELOPMENT OF SUPERHYDROPHOBICITY IN SILANE TREATED DIATOMACEOUS EARTH AND POLYMER COATINGS

Major Field: CHEMISTRY

Abstract:

This dissertation describes the development of superhydrophobicity in fluorosilane treated diatomaceous earth (DE) particles and polymer coatings. The amount of silane coupling agent on the surface of DE particles has been determined by thermogravimetric analysis (TGA). The presence of silane coupling agents on the DE particles has been confirmed by Fourier transform infrared spectroscopy (FTIR). The minimum amount of fluorosilane coupling agent required to exhibit superhydrophobicity has been determined. The development of the superhydrophobicity in the coatings with simple polymers like polystyrene (PS) or poly(vinyl acetate) (PVAc) as binders has been followed as a function of the particle loading using contact angle measurements and scanning electron microscopy.

The effect of particle morphology in the development of superhydrophobicity has been studied systematically. It was found that less-dense treated CelTix DE particles produced superhydrophobicity at 30 wt% of particles loading compared to more dense treated DiaFil DE (rod-shaped) and EcoFlat DE (irregularly shaped) particles with low molecular mass polystyrene binder system. The effects of particle morphology, surface area, porosity and density in the development of superhydrophobicity have been described.

The effect of viscosity of the binder solution in the development of superhydrophobicity has been observed. Changes in the solvent systems have not affected the superhydrophobicity for similar coating compositions. The DE particles were found to be robust and the coatings prepared with the sonicated DE samples also exhibited superhydrophobicity.

Additionally, untreated and treated diatomaceous earth particles and epoxy composites have been prepared. The thermal and dynamic mechanical properties of DE/epoxy composites have been evaluated. The mechanical properties of the DE/epoxy composites revealed that treated DE particles act as better reinforcing agents compared to untreated DE particles.

TABLE OF CONTENTS

Chapters Pages

LIST OF TABLES

Table Page

LIST OF FIGURES

.

CHAPTER I

INTRODUCTION

1.1. DIATOMACEOUS EARTH

Diatoms are unicellular photosynthetic algae. They differ from other microalgae due to the presence of siliceous cell walls.[1] Diatoms are found in most aquatic and moist environments. The size of diatoms vary, from 2 nm up to several mm. There are an estimates of at least 100,000 different species and 250 genera of diatoms.[2] The species differ from each other in the complex morphological features of the siliceous cell wall (frustules). Diatoms can be categorized into two major groups: 1) Coscinodiscophyceae, or centric diatoms, cells with radial symmetry (about a central point) and 2) Bacillariophyceae, or pennate diatoms, cells with bilateral symmetry (about a central line).[3] The fossilized skeletons of diatoms are known as diatomite or diatomaceous earth (DE).

Diatoms frustules have resulted from the evolution over millions of years to generate intricate nanostructures. It would be extremely difficult to produce material of such complexity using artificial techniques. The various intricate patterns of the frustules have made them attractive materials for various applications including nanotechnology. The global demand of nanomaterials in electronic, optical, chemical and biomedical devices has influenced the industrial development of synthetic nanotechnology. Diatomaceous earth is an inexpensive material and can be used to manufacture nano-materials on large scales.[4-6] Diatoms frustules are considered as ideal natural materials for technological exploitation.[7-10]

The frustules of diatoms vary in shape, size, nano-patterning, internal volume, mechanical and optical properties as well as diffusion potential through the pores. Diatoms can produce a high degree of complexity and hierarchical structure under mild conditions using basic nutrients and sunlight. They require CO_2, water, inorganic salts and sunlight to grow. They can be cultured in fresh or sea water without using expensive supplements.[11] The culturing of diatoms does not compete with agriculture cropland. They can be grown in fermenters located on unproductive land-like deserts.[12]

Fig. 1.1. A collection of diatoms showing varieties of shapes. This diagram was taken from http://www.micromagus.net/microscopes/pondlife_plants01.html

1.2. APPLICATIONS OF DIATOMACEOUS EARTH

DE is inexpensive and the most abundant form of amorphous silica. It has many unique physical and chemical characteristics. It has highly developed mesoporosity

and/or microporosity. Losic and coworkers[13] have shown the presence of pores of different size, shape, density and arrangement in morphologically different diatoms species. They have further reported that frustules of centric diatoms have layered porous structures. The number of porous layered structures differ from one species to another.[13] The diatoms' frustules have been exploited for various applications.[14-17] The next few paragraphs describe the versatile applications of diatomaceous earth.

DE has been used as a support to make various types of catalysts. The use of DE-immobilized bismuth (III) oxyiodide (BiOI) hybrid in catalysis has been reported.[18] DE was used as a support to prepare TiO_2/diatomite composites,[19, 20] ytterbium-doped titanium dioxide (Yb-TiO_2)/diatomite composites,[21] cuprous oxide and zinc oxide/DE composites which are efficient catalysts.

Modified DE has been used to adsorb various types of heavy metals. Reports are available on the adsorption of Cu (II) by γ-aminopropyltriethoxysilane (APTES) treated DE.[22] The use of DE has been reported as adsorption of some metal ions (e.g., Ni(II),[23, 24] Pb(II),[25-27] Cu(II),[24] Cd(II),[26] Cr,[28] and Th (IV)[29] and organic contaminants[30] on raw diatomite and the effects of aqueous chemistry conditions, such as pH and temperature, on the adsorptions. Losic et al. have reported the effects of 3-mercapto-propyl-trimethoxysilane modification on improving the Au(III) adsorption of diatomaceous earth.[31] Branton et al. have investigated the adsorption capacity of diatomite towards heavy metals and their adsorption mechanism.[32] Khraisheh et al. have studied on DE and Mn-diatomite for heavy metal removal from freshwater.[33] Aytas and his group have investigated the removal of uranium from aqueous solutions by DE fine particles.[34]

Garcia et al. have used Bolivian DE as a silica source to synthesize Zeolite Y.[35] They have investigated diatomites originating from different locations containing different types and amount of minerals and clays as impurities. They have optimized the conditions for zeolite Y synthesis and mentioned that DE enabled the synthesis of high silica zeolite Y which was similar to colloidal silica in traditional synthesis.[35]

Reports are available on the use of DE for the removal of dyes. Maeda et al. have prepared calcium silicate hydrate gel and DE composites with high surface area. They found higher methylene blue adsorption capacity of the composites compared to DE alone.[36] Inchaurrondo and coworkers have performed Fenton-like oxidation of the anionic azo-dye batch wise using thermally treated commercial grade diatomites.[37] Erdem and his group have investigated adsorption of textile dyes such as Dif Blau BRF (SB), Everzol Brill Red 3BS (EBR), and Int Yellow 5GF (IY) using DE. They have reported the effect of particle size of diatomite, diatomite concentration, initial dye concentrations and shaking time on adsorption.[38] Gao et al. have modified DE with polyethyleneimine by using impregnation method. They, later, studied the trapping behavior of modified DE for phenol using a 4-aminoantipyrine (4-AAP) and a spectrophotometric method.[39]

DE particles have been used as filters to remove viruses and other impurities. Farrah et al. have made filters containing DE modified by in situ precipitation of a combination of ferric chloride and aluminum chloride for the removal of enteroviruses (poliovirus 1, echovirus 5 and coxsackievirus B5 and coliphage MS2).[40] Hadjar and coworkers have prepared inorganic composite materials (ICM) from Algerian DE and charcoal from pine

and found that they were as promising materials for use as industrial adsorbents in different applications wastewater and air treatment, and for solvent recuperation.[41] Xiong et al. have made ferrihydrite-modified DE and have reported increased phosphorus (P) adsorption capacity in modified DE compared to raw DE.[42]

Yilmaz et al. have investigated the use of raw and calcined DE cement production. They have reported the physical, chemical, mineralogical, micro-structural and mechanical tests of the mortars, prepared by mixing Portland cement clinkers with 5%, 10% and 20% raw and calcined DE (w/w) and gypsum.[43]

Osmanlioglu et al. have tested natural DE as an alternative material for removal of radioactivity from liquid waste. They have designed a pilot-scale column-type device and used natural diatomite as sorption media. After the treatment by diatomite, the radioactivity of liquid was reduced from the initial 2.60 Bq.ml to less than 0.40 Bq/ml.[44]

DE particles in modified form have been used in drug delivery applications. Aw et al. have investigated the drug delivery concept based on diatoms for implant and oral drug delivery using indomethacin as a model for a water poorly soluble drug.[45-47] Bariana and coworkers have studied the impact of engineered surface chemistry of DE micro-particles on their drug loading and release properties.[48] Zhang et al. have evaluated the potential of diatom silica micro-particles (DSMs) for the delivery of mesalamine and prednisone.[49] Maher et al. have revealed that diatomaceous earth has a set of unique properties including favorable microcapsule structure with high surface area and micro/mesoporosity providing high drug loading, fast biodegradability, and intrinsic luminescence, suitable for low-cost production of advanced drug micro-carriers.[50]

Jenicijevic et al. have evaluated drug loading capacity in adsorption using diclofenac sodium (DS) as a model drug.[51] Ruggiero and coworkers have functionalized diatomite nanoparticles and reported as efficient cellular uptake and homogeneous distribution of nanoparticles in cytoplasm and nucleus, thus suggesting their potentiality as nano-carriers for drug delivery.[52] Vasani and their group have employed surface initiated atom transfer radical polymerisation to graft thermo-responsive copolymers of oligo(ethylene glycol) methacrylates from the surface of diatom biosilica microcapsules. They have demonstrated the application of the resulting composites for thermo-responsive drug delivery.[53] Delalat et al. have used diatom-derived nanoporous biosilica to deliver chemotherapeutic drugs to cancer cells.[54]

DE can be used in the preparation of conductive devices. Li et al. have obtained a conductive diatomite by surface modification of diatomite with polyaniline. They have characterized the modified DE via Fourier transform Raman spectra, UV-Vis-absorption spectra, thermogravimetric analysis and scanning electron microscopy, as well as conductivity. Their thermogravimetric analysis results suggested that its conductivity was 2.8×10^{-2} S cm^{-1} at 20 ^{o}C with 8% of polyaniline on DE surface by mass.[55]

DE has been considered as an excellent material for nano-technological applications. Yu et al. have fabricated self-supporting gold microstructures with complex 3D morphologies by using electroless gold deposition onto a diatom silica substrate, followed by the substrate removal by acid dissolution.[14] Their work has demonstrated that gold diatom replicas with distinct micro to nano scale structures can be created by a simple and scalable process based on electroless gold deposition. They have mentioned

that this approach could be applied for the preparation of a wide range of different metals (Pt, Pd, Ag, Ni, etc.) offering more efficient catalytic, optical, or magnetic properties.[14]

Modified natural diatomaceous earth (DE) and commercial silica gel $60GF_{254}$ (Si-$60GF_{254}$) have been used as a principal component of the stationary phase in normal thin-layer chromatography (TLC) applications. DE has been modified by flux calcination and refluxing with acid for this application.[56]

Recently, few reports were published on the use of DE for preparation of superhydrophobic surfaces. Simpson and D'Urso have made superhydrophobic surfaces using treated DE powder.[57] Oliveira et al. have modified DE by fluorosilanization and plasma treatment and used those modified DE particles to prepare superhydrophobic surfaces.[58] Polizos et al. have fluorinated diatom frustules of cylindrical and circular structures to make them superhydrophobic and mentioned the effect of particle geometry on the abrasion resistance.[59] Puretskey and coworkers have reported a new approach for the design of functional coatings using DE particles decorated by a thin layer of grafted polymer chains.[60] Nine et al. have prepared graphene-based superhydrophobic composite coatings with robust mechanical strength, self-cleaning, and barrier properties.[61] Parera and coworkers have mentioned the superhydrophobic surface from treated DE/resin system.[62]

1.3. MOTIVATION

Artificial superhydrophobic surface requires a combination of multiscale roughness and low surface energy interfaces.[63] Many techniques and strategies have been used to

prepare artificial hierarchical structures required for superhydrophobic surfaces. Researchers have spent much time, money and energy to make such structured surfaces.[64-70] An inexpensive, environmentally benign and natural material with structured surface topography has been provided to us by nature as diatoms. The exoskeletons of diatoms are microstructures with nano-textures on their surface and consist of mostly amorphous silica. DE particles have varieties of structures. The use of naturally available materials with micro- and nano- structures to make superhydrophobic surfaces with different types of binders systems have not been explored systematically yet. Naturally available different types of DE particles motivated us to explore the development of superhydrophobicity using simple polymers as binder systems. In this research work, DE particles with different structures have been treated with silane coupling agents and treated DE particles have been mixed with high and low molecular mass homopolymers. The development of superhydrophobicity has been studied systematically in both bare treated DE particles coatings and treated DE particles/polymer coatings.

1.4. RESEARCH OBJECTIVES

This dissertation focuses on the understanding of development of superhydrophobicity in silane treated DE particles and treated DE particles/polymer coatings.

Objective 1: The key components of the research are to find the minimum amount of silane coupling agent needed on the surface of DE particles to make them superhydrophobic, the minimum amount of treated DE particles needed in the polymer

DE mixture to make a superhydrophobic coating, and the characterization of the behavior of treated DE in different polymer solutions, which act as binders.

Objective 2: To understand the effect of the DE particle morphologies in the development of superhydrophobicity in the treated DE/polymer coatings. To find out the minimum amount of silane coupling agent required to make superhydrophobic surfaces in morphologically different DE particles. To observe the behavior of morphologically different particles with a polystyrene binder system.

Objective 3: To understand the effect of viscosity, solvent systems, and sonication for treated DE/polymer based coatings.

Objective 4: To understand the nature of superhydrophobic surfaces obtained from structurally different treated DE particles.

Objective 5: To study the effect of superhydrophobic and superhydrophilic DE particles on the thermal and mechanical properties of treated DE/epoxy composites.

1.5. STRUCTURE OF DISSERTATION

CHAPTER II of this dissertation focuses on the background of superhydrophobicity, natural superhydrophobic surfaces, and artificial superhydrophobic surfaces. It also reviews various efforts that have been undertaken to fabricate artificial superhydrophobic surfaces, modification of diatomaceous earth with silane coupling agents, techniques used to characterize modified DE particles, and techniques used to characterize superhydrophobic surfaces and their basic principles.

CHAPTER III discusses development of supherhydrophobicity in 3-heptafluoro-isopropoxypropyl trimethoxysilane (HFIP-TMS) treated DE (HFIP-DE) and simple polymer based coatings. It describes the minimum amount of HFIP-TMS required to make DE particles superhydrophobic. The minimum loadings of treated DE particles required to prepare superhydrophobic coatings with simple polymeric binder systems have been determined.

CHAPTER IV focuses on DE particle morphology dependent superhydrophobicity in HFIP-TMS treated DE and polystyrene binder system. This chapter provides information about selection of the best DE particles to make superhydrophobic surfaces among three different available common DE products in the market.

CHAPTER V covers the effects of viscosity, solvents and sonication for HFIP-TMS treated DE and polystyrene binder system. It describes the behavior of superhydrophobic DE particles after drying of the mixture of high molecular mass and low molecular mass polymer solutions and treated DE particles under ambient conditions. It highlights the robustness of DE particles under extreme physical conditions.

CHAPTER VI describes the thermal and dynamic mechanical analysis of treated DE and epoxy composites. It helps to understand the effect of superhydrophobic DE filler on the epoxy matrix and mechanical properties of their composites.

1.6. REFERENCES

1. Round, F.; Crawford, R.; Mann, D., The diatoms biology and morphology of the genera, Cambridge University Press, Cambridge, 1990.

2. Norton, T. A.; Melkonian, M.; Andersen, R. A., Algal biodiversity. *Phycologia* **1996,** *35*, 308-326.

3. Townley, H. E., Diatom frustules: physical, optical, and biotechnological applications. In *The Diatom World*, Springer 2011,US; pp 273-289.

4. Losic, D.; Mitchell, J. G.; Voelcker, N. H., Diatomaceous lessons in nanotechnology and advanced materials. *Adv. Mater.* **2009,** *21*, 2947-2958.

5. Gordon, R.; Losic, D.; Tiffany, M. A.; Nagy, S. S.; Sterrenburg, F. A., The glass menagerie: diatoms for novel applications in nanotechnology. *Trends Biotechnol.* **2009,** *27*, 116-127.

6. Gordon, R.; Parkinson, J., Potential roles for diatomists in nanotechnology. *J. Nanosci. Nanotechnol.* **2005,** *5*, 35-40.

7. Drum, R. W.; Gordon, R., Star Trek replicators and diatom nanotechnology. *Trends Biotechnol.* **2003,** *21*, 325-328.

8. Hamm, C. E., The evolution of advanced mechanical defenses and potential technological applications of diatom shells. *J. Nanosci. Nanotechnol.* **2005,** *5*, 108-119.

9. Fuhrmann, T.; Landwehr, S.; El Rharbi-Kucki, M.; Sumper, M., Diatoms as living photonic crystals. *Appl. Phys. B* **2004,** *78*, 257-260.

10. Rosi, N. L.; Thaxton, C. S.; Mirkin, C. A., Control of Nanoparticle Assembly by Using DNA-Modified Diatom Templates. *Angew. Chem. Int. Ed.* **2004,** *116*, 5616-5619.

11. Lopez, P. J.; Desclés, J.; Allen, A. E.; Bowler, C., Prospects in diatom research. *Curr. Opin. Biotechnol.* **2005,** *16*, 180-186.

12. Gordon, J. M.; Polle, J. E., Ultrahigh bioproductivity from algae. *Appl. Microbiol. Biotechnol.* **2007,** *76*, 969-975.

13. Losic, D.; Rosengarten, G.; Mitchell, J. G.; Voelcker, N. H., Pore architecture of diatom frustules: potential nanostructured membranes for molecular and particle separations. *J. Nanosci. Nanotechnol.* **2006,** *6*, 982-989.

14. Yu, Y.; Addai-Mensah, J.; Losic, D., Synthesis of self-supporting gold microstructures with three-dimensional morphologies by direct replication of diatom templates. *Langmuir* **2010,** *26*, 14068-14072.

15. van Garderen, N.; Clemens, F. J.; Kaufmann, J.; Urbanek, M.; Binkowski, M.; Graule, T.; Aneziris, C. G., Pore analyses of highly porous diatomite and clay based materials for fluidized bed reactors. *Microporous Mesoporous Mater.* **2012,** *151*, 255-263.

16. Yuan, P.; Liu, D.; Fan, M.; Yang, D.; Zhu, R.; Ge, F.; Zhu, J.; He, H., Removal of hexavalent chromium [Cr (VI)] from aqueous solutions by the diatomite-supported/unsupported magnetite nanoparticles. *J. Hazard. Mater.* **2010,** *173*, 614-621.

17. Skubiszewska-Zięba, J.; Charmas, B.; Leboda, R.; Gun'ko, V., Carbon-mineral adsorbents with a diatomaceous earth/perlite matrix modified by carbon deposits. *Microporous Mesoporous Mater.* **2012,** *156*, 209-216.

18. Li, B.; Huang, H.; Guo, Y.; Zhang, Y., Diatomite-immobilized BiOI hybrid photocatalyst: Facile deposition synthesis and enhanced photocatalytic activity. *Appl. Surf. Sci.* **2015,** *353*, 1179-1185.

19. Wang, B.; de Godoi, F. C.; Sun, Z.; Zeng, Q.; Zheng, S.; Frost, R. L., Synthesis, characterization and activity of an immobilized photocatalyst: Natural porous diatomite supported titania nanoparticles. *J. Colloid Interface Sci.* **2015,** *438,* 204-211.

20. Hsien, K. J.; Tsai, W. T.; Su, T. Y., Preparation of diatomite-TiO2 composite for photodegradation of bisphenol-A in water. *J. Sol-Gel Sci. Technol.* **2009,** *51*, 63-69.

21. Tang, W.; Qiu, K.; Zhang, P.; Yuan, X., Synthesis and photocatalytic activity of ytterbium-doped titania/diatomite composite photocatalysts. *Appl. Surf. Sci.*

22. Yuan, P.; Liu, D.; Tan, D. Y.; Liu, K. K.; Yu, H. G.; Zhong, Y. H.; Yuan, A. H.; Yu, W. B.; He, H. P., Surface silylation of mesoporous/macroporous diatomite (diatomaceous earth) and its function in Cu (II) adsorption: the effects of heating pretreatment. *Microporous Mesoporous Mater.* **2013,** *170*, 9-19.

23. Sheng, G.; Yang, S.; Sheng, J.; Hu, J.; Tan, X.; Wang, X., Macroscopic and microscopic investigation of Ni (II) sequestration on diatomite by batch, XPS, and EXAFS techniques. *Environ. Sci. Technol.* **2011,** *45*, 7718-7726.

24. Dantas, T. D. C.; Neto, A. D.; Moura, M. D. A., Removal of chromium from aqueous solutions by diatomite treated with microemulsion. *Water Res.* **2001,** *35,* 2219-2224.

25. Sheng, G.; Wang, S.; Hu, J.; Lu, Y.; Li, J.; Dong, Y.; Wang, X., Adsorption of Pb (II) on diatomite as affected via aqueous solution chemistry and temperature. *Colloids Surf., A* **2009,** *339,* 159-166.

26. Khraisheh, M. A.; Al-degs, Y. S.; Mcminn, W. A., Remediation of wastewater containing heavy metals using raw and modified diatomite. *Chem. Eng. J.* **2004,** *99*, 177-184.

27. Al-Degs, Y.; Khraisheh, M. A. M.; Tutunji, M. F., Sorption of lead ions on diatomite and manganese oxides modified diatomite. *Water Res.* **2001,** *35*, 3724-3728.

28. De-Castro-Dantas, T. N.; Neto, A. A. D.; De A. Moura, M. C. P., Removal of chromium from aqueous solutions by diatomite treated with microemulsion. *Water Res.* **2001,** *35*, 2219-2224.

29. Sheng, G.; Hu, J.; Wang, X., Sorption properties of Th (IV) on the raw diatomite-effects of contact time, pH, ionic strength and temperature. *Appl. Radiat. Isot.* **2008,** *66*, 1313-1320.

30. Aivalioti, M.; Vamvasakis, I.; Gidarakos, E., BTEX and MTBE adsorption onto raw and thermally modified diatomite. *J. Hazard. Mater.* **2010,** *178*, 136-143.

31. Yu, Y.; Addai-Mensah, J.; Losic, D., Chemical functionalization of diatom silica microparticles for adsorption of gold (III) ions. *J. Nanosci. Nanotechnol.* **2011,** *11*, 10349-10356.

32. Branton, P.; Carrott, P.; Llewellyn, P.; Müller, E.; Flores-Cano, J.; Leyva-Ramos, R.; Padilla-Ortega, E.; Mendoza-Barron, J., Adsorption of heavy metals on diatomite: mechanism and effect of operating variables. *Adsorpt. Sci. Technol.* **2013,** *31*, 275-292.

33. Khraisheh, M. A. M.; Al-degs, Y. S.; McMinn, W. A. M., Remediation of wastewater containing heavy metals using raw and modified diatomite. *Chem. Eng. J.* **2004,** *99*, 177-184.

34. Aytaş, Ş. Ö.; Akyil, S.; Aslani, M.; Aytekin, U., Removal of uranium from aqueous solutions by diatomite (Kieselguhr). *J. Radioanal. Nucl. Chem.* **1999,** *240*, 973-976.

35. Garcia, G.; Cardenas, E.; Cabrera, S.; Hedlund, J.; Mouzon, J., Synthesis of zeolite Y from diatomite as silica source. *Microporous Mesoporous Mater.* **2016,** *219*, 29-37.

36. Maeda, H.; Ishida, E. H., Hydrothermal preparation of diatomaceous earth combined with calcium silicate hydrate gels. *J. Hazard. Mater.* **2011,** *185*, 858-861.

37. Inchaurrondo, N.; Font, J.; Ramos, C. P.; Haure, P., Natural diatomites: Efficient green catalyst for Fenton-like oxidation of Orange II. *Appl. Catal., B* **2016,** *181*, 481-494.

38. Erdem, E.; Çölgeçen, G.; Donat, R., The removal of textile dyes by diatomite earth. *J. Colloid Interface Sci.* **2005,** *282*, 314-319.

39. Gao, B.; Jiang, P.; An, F.; Zhao, S.; Ge, Z., Studies on the surface modification of diatomite with polyethyleneimine and trapping effect of the modified diatomite for phenol. *Appl. Surf. Sci.* **2005,** *250*, 273-279.

40. Farrah, S.; Preston, D.; Toranzos, G.; Girard, M.; Erdos, G.; Vasuhdivan, V., Use of modified diatomaceous earth for removal and recovery of viruses in water. *Appl. Environ. Microbiol.* **1991,** *57*, 2502-2506.

41. Hadjar, H.; Hamdi, B.; Jaber, M.; Brendlé, J.; Kessaïssia, Z.; Balard, H.; Donnet, J. B., Elaboration and characterisation of new mesoporous materials from diatomite and charcoal. *Microporous Mesoporous Mater.* **2008,** *107*, 219-226.

42. Xiong, W.; Peng, J., Development and characterization of ferrihydrite-modified diatomite as a phosphorus adsorbent. *Water Res.* **2008,** *42*, 4869-4877.

43. Yılmaz, B.; Ediz, N., The use of raw and calcined diatomite in cement production. *Cem. Concr. Compos.* **2008,** *30*, 202-211.

44. Osmanlioglu, A. E., Natural diatomite process for removal of radioactivity from liquid waste. *Appl. Radiat. Isot.* **2007,** *65*, 17-20.

45. Aw, M. S.; Simovic, S.; Yu, Y.; Addai-Mensah, J.; Losic, D., Porous silica microshells from diatoms as biocarrier for drug delivery applications. *Powder Technol.* **2012,** *223*, 52-58.

46. Aw, M. S.; Bariana, M.; Yu, Y.; Addai-Mensah, J.; Losic, D., Surface-functionalized diatom microcapsules for drug delivery of water-insoluble drugs. *J. Biomater. Appl.* **2013,** *28*, 163-174.

47. Bariana, M.; Aw, M. S.; Losic, D., Tailoring morphological and interfacial properties of diatom silica microparticles for drug delivery applications. *Adv. Powder Technol.* **2013,** *24*, 757-763.

48. Bariana, M.; Aw, M. S.; Kurkuri, M.; Losic, D., Tuning drug loading and release properties of diatom silica microparticles by surface modifications. *Int. J. Pharm.* **2013,** *443*, 230-241.

49. Zhang, H.; Shahbazi, M. A.; Mäkilä, E. M.; da Silva, T. H.; Reis, R. L.; Salonen, J. J.; Hirvonen, J. T.; Santos, H. A., Diatom silica microparticles for sustained release

and permeation enhancement following oral delivery of prednisone and mesalamine. *Biomaterials* **2013,** *34*, 9210-9219.

50. Maher, S.; Alsawat, M.; Kumeria, T.; Fathalla, D.; Fetih, G.; Santos, A.; Habib, F.; Losic, D., Luminescent silicon diatom replicas: self-reporting and degradable drug carriers with biologically derived shape for sustained delivery of therapeutics. *Adv. Funct. Mater.* **2015,** *25*, 5107-5116.

51. Janićijević, J.; Krajišnik, D.; Čalija, B.; Dobričić, V.; Daković, A.; Krstić, J.; Marković, M.; Milić, J., Inorganically modified diatomite as a potential prolonged-release drug carrier. *Mater. Sci. Eng., C* **2014,** *42*, 412-420.

52. Ruggiero, I.; Terracciano, M.; Martucci, N. M.; De Stefano, L.; Migliaccio, N.; Tatè, R.; Rendina, I.; Arcari, P.; Lamberti, A.; Rea, I., Diatomite silica nanoparticles for drug delivery. *Nanoscale Res. Lett.* **2014,** *9*, 1-7.

53. Vasani, R.; Losic, D.; Cavallaro, A.; Voelcker, N., Fabrication of stimulus-responsive diatom biosilica microcapsules for antibiotic drug delivery. *J. Mater. Chem. B* **2015,** *3*, 4325-4329.

54. Delalat, B.; Sheppard, V. C.; Ghaemi, S. R.; Rao, S.; Prestidge, C. A.; McPhee, G.; Rogers, M.-L.; Donoghue, J. F.; Pillay, V.; Johns, T. G., Targeted drug delivery using genetically engineered diatom biosilica. *Nat. Commun.* **2015,** *6*.

55. Li, X.; Bian, C.; Chen, W.; He, J.; Wang, Z.; Xu, N.; Xue, G., Polyaniline on surface modification of diatomite: a novel way to obtain conducting diatomite fillers. *Appl. Surf. Sci.* **2003,** *207*, 378-383.

56. Ergül, S.; Kadan, İ.; Savaşcı, Ş.; Ergül, S., Modified diatomaceous earth as a principal stationary phase component in TLC. *J. Chromatogr. Sci.* **2005,** *43*, 394-400.

57. Simpson, J. T.; D'urso, B. R., Superhydrophobic diatomaceous earth. U.S. Patent No. 8,216,6742012.

58. Oliveira, N. M.; Reis, R. L.; Mano, J. F., Superhydrophobic surfaces engineered using diatomaceous earth. *ACS Appl. Mater. Interfaces* **2013,** *5*, 4202-4208.

59. Polizos, G.; Winter, K.; Lance, M. J.; Meyer, H. M.; Armstrong, B. L.; Schaeffer, D. A.; Simpson, J. T.; Hunter, S. R.; Datskos, P. G., Scalable superhydrophobic coatings based on fluorinated diatomaceous earth: Abrasion resistance versus particle geometry. *Appl. Surf. Sci.* **2014,** *292*, 563-569.

60. Puretskiy, N.; Chanda, J.; Stoychev, G.; Synytska, A.; Ionov, L., Anti-icing superhydrophobic surfaces based on core-shell fossil particles. *Adv. Mater. Interfaces* **2015,** *2*, 1500124-1500131.

61. Nine, M. J.; Cole, M. A.; Johnson, L.; Tran, D. N.; Losic, D., Robust superhydrophobic graphene-based composite coatings with self-cleaning and corrosion barrier properties. *ACS Appl. Mater. Interfaces* **2015,** *7*, 28482-28493.

62. Perera, H. J.; Khatiwada, B. K.; Paul, A.; Mortazavian, H.; Blum, F. D., Superhydrophobic surfaces with silane-treated diatomaceous earth/resin systems. *J. Appl. Polym. Sci.* **2016,** *133*, 44072-44081.

63. Cassie, A.; Baxter, S., Wettability of porous surfaces. *Trans. Faraday Soc.* **1944,** *40*, 546-551.

64. Jung, Y. C.; Bhushan, B., Dynamic effects induced transition of droplets on biomimetic superhydrophobic surfaces. *Langmuir* **2009,** *25*, 9208-9218.

65. Reyssat, M.; Quéré, D., Contact angle hysteresis generated by strong dilute defects. *J. Phys. Chem. B* **2009,** *113*, 3906-3909.

66. Jung, Y. C.; Bhushan, B., Mechanically durable carbon nanotube-composite hierarchical structures with superhydrophobicity, self-cleaning, and low-drag. *ACS Nano* **2009,** *3*, 4155-4163.

67. Shi, F.; Liu, Z.; Wu, G. L.; Zhang, M.; Chen, H.; Wang, Z.; Zhang, X.; Willner, I., Surface imprinting in layer-by-layer nanostructured films. *Adv. Funct. Mater*. **2007,** *17*, 1821-1827.

68. Lai, Y.; Lin, C.; Wang, H.; Huang, J.; Zhuang, H.; Sun, L., Superhydrophilic-superhydrophobic micropattern on TiO2 nanotube films by photocatalytic lithography. *Electrochem. Commun.* **2008,** *10*, 387-391.

69. Lee, S. M.; Jung, I. D.; Ko, J. S., The effect of the surface wettability of nanoprotrusions formed on network-type microstructures. *J. Micromech. Microeng.* **2008,** *18*, 125007.

70. Bravo, J.; Zhai, L.; Wu, Z.; Cohen, R. E.; Rubner, M. F., Transparent superhydrophobic films based on silica nanoparticles. *Langmuir* **2007,** *23*, 7293-

CHAPTER II

BACKGROUND

2.1. SUPERHYDROPHOBIC SURFACES

An important property of a solid surface is its wettability.[1] Wettability of a solid surface depends upon two factors. One of the factors is chemical and the other factor is the structure of the surface.[2] Wettability of a surface with water can be measured by a water contact angle. Surface energy and structure determine the water contact angle of a solid surface. Flat surfaces with low surface energy and surfaces with packed -CF_3 groups, give contact angles as high as 120^o.[3] These surfaces are hydrophobic, but do not have self-cleaning properties. Structured surfaces with low surface energies are required to achieve large water contact angles.[4] Surfaces with water contact angles larger than 150^o are usually called superhydrophobic (SH) surfaces.[5] Superhydrophobic surfaces show functional properties like anti-sticking,[6] anti-contamination,[7] and self-cleaning[8] etc. All such functional properties are desirable for some industrial and biological applications. Some of the important applications of superhydrophobic surfaces are self-cleaning windshields for automobiles,[9] metal refining, stain resistant textiles, anti-soiling architectural coatings,[10] antifouling paints for boats,[11] anti-sticking of snow for antennae and windows[12]. In nature, many species such as lotus leaves,[1] water strider's legs,[13] and cicada ornis wings[14] are superhydrophobic. Water droplets roll off on those superhydro-

phobic surfaces at small tilt angles (sliding angle) removing contaminants from the surfaces.[15]

2.2. THEORETICAL BACKGROUND

Young's equation[16] is used to express the wettability of a flat surface. The contact angle (CA) of a surface is given by

$$\cos\theta = \frac{\gamma_{SV} - \gamma_{SL}}{\gamma_{LV}} \qquad (1)$$

where, γ_{SV}, γ_{SL} and γ_{LV} refer to the interfacial surface tensions with S, L, and V as solid, liquid, and gas (vapor), respectively. Young's angle (θ) represents thermodynamic equilibrium of the free energy at the solid-liquid-vapor interphase.[16]

Solid surfaces can be categorized into four different types, superhydrophilic (CA < 10^o), hydrophilic ($10^o \leq CA \leq 90^o$), hydrophobic ($90^o \leq CA \leq 150^o$) and superhydrophobic (CA > 150^o) depending upon the water contact angle values.[17] In general, two types of CA values are used. Static and dynamic CAs describe the contact angle of a droplet on a surface. If a surface is flat, the static contact angle of such a surface is close to the Young's angle. The sessile drop method is often used to determine static CAs. In such measurements a drop is placed on the surface and the value of the contact angle is determined using a goniometer.[18]

Water contact angles taken during the growth of a water droplet are known as advancing CAs, θ_a. Similarly, contact angles measured during the shrinkage of a water droplet are receding CAs, θ_r. The difference between advancing CA, θ_a, and receding CA,

θ_r, is referred as contact angle hysteresis ($\Delta\theta$). Larger contact angle hysteresis results from chemical heterogeneity and roughness.[19, 20]

Superhydrophobic surfaces are composed of micro- and nanoscale asperities. A water droplet on a rough surface may show different behaviors which at extremes could be shown as in the Fig. 2.1.

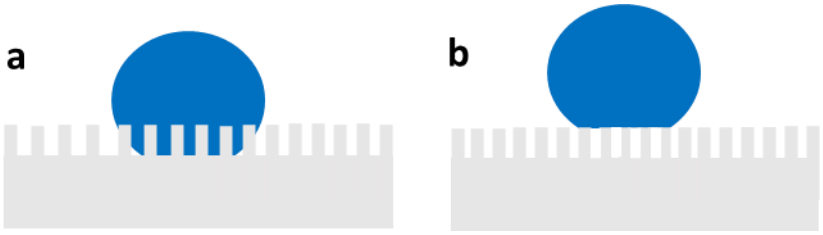

Fig. 2.1. A liquid droplet behavior on a rough surface: a) liquid penetrates into the spikes (Wenzel state) and b) liquid suspends on the spikes (Cassie-Baxter state).

Water droplets can penetrate the asperities or suspend above the asperities. In such structured surfaces, the water contact angles observed are larger compared to corresponding flat surfaces. These two conditions of water droplets on the rough surface are named the Wenzel state (penetration) or homogenous wetting state and Cassie-Baxter state (suspension) or heterogeneous wetting state after the Wenzel[21] and Cassie-Baxter (CB)[22] models. These two models are used as the basic ones for the study of various natural and artificial superhydrophobic surfaces.[23]

Real surfaces having non-ideal surface structures, in many cases, cannot be fully explained by Young equation. Wenzel proposed an equation that relates contact angles to surface roughness and surface energies. It can be written as,

$$r(\gamma_{sv-}\gamma_{sL}) = \gamma_{Lv}\cos\theta_w \qquad (2)$$

where, θ_w is the apparent Wenzel contact angle and it is influenced by roughness of solid surface and r is known as roughness factor. The roughness factor[21] is simply defined as the ratio of the actual surface area and the geometric surface area. The actual surface area and geometric surface area of ideal liquid-liquid or liquid-gas interfaces are identical due to their smooth surface (r = 1). But for real solid surfaces, the actual surface area is always greater than geometric surface area because of the surface roughness. Therefore, for a real solid surface or rough surface, values of r are > 1.[21, 24]

Using equation 1 and 2, the Wenzel equation can be further modified as,

$$\cos\theta_w = r\ \cos\theta \qquad (3)$$

where, θ_w represents to the apparent contact angle, r the roughness factor, and θ refers to Young's angle. The contact angle and its hysteresis depends on the surface roughness and increases with increases in roughness factor. According to Wenzel Model, the contact angle increases steadily with roughness factor up to 1.7 and after that the contact angle hysteresis starts decreasing.[25, 26] The decrease in the contact angle hysteresis is believed to occur due to the switching from the Wenzel to the Cassie-Baxter state. The increased air fraction as shown in Fig. 2.1b leads to the suspension of water droplet on top of the asperities.

According to the Cassie-Baxter (CB) model,[22] for a suspended water droplet on the asperities, the apparent contact angle is the sum of all the contributions of the different phases as described by following equation:

$$cos\ \theta_c = f_1 \cos\theta_1 + f_2\ \cos\theta_2 \qquad (4)$$

where, θ_c is the apparent CA, f_1 and f_2 surface fraction of phase 1 and 2, respectively; θ_1 and θ_2 CA of phase 1 and phase 2, respectively. For a rough surface containing only one type of asperity, given *f* is the solid fraction, then the air fraction is $(1 - f)$. With $(\theta = 180°)$ for air, the resulting CA can be estimated by the following equation:

$$\cos\theta_c = f(1 + \cos\theta) - 1 \qquad (5)$$

Thus, for the CB model, the apparent contact angle, θ_c, is a function of the solid fraction for a given surface with contact angle, θ. To obtain a superhydrophobic surface, the contribution of the solid part should be as small as possible. It is very important to know some guidelines for the prediction of surface behavior. Modeling of surfaces provide such guidelines, which can be very critical for designing superhydrophobic surfaces. Thus, many research projects have been devoted to modeling and creation of superhydrophobic surfaces.[27-32]

Many superhydrophobic surfaces are found in nature. Researchers have mimicked nature and made many different artificial superhydrophobic surfaces.

2.3. NATURAL SUPERHYDROPHOBIC SURFACES

Lotus plant leaves are well known examples of natural superhydrophobic surfaces. Their leaves can remove dirt and pathogenic organisms. Barthlott and Neinhuis are the pioneers of the recent research of superhydrophobic surfaces inspired by nature.[7, 33] They revealed that suitable surface roughness is necessary for extreme repellency against liquid droplets. Subsequently, other researchers found that plant cuticle is a composite of a network of cutin and hydrophobic waxes. After that, researchers noticed different levels of hierarchical structures on the leaves' surfaces. The hierarchical structure on the surface of leaves are formed by convex cells and a much smaller superimposed layer of hydrophobic three-dimensional wax tubules.[17] Air is found enclosed in the cavities of the convex cell structures. The trapped air is responsible for minimal wetting of such surface.

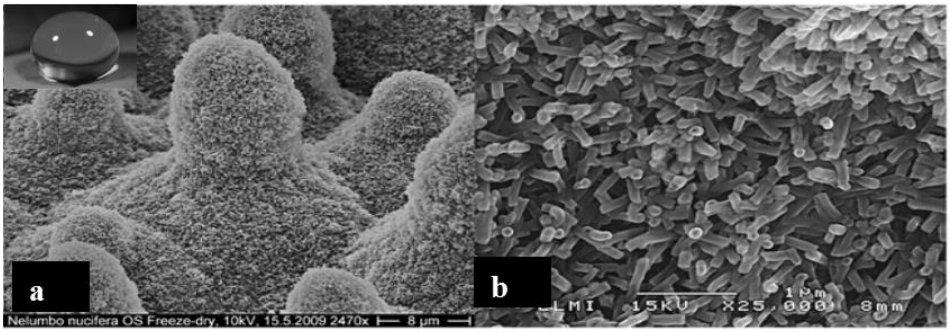

Fig. 2.2. a) The upper side surface of the lotus leaf and water droplet on the surface of lotus leaf (inset); scale bar = 8 µm; b) wax tubules from the upper side of the lotus leaf; scale bar = 1 µm.[34] This figure was reproduced from reference 34.

There are other superhydrophobic surfaces present in the plant kingdom. Taro (*Colocasia esculenta*) leaves show a self-cleaning effect.[7] In taro leaves, elliptic

protrusions (~10 μm) form the microstructures and the nano-scaled pins form hierarchical structures with the appropriate microstructure.[35]

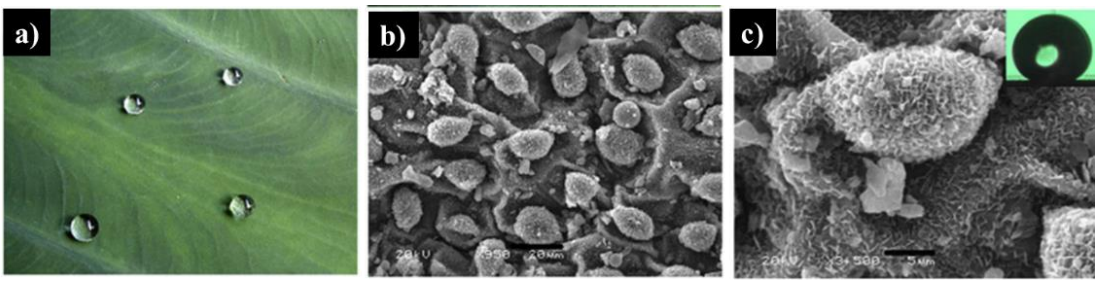

Fig. 2.3. a) A few water droplets on a taro leaf; b) and c) SEM images of a taro leaf with different magnifications.[35] The inset of c) was a water droplet on a taro leaf, with a contact angle of 159 ± 2°. The scale bars of b) and c) were 20 μm and 5 μm, respectively. This figure was reproduced from reference 35.

Similarly, India canna (*canna generalis bailey*) leaves and rice leaves (of different varieties) also exhibit superhydrophobicity and have micro- and nanostructures on the surfaces.[35] Lotus leaves, India canna, and Taro leaves form tubule-like and platelet like wax structures. The arrangement of those structures on the surfaces affect the wettability of the surface.[36] A sliding angle of a lotus leaf is less than 2°.[37] This small angle is expected due to homogeneous arrangement of surface protrusions. A colocasia leaf shows superhydrophobicity, but has different structures than a lotus leaf.[38] The Colocasia leaf has bumps similar to the lotus, but the bumps are separated by the surrounding ridges. The hydrophobic nature results from both bumps and ridges present on the surface since they might create air pockets between the water droplets and surface. All these reports

suggest that the surface cuticle and its waxes are important to surface wettability by folding cuticles or by forming three dimensional wax crystals on plant surface.[17]

Not only in plants, but numerous natural surfaces with hierarchical structures and roughness are found in animal kingdom. It has been reported that the leg of water strider has numerous oriented needle-shaped setae with diameters ranging from few micrometers to several hundred nanometers.[13, 39] Many nano-scaled grooves were observed on each micro-seta, forming a hierarchical structure. This hierarchical topography with secreted wax origins superhydrophobicity on water strider's legs.[40]

On the other hand, the scales on the wings of some butterflies have regular overlapping structures like roof tiles.[41] The length and widths of individual scales are in the micro (50-150 μm) and nanometer (35-70 nm) range. A gecko foot contains hundreds of thousands of keratinous hairs or setae.[42, 43] Each seta is approximately 30-130 μm long and contains hundreds of submicron spatula forming hierarchical morphologies.[44] Byun et al. investigated 10 orders and 24 species of insects to characterize the functions of natural structures by focusing on both lower and upper surfaces of the insect wings.[45] They have mentioned that hierarchical structure with micro- and nano-scaled layers on the upper surface of insects' wings enabled hydrophobicity. Such surface structures are essential for water droplets to roll off and remove the dirt particles.

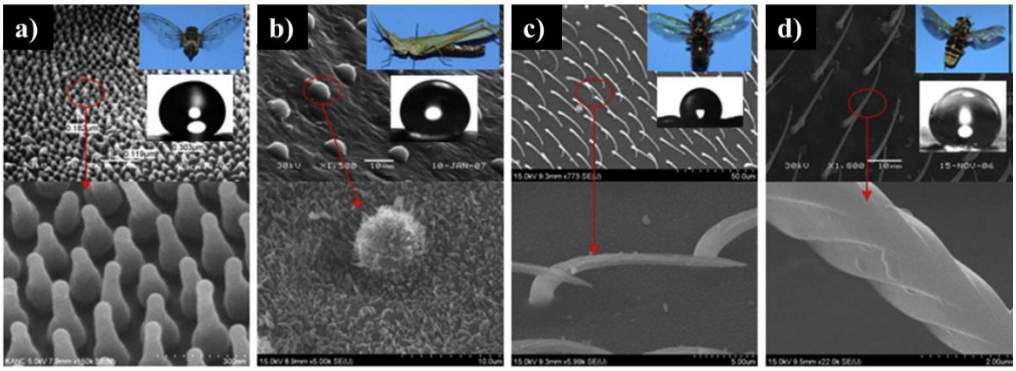

Fig. 2.4. SEM images and measured contact angles on upper wing surfaces of insects.[46] (a) *Homoptera Meimuna opalifera* (Walker), water contact angle of 165°; (b) *Orthoptera Acrida cinerea cinerea* (Thunberg), water contact angle of 151°; (c) *Hymenoptera Vespa dybowskii* (Andre), water contact angle 126°; (d) *Diptera Tabanus chrysurus* (Loew), water contact angle of 156°. This figure was reproduced from reference 46.

All of these reports suggest that many hierarchical structures are present in natural animal surfaces. This indicates the importance of the pattern of surface structures to wettability and all natural surfaces are not superhydrophobic.

The nature of all superhydrophobic surfaces are not the same in every aspect. Water droplets on the petal surface of a red rose (*rosea Rehd*) form a spherical shape, but the droplets do not fall when the petal is turned upside down.[47] This special property is known as petal effect. The Lotus effect differs from petal effect due to the difference in their microstructures. When a water droplet wets the petal surface, the liquid film impregnates the textured regime. The liquid only wets the grooves between the projected pillars leaving the plateaus dry which form Cassie impregnating state. For the petal

surface, the dimensions of hierarchical micro- and nano-structures both are found to be larger than those related to the lotus leaf.[47]

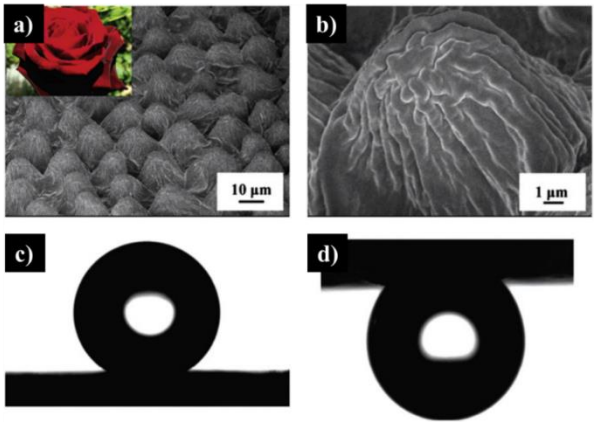

Fig. 2.5. SEM images (a, b) of a red rose petal, with a periodic array of micro-papillae and nano-folds; (c) a water droplet on the petal's surface, water contact angle of 152°; (d) a water droplet on the petal surface when turned upside down.[47] This figure was reproduced from reference 47.

In the Cassie impregnating wetting regime, water droplets enter in to the large grooves of petal, but not in to the small ones. However, the common characteristic of superhydrophobic surfaces rest on the periodic structures that are hierarchically organized into micro- and nano-scales.[47]

2.4. ARTIFICIAL SUPERHYDROPHOBIC SURFACES

After discovering natural superhydrophobic surfaces structures, various work has been done to mimic natural textured surfaces and their superhydrophobicity.

2.5. METHODS FOR FABRICATING ARTIFICIAL SUPERHYDROPHOBIC SURFACES

Superhydrophobic films have been made using a combination of poly(vinyl chloride) (PVC) and ethanol.[48] The structure of such surfaces can be controlled by varying the ethanol content in the PVC solution. Those superhydrophobic surfaces had lotus leaf like structures with nanoparticles of size ranging from 100 to 300 nm.[48]

Various methods have been employed to prepare structured surfaces required for superhydrophobicity. Suitable surface structures for superhydrophobicity can be achieved using lithographic methods,[49-51] template based techniques,[52, 53] plasma treatment,[54, 55] self-assembly and self- organization,[105,106] chemical deposition,[56-60] layer-by-layer (LBL) deposition,[61-67] colloidal assembly,[99,100] and electrospinning.[68-70]

Fabrication of superhydrophobic surfaces using imprinting technique involves lithography, templating, and plasma treatment. Lithography is well-known technique and its sub-techniques are optical lithography (photolithography),[49-51] soft lithography,[56, 71, 72] nano-imprint lithography,[37, 73] electron beam lithography,[74, 75] X-ray lithography[76] and colloidal lithography.[77] Many superhydrophobic surfaces have been made by template-based methods.[52, 53] Various materials such as filter paper,[78] insect wings,[79] reptile skins,[80] and plant leaves[81] have been used as templates to fabricate superhydrophobic surface patterns. Generally, templating processes involve preparing a textured template master, molding the replica, and finally removal of the templates One example involving such a process is mimicking of gecko's feet to make superhydrophobic surface.[80] A large number of samples can be made using the same high-quality template. Operators need to

be careful, especially for micro- and nano-scaled structures, to avoid damaging both the samples and the templates.

Researchers have reported the formation of surface patterns by the plasma treatment after lithography or templating methods.[77, 82] Plasma treatments can also be used before lithography or templating.[54, 55] Sometimes plasma treatment and lithography can be alternate options during the surface processing.[83] Plasma treatment is more connected to etching techniques to prepare superhydrophobic surface patterns. Superhydrophobic surfaces with sharp tips at nanoscale have been prepared by using deep reactive ion etching (DRIE).[84-86] Argon plasma treatment on a structured surface has been used to control the wettability of surfaces.[87] Many other plasma treatments that have been used to make superhydrophobic surfaces include plasma polymerization,[88, 89] plasma electrospray,[90] plasma-enhanced vapor deposition,[58, 60, 91] and plasma immersion ion implantation (PIII).[92] So, plasma treatment alone or coupled with other techniques can be used to fabricate superhydrophobic surfaces.

Another way of fabricating superhydrophoic surfaces is chemical deposition of a thin film on the textured surfaces. Chemical vapor deposition (CVD),[56-60] electrochemical deposition, and layer-by-layer deposition,[61-67] are the typical chemical deposition methods. In a common CVD process, selected substrate is exposed to a gaseous precursor to deposit the desired film or powder, and chemical reaction occurs during the process. Electrochemical deposition processes can deposit films of solid metal or their oxides on to electrically conductive substrates. LBL deposition is another method to make superhydrophobic surfaces. In this process, assembling of layers occurs by spontaneous

adsorptions and varieties of substrates can be used. This method is relatively facile and economical because there is no need to prepare master for replication like imprinting methods or provide a particular environmental chamber like plasma treatment and CVD.

Colloidal assembly is a process of forming assemblies of monodispersed particles through chemical bonding or van der Waals forces. Multilayered roughness can be formed by controlling the assembly of the particles.[93] Immersing the substrate into a solution of particles and spin coating techniques can be used to form multilayers onto the substrates.[94, 95] Min et al. have reported spin coating of monodispersed silica particles (~70 nm) over a large area.[96] In this technique, superhydrophobic states with multilayered colloids crystals formation occurs by self-assembly methods. Self-assembly of particles result due to the internal interaction or forces among the colloidal particles.[97, 98] Colloidal assembly and aggregates are very effective in modifying surface energy and increasing surface roughness.

Superhydrophobic surfaces have been prepared by sol-gel methods.[99-103] In this method, a chemical solution or sol is utilized as a precursor by chemical solution deposition on the selected surface to form a gel like network. A rough surface required for superhydrophobicity and can be created by adding materials of low surface energy and micro- and nanoparticles into the network. This method is suitable for making superhydrophobic films on glass surfaces.[23, 104-107] Use of a eutectic liquid in a sol-gel process has been reported to form silica films with optical transparency and superhydrophobicity.[105]

Electrospinning is a simple and versatile method to make polymer fibers in macro- and nano-scale.[68-70] This technique can be used to increase roughness for the creation of superhydrophobic surfaces.[108] Electrospraying is not limited to fibers. By electrospraying, polymer films of different shapes ranging from spheres to fibers can be deposited.[109] Generally, fibers are produced by electrospinning process and beads are formed during electrospraying.[110-114]

The next section will discuss about silane coupling agents and reaction of diatomaceous earth with silane coupling agents.

2.6. TREATMENT OF DE PARTICLES WITH SILANES

DE particles have been treated with three different types of silane coupling agents. The reactions of DE particles have been carried out in plastic container, using *p*-toluene sulfonic acid (PTSA) as a catalyst and toluene as a solvent.

2.6.1. Silane coupling agents

Silane coupling agents are silicon containing compounds which have two types of reactive groups, both inorganic and organic, in the same molecule. They usually form an interface between an inorganic substrate (glass, metal or mineral) and an organic material (polymer, coating or adhesive).[115]

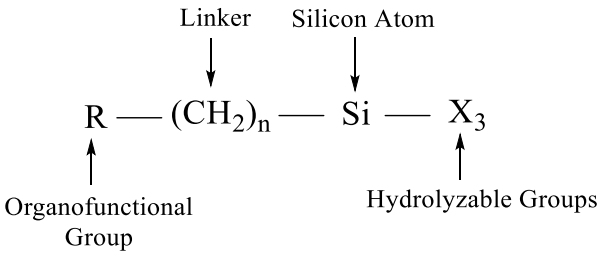

Fig. 2.6. General structure of silane coupling agents

As shown in Fig. 2.6, silane coupling agents have two kinds of functionality, where X represents a hydrolysable group such as alkoxy, acyloxy, halogen or amine. After hydrolysis, reactive silanol groups are formed, which undergo condensation reactions on the surface of siliceous fillers or in solution resulting in the formation of siloxane linkages.[116-118]

The R group is a non-hydrolysable organic species and it differs in different silanes to impart different desired characteristics. The substrates, after reacting with an organosilane, exhibit different wetting or adhesion characteristics. Modified substrates are often the basis to form covalent bonds between organic and inorganic materials.

2.6.2 Acid catalyzed silane and silica reactions.

Reaction of silanes occurs in four steps (shown in an idealized mechanism in Fig. 2.7). Initially, hydrolysis of the reactive groups occurs. Water for hydrolysis may come from several sources. It may be added, it may be present on the substrate surface, or it may come from the atmosphere. The degree of polymerization of the silane is determined by the amount of water available and the organic substituent. Then, condensation reactions give rise to oligomers if the concentration is large enough. The oligomers then

form hydrogen bonds with -OH groups of the substrate. Finally, during drying or curing, a covalent linkage is formed with the substrate after dehydration. These reactions may occur simultaneously after the initial hydrolysis step. The R group of organosilanes remain available for covalent or physical interaction with other phases.[119] Steric hindrance and bond constraints prevent uniform simple attachment of silanes to surfaces as an “idealized” monolayer.

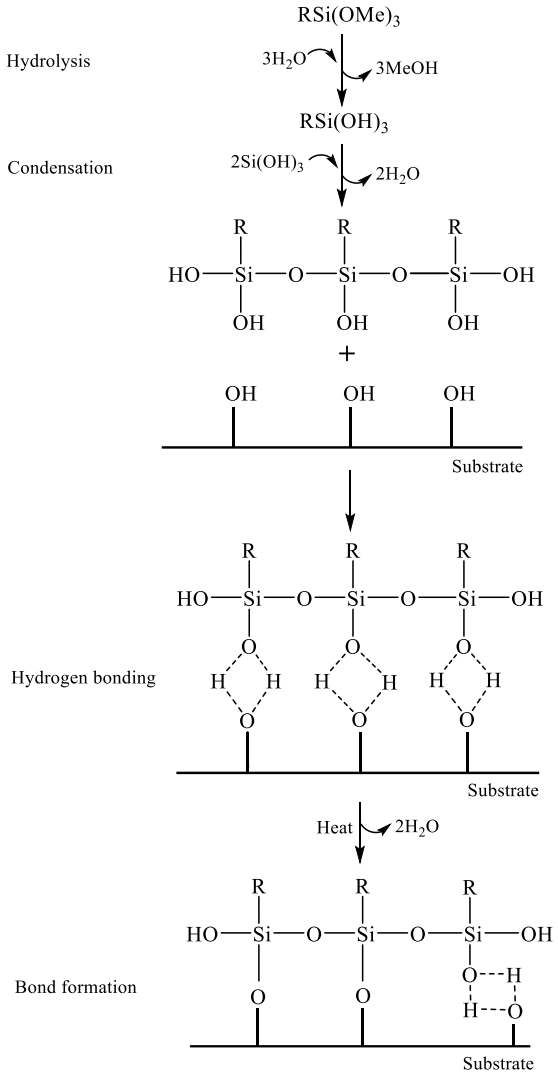

Fig. 2.7. Idealized mechanism for the hydrolytic deposition of silanes.[120]

N. Garcia and co-workers[121] have shown the organic modification of silica (Aerosil 200) with a series of mono- and trifunctional alkoxysilanes. They have used strong organic acids as a catalyst, for example p-toluene sulfonic acid (PTSA) for modification of silica. PTSA dissolves both in the organic phase and in the aqueous layer on the silica. Firstly, the acid catalyzes the hydrolysis of the silanes to silanols. According to them, if the concentration of methoxysilane is small, a step like condensation reaction occurs on the silica particle surface. A first trimethoxysilane hydrolyzes in the aqueous layer and reacts with nearby silica silanols. The remaining two methoxy groups may hydrolyze and condense with eventual alkyltrimethoxysilane molecules in the vicinity. Once condensation brings the siloxane chain out of the aqueous layer, the probability of further condensation decreases as hydrolysis becomes difficult.[121] Reaction of DE samples reported in this dissertation has been done by slight modifications of above method.

In this work, DE samples have been treated with three different trimethoxysilanes. During the treatment of DE with silanes, DE samples, as received, were placed in a plastic bottle. Toluene was added to the bottle. PTSA equivalent to 1 wt% of DE sample was added into the reaction vessel. Increasing amounts of silane (0.0001 to 1 mL) was added to get the DE sample with increased loading of grafted silanes on the surfaces. The reaction vessel was heated at 50 ^{o}C in a mechanical shaker for 4 h. The modified DE samples were washed with sufficient amounts of hexane and methanol to remove unreacted silanes from the reaction mixtures. Silane coupling agents can go on the surface of DE in varieties of ways. A schematic diagram for the reaction of 3-heptafluoroisopropoxypropyl trimethoxysilane (HFIP) and DE is shown in Fig. 2.8.

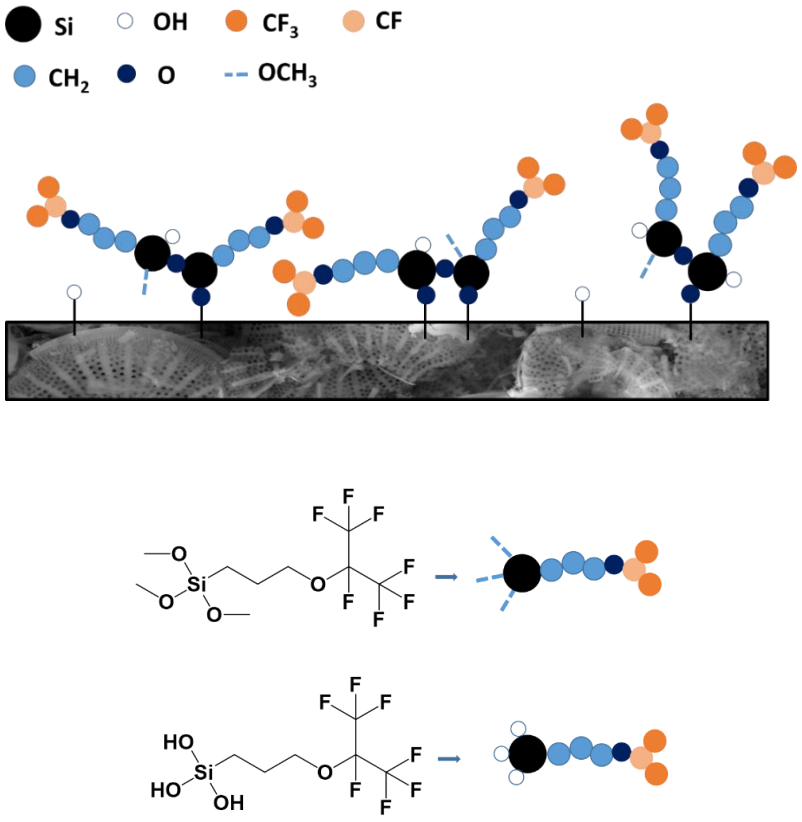

Fig. 2.8. Schematic representation of 3-heptafluoroisopropoxypropyl trimethoxysilane treated DE surface.

2.7. SUPERHYDROPHOBIC SURFACES FROM DE PARTICLES

Diatomaceous earth particles have been used to prepare artificial superhydrophobic surfaces. Simpson and D'Urso were first to make superhydrophobic surfaces using DE particles and then patented the process.[122] Since then, others have used similar processes to fabricate superhydrophobic surfaces using DE[123-128].

2.7.1. Bare treated DE particles coatings

Superhydrophobic surfaces have been made using treated DE particles alone (without binder). Of course, these particles do not hold together well enough for use as a commercial coating. For the preparation of silane treated DE particles, a slurry of treated DE particles in tetrahydrofuran was prepared. A suspension of treated DE particles was used to coat paper strips or microscopic cover slips. These surfaces, after drying in air, were subjected to contact angle measurement and other surface characterization techniques.

2.7.2. Treated DE particles and polymer coatings

Superhydrophobic coatings have also been prepared using treated DE particles with polymers as binders. Low molecular mass polystyrene (number average molecular mass, M_n = 20,000 g/mole), high molecular mass polystyrene (number average molecular mass, M_n = 280,000 g/mole) and high molecular mass polyvinyl acetate (number average molecular mass, M_n = 260, 000 g/mole) have been used as binders to prepare coatings. A series of coating mixtures have been prepared using different percentages of treated DE particles in polymer dispersions. During the preparation of the coatings, treated DE particles were added to polymer solutions and the mixtures were shaken in a mechanical shaker for 4 h at room temperature. The treated DE particles and polymer mixtures have been used to coat aluminum pans. The coated aluminum pans were dried in air at ambient conditions. The coated pan surfaces have been characterized by contact angle measurements and other techniques.

2.8. EXPERIMENTAL TECHNIQUES

Treated DE particles and the coatings prepared from treated DE and polymers were characterized by variety of experimental techniques as described below.

2.8.1. Thermogravimetric analysis (TGA)

TGA was used to determine the percentage of silane couplings agents on diatomaceous earth particles. It was used to measure the mass change of a sample over a range of temperatures. A TGA instrument consists of a sample pan that is connected by a microgram balance arm to a tared pan. When a sample is heated, a change in mass occurs. This change is used to determine the composition of a material or its thermal stability. During heating, a change in mass usually occurs due to decomposition, reaction, or evaporation. While in use, the TGA instrument tracks the change in mass of the sample via a microgram balance. The change in temperature is monitored via a thermocouple. The TGA has an ability to track changes in mass as a function of time and, consequently, temperature. Data can be graphed as mass fraction vs. temperature (^{o}C) as shown in Fig. 2.9. In some cases, materials decompose in the presence of an inert atmosphere to eliminate the formation of side products. In a TGA experiment, first of all, the TGA pan on the balance is tared. Then, the sample is placed on the pan and loaded on the balance. After that, the sample is heated from room temperature to the desired

temperature at a specific heating rate (for example 20 ^{o}C/min) under air/nitrogen flow.

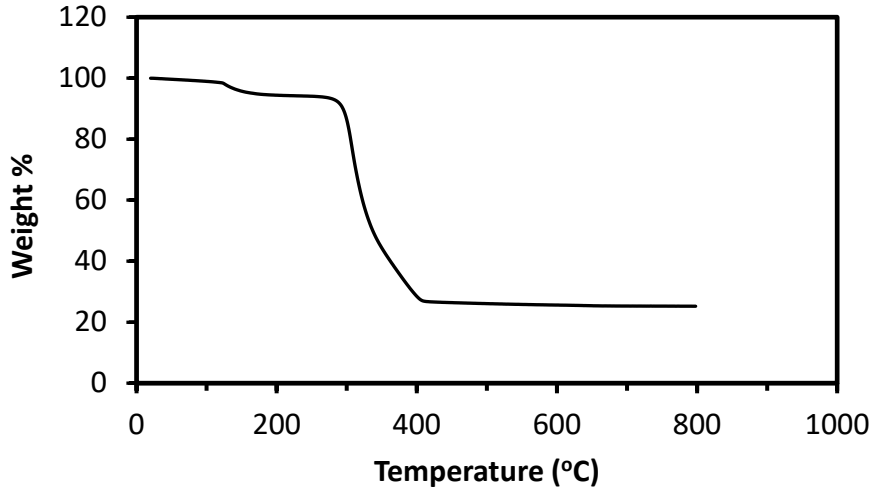

Fig. 2.9. A typical TGA thermogram.[129]

2.8.2. Fourier-transform infrared spectroscopy (FTIR) with an attenuated total reflection (ATR) unit

An FTIR instrument with ATR unit has been used to characterize the silane treated DE particles. FTIR spectroscopy is important technique to identify the functional groups like C=O, C-H or N-H etc. present in a compound. Most of the substances show a characteristic spectrum with characteristic resonances and can be identified by this technique similar to human fingerprint. All types of samples which may be solid, liquid or gas can be identified by FT-IR spectroscopy although the details of the experiment or sample preparation may vary with the sample.[130]

In order to avoid the problems associated with KBr pellets, liquid cells, and scattering, IR-measurements can also be performed in ATR mode. This technique is usually more appropriate to use for solids and dispersions than the conventional

transmission mode, though it suffers from other complications. All types of samples (e.g. solids, liquids, powders, pastes, pellets, slurries, fibers etc.) can usually be used without dilution on the ATR crystal. The measurement is typically performed within seconds.

In ATR, the IR beam is directed into a crystal of relatively high refractive index. The IR beam reflects from the internal surface of the crystal and creates an evanescent wave which projects orthogonally into the sample in intimate contact with the ATR crystal. Some of the energy of the evanescent wave is absorbed by the sample and the reflected radiation is returned to the detector as shown in Fig. 2.10.

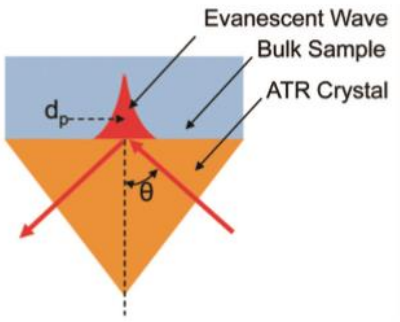

Fig. 2.10. Graphical representation of a single reflection ATR. This figure was reproduced from http://www.piketech.com/files/pdfs/ATRAN611.pdf

The following equation describes the angle of refraction, θ, and its dependence on refractive indices in ATR sampling techniques,

$$\theta_c = \sin^{-1}\left(\frac{n_2}{n_1}\right) \qquad (1)$$

where, n_2 is the refractive index of the sample, n_1 is the refractive index of the crystal, θ is angle of incidence, and θ_c is the critical angle.

To observe a pure ATR spectra, the incident angle needs to be greater than the critical angle, θ_c. If the critical angle is not exceeded, a combined ATR and external reflectance result will be observed. This situation may happen if the angle of incidence of the IR beam is too small, if the refractive index of the crystal is too small, if the refractive index of the sample is too large, or a combination of these three factors.

Most ATR units have horizontal crystals with a clamping utility to ensure good sample contact of solids. Most commonly used crystal materials include diamond, zinc selenide (ZnSe) and germanium. ZnSe is an inexpensive common material and ideal for analyzing liquids and "soft" samples. Diamond is very robust and chemically inert material. So, it is an ideal crystal material for routine measurements with a wide range of possible samples.[131]

The basic procedure of an ATR-measurement is very easy. First of all, the crystal is cleaned (e.g. cellulose tissue with isopropanol) and background is measured with the ATR unit. Then, the sample is placed on the crystal ensuring good contact. Finally, IR spectra of the sample is taken.

2.8.3. Surface Area Determination: BET Theory

BET theory [132] was named after three scientists Brunauer, Emmett, and Teller. It is a modified form of the Langmuir adsorption isotherm. The basic assumptions of BET theory are summarized as follows.[132]

1. Adsorption of the first layer occurs on the well-defined surface sites of uniform energy (one molecule per site).

2. Formation of multiple adsorbate layers occurs from stacking of one layer above another. When, $p = p_o$ (at the saturated vapor pressure of the adsorptive layer), an infinite number of layers will form.

3. At equilibrium, the rate of condensation equals with rate of evaporation for each individual layer.

4. It assumes that no interactions exist between the adsorbate molecules.

The surface area of the adsorbent is determined by the following BET equation 1.

$$\frac{1}{W \times \left(\left(\frac{P}{P_o}\right)\right) - 1} = \frac{1}{W_m \times C} + \frac{C - 1}{W_m \times C} \times \left(\frac{P}{P_o}\right) \qquad (1)$$

The slope (s) and intercept (i) corresponding to equation (1) can be obtained from the plot of $\frac{1}{W \times \left(\frac{P}{P_o}\right) - 1}$ versus relative pressure (shown in Fig. 2.11). W_m (amount of monolayer adsorbed gas) can be derived from equation 2. The total surface area can be calculated from the equation 3.

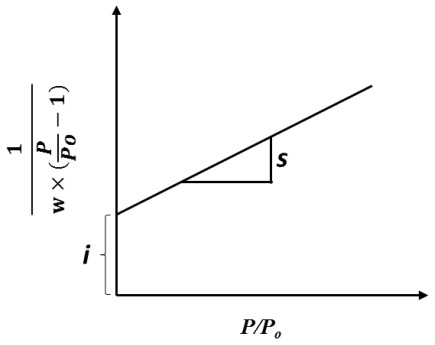

Fig. 2.11. A typical BET plot.[132]

$$s = \frac{C-1}{W_m \times C} \; and \; i = \frac{1}{W_m \times C} \qquad (2)$$

$$S_t = \frac{W_m \times N \times A_{CS}}{M} \qquad (3)$$

In equations (2) and (3), *s* and *i* are the slope and intercept, respectively. S_t is the total surface area, W_m is the amount of monolayer adsorbed gas, *N* is Avogadro's number, A_{cs} is the cross-sectional area of the adsorbate (nitrogen) which is 16.2 $Å^2$ for nitrogen gas, *M* is the molecular mass of nitrogen, and W_s is the mass of the sample. The specific surface area can be calculated from total surface area as shown in equation 4.

$$S = \frac{S_t}{w_s} \qquad (4)$$

2.8.4. Differential scanning calorimetry (DSC)

DSC is a technique used to measure some of the thermal characteristics of samples. It can also be used to determine the temperature for the onset local segmental motions of

polymeric chains which occur with a change in heat capacity. It is routinely used to determine the thermal properties of polymers such as glass transition temperature (T_g), melting temperature (T_m), and crystallization temperature (T_c). A schematic diagram of the DSC instrument and a typical DSC thermogram are shown in Fig. 2.12 and 2.13, respectively. The pan with a sample is referred to as "sample pan", whereas the one without the sample is referred to as "reference pan". This pan is usually empty. In DSC experiments, the sample and reference pans are heated simultaneously to the same temperature at the same time. The difference in heat flows of sample and reference pans is recorded and plotted as the function of temperature.

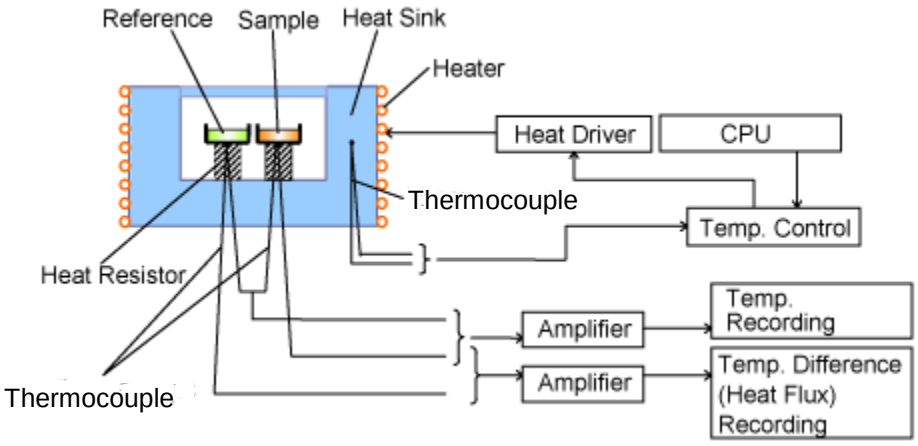

Fig. 2.12. Block diagram of heat flux DSC. Diagram was taken from http://www.hitachi-hightech.com/global/products/science/tech/ana/thermal/descriptions/dsc.html

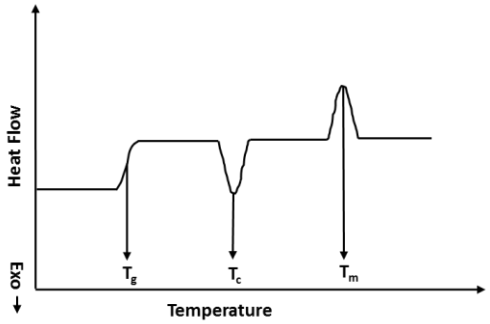

Fig. 2.13. A typical DSC thermogram of a semicrystalline material.

To interpret DSC thermograms, it is important to understand the first order and second order transitions. A first order transition involves both latent heat (heat evolved or absorbed) and heat capacity. Melting of a polymer sample occurs by absorption of heat and is an endothermic process. Crystallization of polymers occur by evolution of heat and is an exothermic process. In contrast, a second order transition such as a glass transition temperature occurs only with a change heat capacity. As polymers have large heat capacities changes at the glass transition temperature, a small increase in temperature will increase the heat flow around this transition resulting in a transition in the thermogram.

2.8.5. Scanning electron microscopy (SEM)

An electron microscope uses an electron beam to produce an image of an object and magnification is obtained by electromagnetic fields. The smaller the wavelength of radiation, the greater is resolving power of a microscope. An electron microscope can resolve objects as small as 0.001 μm (=10 Å), as compared to 0.2 μm by a light microscope. The resolving power of an electron microscope is 200 times greater than that of a light microscope. It can produce magnification up to 400,000 times.

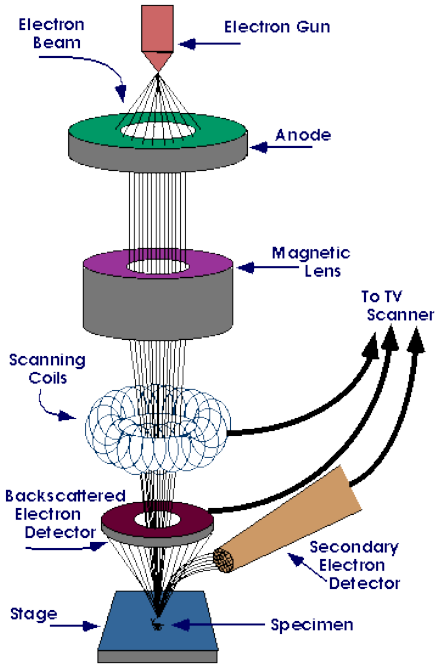

Fig. 2.14. Schematic diagram for scanning electron microscope. This figure was reproduced from https://www.purdue.edu/ehps/rem/rs/sem.htm.

In a scanning electron microscope, the sample to be analyzed is exposed to a narrow electron beam from an electron gun. The electron beam rapidly moves over or scans the surface of the specimen (Fig. 2.14). As a result of the beams, a shower of secondary electrons and other types of radiations from the specimen surface are released. The intensity of released secondary electrons depends upon the structure and the chemical composition of the irradiated sample. These electrons are gathered by a detector, which generates electronic signals. These signals are scanned, as in a television system, to produce an image on a cathode ray tube (CRT). Thus, the formed image is recorded by capturing it from the CRT. Modern scanning electron microscopes have the ability to record the photograph using a digital camera. These microscopes are used to observe the surface topography of microscopic objects.

2.8.6. Contact angle goniometer

A goniometer is an instrument which is used to measure an angle. Water contact angles can also yield the surface tension and interfacial tension. The sessile drop method is a simple and useful method for measuring contact angles. In this dissertation, a home built sessile drop device has been used for measuring water contact angles and is shown in Fig.2.15. The device has a stage for placing the sample and a camera equipped with microscopic lens for obtaining images of water droplets. The magnification and focus of the camera is manually adjusted to obtain the correct perspective of the water droplet. This perspective is achieved by moving the lens forward and backwards by using two mounting screws. The device has a place to hold a micropipette (1-20 µl). With the aid of micropipette water droplets are put on the flat sample surface. The height of the stage is adjusted to obtain the best image of the water droplets on the sample surface.

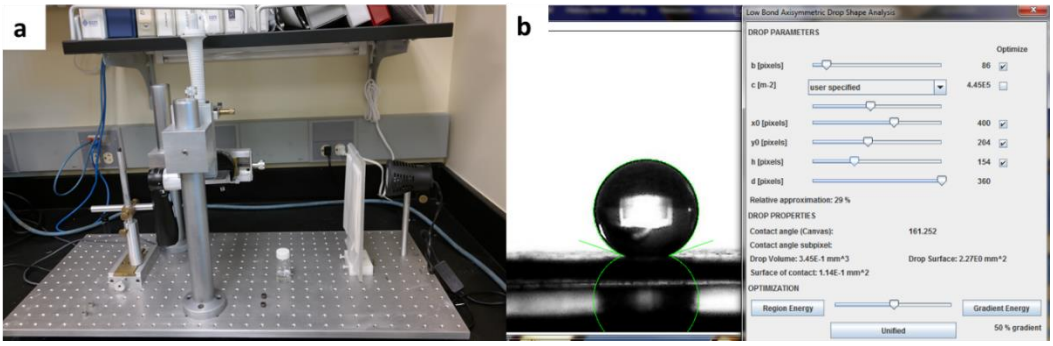

Fig. 2.15. a) Home built goniometer (built by Hamid Mortazavian) and b) analysis of water droplet images by ImageJ software using plugin method LB-ADSA.

After placing the water droplet on the sample surface, a pro-scope camera software is used to observe the image of a water droplet. The height and position of the water droplet is adjusted manually using adjusting screws. After that, the stage with the sample and water droplet is moved forward and backward for proper focus of the camera. The light intensity is also adjusted using a light source which is on the opposite side of camera. After adjusting camera focus, height, position and light, a best image of water droplet is captured and saved. For each sample, three different positions are selected and images were taken. These water droplets images were then analyzed by ImageJ (NIST) software using plugin method low bond axisymmetric drop shape analysis (LB-ADSA).

2.8.7. Particle size analyzer

A CILAS 1180 particle-size-analyzer has been used for the particle size measurements of the DE samples. The CILAS 1180 particle-size-analyzer has integrated wet and dry dispersion modes, built in video camera, and short optical path. The CILAS 1180 provides a measurement range from 0.04 to 2,500 µm**.** Laser diffraction analyzers measure the angular distribution of forward-scattered light from which the most probable particle size distribution of spherical scatterers is inferred.[133] A laser beam of known wavelength is passed through the suspension of the sample. Detectors measure the angular distribution of intensity of the light diffracted by particles.

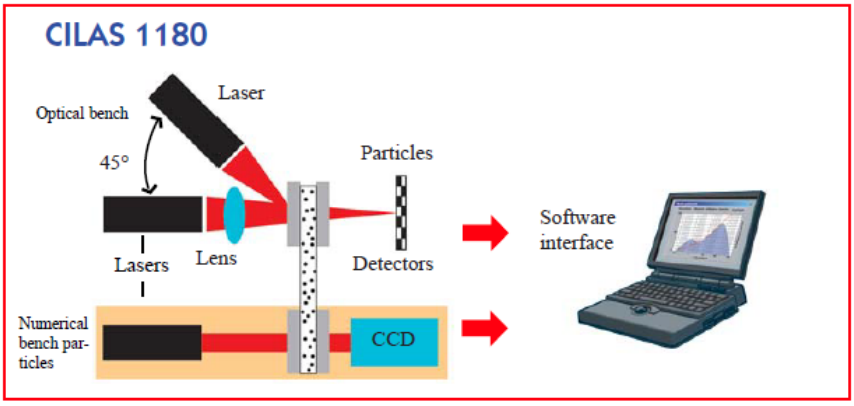

Fig. 2.16. Schematic representation of CILAS 1180. This figure was taken from http://www.es-france.com/pdf/1180_us_doctech.pdf.

About 5 ml of the sample suspension were used to measure the particles size of DE samples. The obscuration value is an important parameter that needs to be adjusted during the measurements (around 17 for DE samples). Obscuration is the percentage of the incident light which is attenuated due to striking the sediment particles. This parameter is used to adjust the amount of sample necessary for an accurate measurement. Values of 12-18 are preferred. A background measurement is done before running each sample. The graphic mean grain size (ϕ) is obtained after completion of experiment. The mean diameter of the DE particles is determined using the relation,[134] $\phi = -log_2 d$ where, *d*, is the diameter in mm.

2.8.8. Dynamic mechanical analyzer (DMA)

DMA is an instrument used for the thermal mechanical analysis of materials. This technique measures the properties of materials as they are deformed under periodic stress.

Specifically, in DMA, a variable sinusoidal stress is applied, and the resultant sinusoidal strain is measured. If the material to be analyzed is purely elastic, the phase difference between the stress and strain sine waves is 0^o (they are in phase). If the materials to be analyzed is purely viscous, the phase difference is 90^o. However, in reality, most real materials are viscoelastic and exhibit a phase difference between these extremes. Viscoelastic materials exist in two distinct states. They show the properties of a glass (high modulus) at low temperatures and those of a rubber (low modulus) at higher temperatures. This phase difference, together with the amplitudes of the stress and strain waves, can be used to determine a variety of fundamental material parameters. Such fundamental material parameters may be storage and loss modulus, tan δ, complex and dynamic viscosity, storage and loss compliance, transition temperatures, creep, and stress relaxation, as well as related performance attributes such as rate and degree of cure, sound absorption and impact resistance, and morphology.

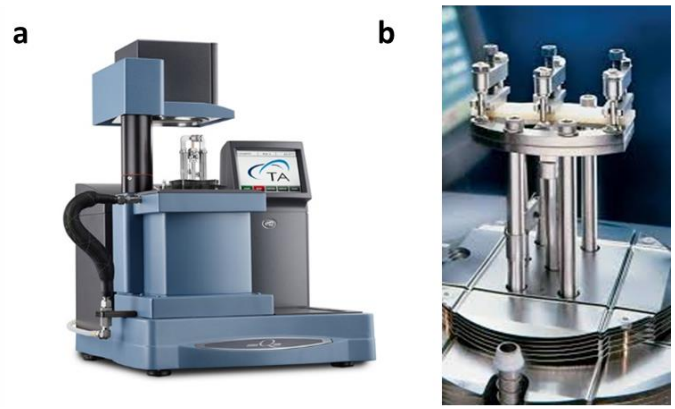

Fig. 2.17. a) Dynamic mechanical analyzer and b) dual cantilever clamp. The images were reproduced from *http://www.tainstruments.com/pdf/brochure/dma.pdf.*

By scanning the temperature during a DMA experiment, the change of state can be observed and the glass transition temperature (T_g) can be determined. The amplitude and phase displacement of a sample in response to an applied oscillating force can be measured. This data provides the stiffness of the sample and can be converted to a modulus to enable sample inter-comparisons. Tan δ, the loss tangent or damping factor can be determined. A temperature scan at constant frequency can produce a fingerprint of the material's relaxation processes and its glass transition temperature (T_g). This technique can help us to understand valuable information on polymer structure and dynamics.

2.8.9. Surface profilometry

The surface profile or surface roughness is an important characteristic of a solid surface. The surface profile of a solid surface is usually measured using an instrument called a profilometer. In this dissertation, two types of profilometers have been used to characterize the surface profiles of the superhydrophobic surfaces.

2.8.9.1. Three dimensional (3-D) profilometer

Nanovea PS50 optical profilometer has been used for measuring the 3D roughness. This profilometer system consists of a base and cluster head relay (CHR). CHR is an axial chromatic optical sensor. It is used for measuring height information of the surface. It uses a light source, where a light passes through an objective lens with high chromatic aberration. When the measured sample is within the range of possible heights of the instrument, the incident white light is focused to form the image of the surface. Only the

focused wavelength is allowed to pass through the spatial filter and spectral analysis is done using diffraction grating. Fig. 2.18 shows the photograph of Nanovea profilometer connected to a computer. An optical pen is a part of the instrument which has been designed to determine vertical measurement range and optical resolutions. Data acquiring software, Nanovea 3D is used to operate the profilometer. A number of roughness parameters are obtained from 3D optical profilometer. The area to be measured is specified by entering the dimensions of area in the software window. Also, the rate of acquisition of the data is specified along with the area software.

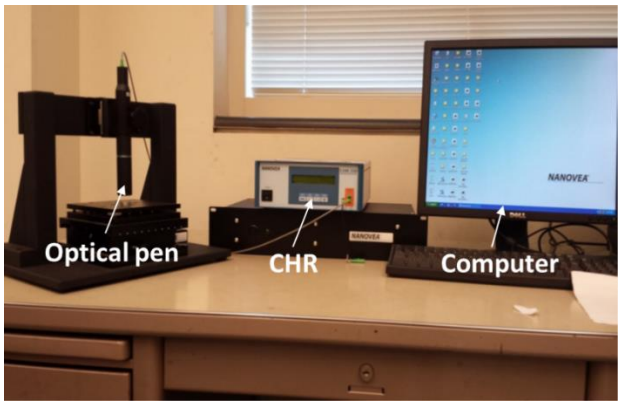

Fig. 2.18. Nanovea optical profilometer.[135] The image was reproduced from reference 135.

At the end of the experiment, a pattern of surface topography of the sample is obtained along with the output.

2.8.9.2. Two dimensional (2-D) Profilometer

The roughness measurements have been performed using two dimensional a stylus type profilometer (Mahr Perthometer). The schematic diagram of profilometer (Mahr Perthometer) used in this study is shown in Fig. 2.19.

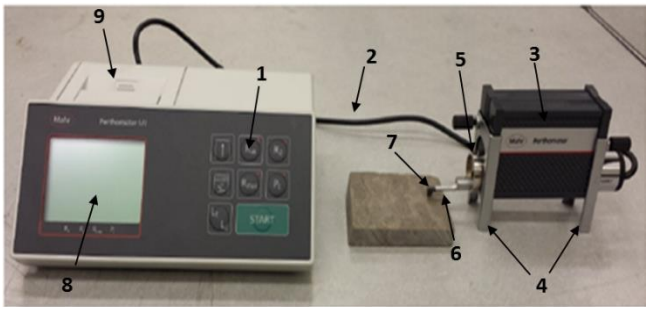

Fig. 2.19. a) Mahr perthometer and its various components.[135] The image was taken from reference 135.

The equipment parts shown in Fig. 2.19 are: Keypad-1; Connecting cable-2; Hand held support-3; Vertical adjusters-4; Dive unit-5; Vee pick up protection-6; Pick up (stylus)-7; Display-8; Printer cover-9.

The profilometer consists of a drive unit which is connected to pick-up with stylus. The drive unit moves in a straight line across the specimen surface during a measuring run at constant speed. During measurement, the pick-up travels in longitudinal direction on the sample surface. The pick-up has the ability to travel in lateral as well as upward directions during the measurements. Vertical adjusters are used to connect the hand held support for the adjustment of the pick-up height. Vee pick-up function is to provide necessary protection for the pick-up. The output of the profilometer provides the roughness parameters, R_a, R_z and R_{max}. The meaning of these parameters are explained

elsewhere in this dissertation. For the measurement, the sample surface is cleaned and the profilometer is switched on. Depending upon the sample, the stylus of the profilometer is adjusted to the height of the measurement. The pick-up travels across the sample surface in the longitudinal direction and measures the roughness parameters. Roughness is measured at three different locations. The average of the three measurements is taken as the average R_a, R_z and R_{max} for the sample.

2.9. REFERENCES

1. Sun, T.; Feng, L.; Gao, X.; Jiang, L., Bioinspired surfaces with special wettability. *Acc. Chem. Res.* **2005,** *38*, 644-652.
2. Hazlett, R. D., Fractal applications: wettability and contact angle. *J. Colloid Interface Sci.* **1990,** *137*, 527-533.
3. Nishino, T.; Meguro, M.; Nakamae, K.; Matsushita, M.; Ueda, Y., The lowest surface free energy based on-CF3 alignment. *Langmuir* **1999,** *15*, 4321-4323.
4. Zhai, L.; Berg, M. C.; Cebeci, F. C.; Kim, Y.; Milwid, J. M.; Rubner, M. F.; Cohen, R. E., Patterned superhydrophobic surfaces: toward a synthetic mimic of the Namib Desert beetle. *Nano Lett.* **2006,** *6*, 1213-1217.
5. Roach, P.; Shirtcliffe, N. J.; Newton, M. I., Progess in superhydrophobic surface development. *Soft Matter* **2008,** *4*, 224-240.
6. Podgornik, B.; Hogmark, S.; Sandberg, O.; Leskovsek, V., Wear resistance and anti-sticking properties of duplex treated forming tool steel. *Wear* **2003,** *254*, 1113-1121.
7. Barthlott, W.; Neinhuis, C., Purity of the sacred lotus, or escape from contamination in biological surfaces. *Planta* **1997,** *202*, 1-8.

8. Blossey, R., Self-cleaning surfaces-virtual realities. *Nat. Mater.* **2003,** *2*, 301-306.

9. Quéré, D., Non-sticking drops. *Rep. Prog. Phys.* **2005,** *68*, 2495.

10. Zielecka, M.; Bujnowska, E., Silicone-containing polymer matrices as protective coatings: Properties and applications. *Prog. Org. Coat.* **2006,** *55*, 160-167.

11. Almeida, E.; Diamantino, T. C.; de Sousa, O., Marine paints: the particular case of antifouling paints. *Prog. Org. Coat.* **2007,** *59*, 2-20.

12. Kako, T.; Nakajima, A.; Irie, H.; Kato, Z.; Uematsu, K.; Watanabe, T.; Hashimoto, K., Adhesion and sliding of wet snow on a super-hydrophobic surface with hydrophilic channels. *J. Mater. Sci.* **2004,** *39*, 547-555.

13. Gao, X.; Jiang, L., Biophysics: water-repellent legs of water striders. *Nature* **2004,** *432*, 36-36.

14. Lee, W.; Jin, M.-K.; Yoo, W. C.; Lee, J.K., Nanostructuring of a polymeric substrate with well-defined nanometer-scale topography and tailored surface wettability. *Langmuir* **2004,** *20*, 7665-7669.

15. Miwa, M.; Nakajima, A.; Fujishima, A.; Hashimoto, K.; Watanabe, T., Effects of the surface roughness on sliding angles of water droplets on superhydrophobic surfaces. *Langmuir* **2000,** *16*, 5754-5760.

16. Young, T., An essay on the cohesion of fluids. *Philosophical Transactions of the Royal Society of London* **1805,** *95*, 65-87.

17. Koch, K.; Bhushan, B.; Barthlott, W., Diversity of structure, morphology and wetting of plant surfaces. *Soft Matter* **2008,** *4*, 1943-1963.

18. Bigelow, W.; Pickett, D.; Zisman, W., Oleophobic monolayers: I. Films adsorbed from solution in non-polar liquids. *J.Colloid Interface Sci.* **1946,** *1*, 513-538.

19. Brzoska, J.; Azouz, I. B.; Rondelez, F., Silanization of solid substrates: a step toward reproducibility. *Langmuir* **1994,** *10*, 4367-4373.

20. Nadkarni, G.; Garoff, S., Reproducibility of contact line motion on surfaces exhibiting contact angle hysteresis. *Langmuir* **1994,** *10*, 1618-1623.

21. Wenzel, R. N., Resistance of solid surfaces to wetting by water. *Ind. Eng. Chem. Chem. Eng.* **1936,** *28*, 988-994.

22. Cassie, A.; Baxter, S., Wettability of porous surfaces. *Trans. Faraday Soc.* **1944,** *40*, 546-551.

23. Hikita, M.; Tanaka, K.; Nakamura, T.; Kajiyama, T.; Takahara, A., Super-liquid-repellent surfaces prepared by colloidal silica nanoparticles covered with fluoroalkyl groups. *Langmuir* **2005,** *21*, 7299-7302.

24. Kamusewitz, H.; Possart, W., Wetting and scanning force microscopy on rough polymer surfaces: Wenzel's roughness factor and the thermodynamic contact angle. *Appl. Phys. A* **2003,** *76*, 899-902.

25. Jopp, J.; Grüll, H.; Yerushalmi-Rozen, R., Wetting behavior of water droplets on hydrophobic microtextures of comparable size. *Langmuir* **2004,** *20*, 10015-10019.

26. Johnson Jr, R. E.; Dettre, R. H., Contact angle hysteresis. III. Study of an idealized heterogeneous surface. *J. Phys. Chem.* **1964,** *68*, 1744-1750.

27. Patankar, N. A., Transition between superhydrophobic states on rough surfaces. *Langmuir* **2004,** *20*, 7097-7102.

28. Patankar, N. A., On the modeling of hydrophobic contact angles on rough surfaces. *Langmuir* **2003,** *19*, 1249-1253.

29. Gao, N.; Yan, Y., Modeling superhydrophobic contact angles and wetting transition. *J. Bionic Eng.* **2009,** *6*, 335-340.

30. Nosonovsky, M.; Bhushan, B., Biomimetic superhydrophobic surfaces: multiscale approach. *Nano Lett.* **2007,** *7*, 2633-2637.

31. Sun, G.; Fang, Y.; Cong, Q.; Ren, L., Anisotropism of the non-smooth surface of butterfly wing. *J. Bionic Eng.* **2009,** *6*, 71-76.

32. Gorb, S. N., Biological attachment devices: exploring nature's diversity for biomimetics. *Phil. Trans. R. Soc. A.* **2008,** *366*, 1557-1574.

33. Neinhuis, C.; Barthlott, W., Characterization and distribution of water-repellent, self-cleaning plant surfaces. *Ann. Bot.* **1997,** *79*, 667-677.

34. Yan, Y.; Gao, N.; Barthlott, W., Mimicking natural superhydrophobic surfaces and grasping the wetting process: A review on recent progress in preparing superhydrophobic surfaces. *Adv. Colloid Interface Sci.* **2011,** *169*, 80-105.

35. Guo, Z.; Liu, W., Biomimic from the superhydrophobic plant leaves in nature: Binary structure and unitary structure. *Plant Sci.* **2007,** *172*, 1103-1112.

36. Barthlott, W.; Neinhuis, C.; Cutler, D.; Ditsch, F.; Meusel, I.; Theisen, I.; Wilhelmi, H., Classification and terminology of plant epicuticular waxes. *Bot. J. Linn. Soc.* **1998,** *126*, 237-260.

37. Lee, S. M.; Kwon, T. H., Effects of intrinsic hydrophobicity on wettability of polymer replicas of a superhydrophobic lotus leaf. *J. Micromech. Microeng.* **2007,** *17*, 687.

38. Hüger, E.; Rothe, H.; Frant, M.; Grohmann, S.; Hildebrand, G.; Liefeith, K., Atomic force microscopy and thermodynamics on taro, a self-cleaning plant leaf. *Appl. Phys. Lett.* **2009,** *95*, 033702.

39. Feng, X.; Jiang, L., Design and creation of superwetting/antiwetting surfaces. *Adv. Mater.* **2006,** *18*, 3063-3078.

40. Feng, X.-Q.; Gao, X.; Wu, Z.; Jiang, L.; Zheng, Q.-S., Superior water repellency of water strider legs with hierarchical structures: experiments and analysis. *Langmuir* **2007,** *23*, 4892-4896.

41. Fang, Y.; Sun, G.; Wang, T.; Cong, Q.; Ren, L., Hydrophobicity mechanism of non-smooth pattern on surface of butterfly wing. *Chin. Sci. Bull.* **2007,** *52,* 711-716.

42. Gao, H.; Wang, X.; Yao, H.; Gorb, S.; Arzt, E., Mechanics of hierarchical adhesion structures of geckos. *Mech. Mater.* **2005,** *37*, 275-285.

43. Liu, K.; Du, J.; Wu, J.; Jiang, L., Superhydrophobic gecko feet with high adhesive forces towards water and their bio-inspired materials. *Nanoscale* **2012,** *4*, 768-772.

44. Nosonovsky, M.; Bhushan, B., Multiscale friction mechanisms and hierarchical surfaces in nano-and bio-tribology. *Mater. Sci. Eng. R. Rep.* **2007,** *58*, 162-193.

45. Byun, D.; Hong, J.; Ko, J. H.; Lee, Y. J.; Park, H. C.; Byun, B. K.; Lukes, J. R., Wetting characteristics of insect wing surfaces. *J. Bionic Eng.* **2009,** *6*, 63-70.

46. Byun, D.; Hong, J.; Saputra; Ko, J. H.; Lee, Y. J.; Park, H. C.; Byun, B.-K.; Lukes, J. R., Wetting Characteristics of Insect Wing Surfaces. *J. Bionic Eng.* **2009,** *6*, 63-70.

47. Feng, L.; Zhang, Y.; Xi, J.; Zhu, Y.; Wang, N.; Xia, F.; Jiang, L., Petal effect: a superhydrophobic state with high adhesive force. *Langmuir* **2008,** *24*, 4114-4119.

48. Chen, H.; Yuan, Z.; Zhang, J.; Liu, Y.; Li, K.; Zhao, D.; Li, S.; Shi, P.; Tang, J., Preparation, characterization and wettability of porous superhydrophobic poly (vinyl chloride) surface. *J. Porous Mat.* **2009,** *16*, 447-451.

49. Kwon, Y.; Patankar, N.; Choi, J.; Lee, J., Design of surface hierarchy for extreme hydrophobicity. *Langmuir* **2009,** *25*, 6129-6136.

50. Chen, M. H.; Hsu, T. H.; Chuang, Y. J.; Tseng, F. G., Dual hierarchical biomimic superhydrophobic surface with three energy states. *Appl. Phys. Lett.* **2009,** *95*, 023702.

51. Steinberger, A.; Cottin-Bizonne, C.; Kleimann, P.; Charlaix, E., High friction on a bubble mattress. *Nat. Mater.* **2007,** *6*, 665-668.

52. Shi, F.; Liu, Z.; Wu, G. L.; Zhang, M.; Chen, H.; Wang, Z.; Zhang, X.; Willner, I., Surface imprinting in layer-by-layer nanostructured films. *Adv. Funct. Mater*. **2007,** *17*, 1821-1827.

53. Lai, Y.; Lin, C.; Wang, H.; Huang, J.; Zhuang, H.; Sun, L., Superhydrophilic-superhydrophobic micropattern on TiO2 nanotube films by photocatalytic lithography. *Electrochem. Commun.* **2008,** *10*, 387-391.

54. Manca, M.; Cortese, B.; Viola, I.; Aricò, A. S.; Cingolani, R.; Gigli, G., Influence of chemistry and topology effects on superhydrophobic CF4-plasma-treated poly (dimethylsiloxane)(PDMS). *Langmuir* **2008,** *24*, 1833-1843.

55. Tsougeni, K.; Papageorgiou, D.; Tserepi, A.; Gogolides, E., "Smart" polymeric microfluidics fabricated by plasma processing: controlled wetting, capillary filling and hydrophobic valving. *Lab Chip.* **2010,** *10*, 462-469.

56. Jung, Y. C.; Bhushan, B., Mechanically durable carbon nanotube-composite hierarchical structures with superhydrophobicity, self-cleaning, and low-drag. *ACS Nano* **2009,** *3*, 4155-4163.

57. Journet, C.; Moulinet, S.; Ybert, C.; Purcell, S. T.; Bocquet, L., Contact angle measurements on superhydrophobic carbon nanotube forests: effect of fluid pressure. *EPL-Europhys. Lett.* **2005,** *71*, 104.

58. Balu, B.; Breedveld, V.; Hess, D. W., Fabrication of "roll-off" and "sticky" superhydrophobic cellulose surfaces via plasma processing. *Langmuir* **2008,** *24*, 4785-4790.

59. Miyahara, Y.; Mitamura, K.; Saito, N.; Takai, O., Fabrication of microtemplates for the control of bacterial immobilization. *J. Vac. Sci. Technol., A* **2009,** *27*, 1183-1187.

60. Milella, A.; Di Mundo, R.; Palumbo, F.; Favia, P.; Fracassi, F.; d'Agostino, R., Plasma nanostructuring of polymers: different routes to superhydrophobicity. *Plasma Processes Polym.* **2009,** *6*, 460-466.

61. Chen, W.; McCarthy, T. J., Layer-by-layer deposition: a tool for polymer surface modification. *Macromolecules* **1997,** *30*, 78-86.

62. Soeno, T.; Inokuchi, K.; Shiratori, S., Ultra-water-repellent surface: fabrication of complicated structure of SiO2 nanoparticles by electrostatic self-assembled films. *Appl. Surf. Sci.* **2004,** *237*, 539-543.

63. Bravo, J.; Zhai, L.; Wu, Z.; Cohen, R. E.; Rubner, M. F., Transparent superhydrophobic films based on silica nanoparticles. *Langmuir* **2007,** *23*, 7293-7298.

64. Cebeci, F. Ç.; Wu, Z.; Zhai, L.; Cohen, R. E.; Rubner, M. F., Nanoporosity-driven superhydrophilicity: a means to create multifunctional antifogging coatings. *Langmuir* **2006,** *22*, 2856-2862.

65. Zhai, L.; Cebeci, F. C.; Cohen, R. E.; Rubner, M. F., Stable superhydrophobic coatings from polyelectrolyte multilayers. *Nano Lett.* **2004,** *4*, 1349-1353.

66. Chunder, A.; Etcheverry, K.; Londe, G.; Cho, H. J.; Zhai, L., Conformal switchable superhydrophobic/hydrophilic surfaces for microscale flow control. *Colloids Surf., A* **2009,** *333*, 187-193.

67. Jindasuwan, S.; Nimittrakoolchai, O.; Sujaridworakun, P.; Jinawath, S.; Supothina, S., Surface characteristics of water-repellent polyelectrolyte multilayer films containing various silica contents. *Thin Solid Films* **2009,** *517*, 5001-5005.

68. Ma, M.; Hill, R. M.; Lowery, J. L.; Fridrikh, S. V.; Rutledge, G. C., Electrospun poly (styrene-block-dimethylsiloxane) block copolymer fibers exhibiting superhydrophobicity. *Langmuir* **2005,** *21*, 5549-5554.

69. Zhu, M.; Zuo, W.; Yu, H.; Yang, W.; Chen, Y., Superhydrophobic surface directly created by electrospinning based on hydrophilic material. *J. Mater. Sci.* **2006,** *41*, 3793-3797.

70. Wang, N.; Zhao, Y.; Jiang, L., Low-cost, thermoresponsive wettability of surfaces: poly (N-isopropylacrylamide)/polystyrene composite films prepared by electrospinning. *Macromol. Rapid Commun.* **2008,** *29*, 485-489.

71. Jung, Y. C.; Bhushan, B., Dynamic effects induced transition of droplets on biomimetic superhydrophobic surfaces. *Langmuir* **2009,** *25*, 9208-9218.

72. Reyssat, M.; Quéré, D., Contact angle hysteresis generated by strong dilute defects. *J. Phys. Chem. B* **2009,** *113*, 3906-3909.

73. Choi, Y. W.; Han, J. E.; Lee, S.; Sohn, D., Preparation of a superhydrophobic film with UV imprinting technology. *Macromol. Res.* **2009,** *17*, 821-824.

74. Wong, T. S.; Huang, A. P. H.; Ho, C. M., Wetting behaviors of individual nanostructures. *Langmuir* **2009,** *25*, 6599-6603.

75. Wang, J.; Zheng, Z.; Li, H.; Huck, W.; Sirringhaus, H., Dewetting of conducting polymer inkjet droplets on patterned surfaces. *Nat. Mater.* **2004,** *3*, 171-176.

76. Fürstner, R.; Barthlott, W.; Neinhuis, C.; Walzel, P., Wetting and self-cleaning properties of artificial superhydrophobic surfaces. *Langmuir* **2005,** *21*, 956-961.

77. Zhang, X.; Zhang, J.; Ren, Z.; Li, X.; Zhang, X.; Zhu, D.; Wang, T.; Tian, T.; Yang, B., Morphology and wettability control of silicon cone arrays using colloidal lithography. *Langmuir* **2009,** *25*, 7375-7382.

78. Hou, W.; Wang, Q., Stable polytetrafluoroethylene superhydrophobic surface with lotus-leaf structure. *J. Colloid Interface Sci.* **2009,** *333*, 400-403.

79. Sato, O.; Kubo, S.; Gu, Z. Z., Structural color films with lotus effects, superhydrophilicity, and tunable stop-bands. *Acc. Chem. Res.* **2008,** *42*, 1-10.

80. Cho, W. K.; Choi, I. S., Fabrication of hairy polymeric films inspired by geckos: wetting and high adhesion properties. *Adv. Funct. Mater.* **2008,** *18*, 1089-1096.

81. Yuan, Z.; Chen, H.; Tang, J.; Gong, H.; Liu, Y.; Wang, Z.; Shi, P.; Zhang, J.; Chen, X., A novel preparation of polystyrene film with a superhydrophobic surface using a template method. *J. Phys. D Appl. Phys.* **2007,** *40*, 3485.

82. Berendsen, C. W.; Škereň, M.; Najdek, D.; Černý, F., Superhydrophobic surface structures in thermoplastic polymers by interference lithography and thermal imprinting. *Appl. Surf. Sci.* **2009,** *255*, 9305-9310.

83. Lee, S. M.; Jung, I. D.; Ko, J. S., The effect of the surface wettability of nanoprotrusions formed on network-type microstructures. *J. Micromech. Microeng.* **2008,** *18*, 125007.

84. Long, C. J.; Schumacher, J. F.; Brennan, A. B., Potential for tunable static and dynamic contact angle anisotropy on gradient microscale patterned topographies. *Langmuir* **2009,** *25*, 12982-12989.

85. Lim, H.; Jung, D. H.; Noh, J. H.; Choi, G. R.; Kim, W. D., Simple nanofabrication of a superhydrophobic and transparent biomimetic surface. *Chin. Sci. Bull.* **2009,** *54*, 3613-3616.

86. Choi, C. H.; Ulmanella, U.; Kim, J.; Ho, C. M.; Kim, C. J., Effective slip and friction reduction in nanograted superhydrophobic microchannels. *Phys. Fluids* **2006,** *18*, 087105.

87. Song, W.; Veiga, D. D.; Custódio, C. A.; Mano, J. F., Bioinspired degradable substrates with extreme wettability properties. *Adv. Mater.* **2009,** *21*, 1830-1834.

88. Ji, Y. Y.; Kim, S. S.; Kwon, O. P.; Lee, S. H., Easy fabrication of large-size superhydrophobic surfaces by atmospheric pressure plasma polymerization with

non-polar aromatic hydrocarbon in an in-line process. *Appl. Surf. Sci.* **2009,** *255*, 4575-4578.

89. Lee, S. M.; Oh, D. J.; Jung, I. D.; Bae, K. M.; Jung, P. G.; Chung, K. H.; Cho, S. J.; Ko, J. S., Fabrication of nickel micromesh sheets and evaluation of their water-repellent and water-proof abilities. *Int. J. Precis. Eng. Manuf.* **2009,** *10*, 161-166.

90. Byun, D.; Lee, Y.; Tran, S. B. Q.; Nugyen, V. D.; Kim, S.; Park, B.; Lee, S.; Inamdar, N.; Bau, H. H., Electrospray on superhydrophobic nozzles treated with argon and oxygen plasma. *Appl. Phys. Lett.* **2008,** *92*, 093507.

91. Intranuovo, F.; Sardella, E.; Rossini, P.; d'Agostino, R.; Favia, P., PECVD of fluorocarbon coatings from hexafluoropropylene oxide: glow vs. afterglow. *Chem. Vapor Depos.* **2009,** *15*, 95-100.

92. Han, Z.; Tay, B.; Shakerzadeh, M.; Ostrikov, K., Superhydrophobic amorphous carbon/carbon nanotube nanocomposites. *Appl. Phys. Lett.* **2009,** *94*, 223106.

93. Sun, C.; Ge, L. Q.; Gu, Z. Z., Fabrication of super-hydrophobic film with dual-size roughness by silica sphere assembly. *Thin Solid Films* **2007,** *515*, 4686-4690.

94. Zhao, Y.; Li, M.; Lu, Q.; Shi, Z., Superhydrophobic polyimide films with a hierarchical topography: combined replica molding and layer-by-layer assembly. *Langmuir* **2008,** *24*, 12651-12657.

95. Hsieh, C. T.; Chen, W. Y.; Wu, F. L.; Shen, Y. S., Fabrication and superhydrophobic behavior of fluorinated silica nanosphere arrays. *J. Adhes. Sci. Technol.* **2008,** *22*, 265-275.

96. Min, W. L.; Jiang, P.; Jiang, B., Large-scale assembly of colloidal nanoparticles and fabrication of periodic subwavelength structures. *Nanotechnol.* **2008,** *19,* 475604.

97. Zhu, Y.; Li, J.; Wan, M.; Jiang, L., Superhydrophobic 3D microstructures assembled from 1D nanofibers of polyaniline. *Macromol. Rapid Commun.* **2008,** *29,* 239-243.

98. Shen, Y.; Wang, J.; Kuhlmann, U.; Hildebrandt, P.; Ariga, K.; Möhwald, H.; Kurth, D. G.; Nakanishi, T., Supramolecular templates for nanoflake-metal Surfaces. *Chem. Eur. J.* **2009,** *15,* 2763-2767.

99. Mahltig, B.; Böttcher, H., Modified silica sol coatings for water-repellent textiles. *J. Sol-Gel Sci. Technol.* **2003,** *27,* 43-52.

100. Shirtcliffe, N.; McHale, G.; Newton, M.; Perry, C., Intrinsically superhydrophobic organosilica sol-gel foams. *Langmuir* **2003,** *19,* 5626-5631.

101. Pilotek, S.; Schmidt, H. K., Wettability of microstructured hydrophobic sol-gel coatings. *J. Sol-Gel Sci. Technol.* **2003,** *26,* 789-792.

102. Yu, M.; Gu, G.; Meng, W. D.; Qing, F. L., Superhydrophobic cotton fabric coating based on a complex layer of silica nanoparticles and perfluorooctylated quaternary ammonium silane coupling agent. *Appl. Surf. Sci.* **2007,** *253,* 3669-3673.

103. Sheen, Y. C.; Chang, W. H.; Chen, W. C.; Chang, Y. H.; Huang, Y. C.; Chang, F. C., Non-fluorinated superamphiphobic surfaces through sol-gel processing of methyltriethoxysilane and tetraethoxysilane. *Mater. Chem. Phys.* **2009,** *114,* 63-68.

104. Shang, H.; Wang, Y.; Limmer, S.; Chou, T.; Takahashi, K.; Cao, G., Optically transparent superhydrophobic silica-based films. *Thin Solid Films* **2005,** *472*, 37-43.

105. Xiu, Y.; Xiao, F.; Hess, D. W.; Wong, C., Superhydrophobic optically transparent silica films formed with a eutectic liquid. *Thin Solid Films* **2009,** *517*, 1610-1615.

106. Tadanaga, K.; Kitamuro, K.; Matsuda, A.; Minami, T., Formation of superhydrophobic alumina coating films with high transparency on polymer substrates by the sol-gel method. *J. Sol-Gel Sci. Technol.* **2003,** *26*, 705-708.

107. Rao, A. V.; Latthe, S. S.; Nadargi, D. Y.; Hirashima, H.; Ganesan, V., Preparation of MTMS based transparent superhydrophobic silica films by sol-gel method. *J. Colloid Interface Sci.* **2009,** *332*, 484-490.

108. Tuteja, A.; Choi, W.; Ma, M.; Mabry, J. M.; Mazzella, S. A.; Rutledge, G. C.; McKinley, G. H.; Cohen, R. E., Designing superoleophobic surfaces. *Science* **2007,** *318*, 1618-1622.

109. Mizukoshi, T.; Matsumoto, H.; Minagawa, M.; Tanioka, A., Control over wettability of textured surfaces by electrospray deposition. *J. Appl. Polym. Sci.* **2007,** *103*, 3811-3817.

110. Zheng, J.; He, A.; Li, J.; Xu, J.; Han, C. C., Studies on the controlled morphology and wettability of polystyrene surfaces by electrospinning or electrospraying. *Polymer* **2006,** *47*, 7095-7102.

111. Ding, B.; Ogawa, T.; Kim, J.; Fujimoto, K.; Shiratori, S., Fabrication of a super-hydrophobic nanofibrous zinc oxide film surface by electrospinning. *Thin Solid Films* **2008,** *516*, 2495-2501.

112. Han, D.; Steckl, A. J., Superhydrophobic and oleophobic fibers by coaxial electrospinning. *Langmuir* **2009,** *25*, 9454-9462.

113. Li, X.; Ding, B.; Lin, J.; Yu, J.; Sun, G., Enhanced mechanical properties of superhydrophobic microfibrous polystyrene mats via polyamide 6 nanofibers. *J. Phys. Chem. C* **2009,** *113*, 20452-20457.

114. Burkarter, E.; Saul, C. K.; Thomazi, F.; Cruz, N. C.; Zanata, S. M.; Roman, L. S.; Schreiner, W. H., Electrosprayed superhydrophobic PTFE: a non-contaminating surface. *J. Phys. D Appl. Phys.* **2007,** *40*, 7778.

115. Xie, Y.; Hill, C. A.; Xiao, Z.; Militz, H.; Mai, C., Silane coupling agents used for natural fiber/polymer composites: A review. *Compos Part A Appl Sci Manuf.* **2010,** *41*, 806-819.

116. Plueddemann, E. P., Nature of adhesion through silane coupling agents. In *Silane Coupling Agents*, Springer1991, US; pp 115-152.

117. Hertl, W., Mechanism of gaseous siloxane reaction with silica. I. *J. Phys. Chem.* **1968,** *72*, 1248-1253.

118. Krasnoslobodtsev, A. V.; Smirnov, S. N., Effect of water on silanization of silica by trimethoxysilanes. *Langmuir* **2002,** *18*, 3181-3184.

119. Arkles, B., Silane coupling agents: connecting across boundaries. *Gelest Inc., Morrisville* **2004**, 1-5.

120. Arkles, B., Tailoring surfaces with silanes. *Chemtech* **1977,** *7*, 766-778.

121. García, N.; Benito, E.; Guzmán, J.; Tiemblo, P., Use of p-toluenesulfonic acid for the controlled grafting of alkoxysilanes onto silanol containing surfaces:

preparation of tunable hydrophilic, hydrophobic, and super-hydrophobic silica. *J. Am. Chem. Soc.* **2007,** *129*, 5052-5060.

122. Simpson, J. T.; D'urso, B. R., Superhydrophobic diatomaceous earth. U.S. Patent No. 8,216,6742012.

123. Oliveira, N. M.; Reis, R. L.; Mano, J. F., Superhydrophobic surfaces engineered using diatomaceous earth. *ACS Appl. Mater. Interfaces* **2013,** *5*, 4202-4208.

124. Puretskiy, N.; Chanda, J.; Stoychev, G.; Synytska, A.; Ionov, L., Anti-icing superhydrophobic surfaces based on core-shell fossil particles. *Adv. Mater. Interfaces* **2015,** *2*, 1500124-1500131.

125. Polizos, G.; Winter, K.; Lance, M. J.; Meyer, H. M.; Armstrong, B. L.; Schaeffer, D. A.; Simpson, J. T.; Hunter, S. R.; Datskos, P. G., Scalable superhydrophobic coatings based on fluorinated diatomaceous earth: Abrasion resistance versus particle geometry. *Appl. Surf. Sci.* **2014,** *292*, 563-569.

126. Nine, M. J.; Cole, M. A.; Johnson, L.; Tran, D. N.; Losic, D., Robust superhydrophobic graphene-based composite coatings with self-cleaning and corrosion barrier properties. *ACS Appl. Mater. Interfaces* **2015,** *7*, 28482-28493.

127. Sedai, B. R.; Khatiwada, B. K.; Mortazavian, H.; Blum, F. D., Development of superhydrophobicity in fluorosilane-treated diatomaceous earth polymer coatings. *Appl. Surf. Sci.* **2016,** *386*, 178-186.

128. Perera, H. J.; Khatiwada, B. K.; Paul, A.; Mortazavian, H.; Blum, F. D., Superhydrophobic surfaces with silane-treated diatomaceous earth/resin systems. *J. Appl. Polym. Sci.* **2016,** *133*, 44072-44081.

129. Haines, P. J., *Principles of thermal analysis and calorimetry*. Royal Society of Chemistry2002.

130. Stuart, B., *Infrared spectroscopy*. Wiley Online Library 2005.

131. Buffeteau, T.; Desbat, B.; Eyquem, D., Attenuated total reflection Fourier transform infrared microspectroscopy: Theory and application to polymer samples. *Vib. Spectrosc.* **1996,** *11*, 29-36.

132. Brunauer, S.; Emmett, P. H.; Teller, E., Adsorption of gases in multimolecular layers. *J. Am. Chem. Soc.* **1938,** *60*, 309-319.

133. Syvitski, J. P. M., *Principles, methods, and application of particle size analysis*. Cambridge University Press: Cambridge; New York, 1991.

134. Pugh, R. S.; McCave, I. N., Particle size measurement of diatoms with inference of their properties: comparison of three techniques. *J. Sediment. Res.* **2011,** *81*, 600-610.

135. Thoroppady Kittu, A., Surface energy characteristics of granite and limestone aggregates with respect to 2D and 3D surface roughness measurements. **2013**.

CHAPTER III

DEVELOPMENT OF SUPERHYDROPHOBICITY IN FLUOROSILANE-TREATED DIATOMACEOUS EARTH POLYMER COATINGS

Note: This chapter was published on *Applied Surface Science* **2016,** *386*, 178-186. DOI: 10.1016/j.apsusc.2016.06.009, and reprinted with permission from Applied Surface Science.

Bhishma R. Sedai[a], Bal K. Khatiwada[a,b], Hamid Mortazavian[a], and Frank D. Blum[a]*

[a]Department of Chemistry, Oklahoma State University, Stillwater, Oklahoma, 74078, USA

[b]Department of Chemistry, University of the Ozarks, Clarksville, Arkansas, 72830, USA

*Corresponding author: Frank D. Blum, fblum@okstate.edu

3.1. ABSTRACT

Superhydrophobic coatings were prepared using 3-(heptafluoroisopropoxy)-propyl-trimethoxy-silane (HFIP-TMS) treated diatomaceous earth (DE) particles with high molecular mass polystyrene or poly(vinyl acetate) as polymer binders. DE is a highly hydrophilic material and treatment of the DE with HFIP-TMS turned it into superhydro-

phobic diatomaceous earth (HFIP-DE). Thermogravimetric analysis (TGA) was used to determine the amount of grafted fluorosilane on the surface of the DE particles. The results showed that approximately 1.8% of HFIP-TMS grafted onto the surface of DE particles resulted in superhydrophobicity with contact angles as high as 164° for the particles themselves and also in coatings. Fourier transformed infrared spectroscopy (FTIR) was used to confirm the presence of HFIP-TMS on the surface of DE particles. The development of the hydrophobicity in the coatings with either polystyrene (PS) or poly(vinyl acetate) (PVAc) as binders was followed as a function of the particle loading using contact angle measurements and scanning electron microscopy. It was found that for these model DE-binder systems, the contact angles of the coatings were independent of the polymers used as long as the particle loading was greater than a minimum amount (~40% treated DE particles). It was also found that more treated DE particles moved to the air interface as the particle loadings in the coatings increased and then leveled off.

3.2. INTRODUCTION

Superhydrophobic surfaces are those surfaces that have a water contact angle greater than 150° and a sliding angle no more than 10°.[1-3] Such surfaces have received much attention recently because of their potential in industrial and biological applications, such as self-cleaning materials, anti-adhesives and corrosion-free coatings.[4] The superhydrophobicity of a surface depends on its surface energy and surface morphology.[5] The models of Wenzel and Cassie-Baxter revealed that suitable surface roughness and low-surface-energy materials are important for achieving self-cleaning.[6-8] Generally, there are two different approaches to achieve superhydrophobicity, namely, enhancing

the roughness of a hydrophobic substrate or modifying a rough surface with lower surface energy molecules.[9]

To date, many efforts have been undertaken to obtain artificial superhydrophobic surfaces with self-cleaning characteristics. Techniques such as plasma etching,[10, 11] electrodeposition,[12, 13] electrohydrodynamics,[14] laser treatment,[15] sol-gel processing,[2] chemical etching,[16, 17] layer-by-layer (LbL) assembly[18] and LbL particle deposition have been used to make artificial superhydrophobic surfaces.[19] One of the most common methods to fabricate a superhydrophobic surface is modification of a rough surface with a self-assembled monolayer of low surface energy coupling agents.[20, 21] While a number of studies have successfully prepared superhydrophobic surfaces, most techniques are either expensive or lack the durability to be useful in commercial applications.

It is highly desirable to develop a facile and cost effective method for fabrication of superhydrophobic coatings. The cost of superhydrophobic coatings can be decreased by using commercially available materials and simple fabrication techniques. One of the materials with potential applications in superhydrophobic coatings can be skeletons from diatoms. Diatoms are unicellular microscopic plants and inhabit all aquatic and moist environments. The dimensions of amorphous silica skeletons range from about 1 to 500 μm, while the regular features like pores, channels, ridges, protuberances distributed on the frustules wall possess characteristic dimensions of 10 to 200 nm.[22-28] DE is an inexpensive and environmentally benign natural material with the micro- and nano-topography required for superhydrophobic surfaces. DE particles have been used in various applications. The variety of unique frustule architectures were attractive materials for optical,[29] mechanical,[30, 31] and transport properties.[32] DE has been modified in

different ways and treated DE has been used in the construction of advanced devices for light harvesting,[33] photonics,[34] molecular separation,[32] sensing,[35, 36] and drug delivery.[37-39] DE also have been used in photo-catalysis,[40, 41] synthesis of zeolite,[42] removal of dye,[43, 44] waste water treatment,[45, 46] cement production,[47] filtration,[48] nanotechnology,[49] chromatography,[50] and mostly as adsorbents.[51-56]

Very few studies have focused on surface modification of fossilized diatomaceous amorphous silica to extend their applications to superhydrophobic surfaces. Simpson and D'Urso demonstrated a procedure to develop superhydrophobic powder using DE. They made the surfaces of wood, plastic, glass, ceramic and metal substrates superhydrophobic by dipping, painting, or spraying methods.[57] Mano and coworkers produced superhydrophobic surfaces using DE and showed that the wettability of such surfaces was controlled by exposing the substrates to plasma treatment for specific times. They showed that the proposed strategy could be applied in substrates, such as glass and polystyrene.[58] Leonid and coworkers have used polymer-modified DE particles for the design of surfaces with superhydrophobic and ice-repellent properties.[59] Nine, et al. have reported robust superhydrophobic graphene and DE based composite coatings with self-cleaning and corrosion barrier properties.[60] Panos and coworkers have investigated the wetting properties and abrasion resistance of coatings based on superhydrophobic DE particles with different geometries and sizes.[61] However, as far as we know, there has not been a systematic study of the amount of fluorosilane required for preparing superhydrophobic surfaces using DE particles and also the amount of treated DE required to prepare superhydrophobic coatings using simple high molecular mass polymer solutions as binder systems.

In this work, we have used 3-(heptafluoroisopropoxy)propyltrimethoxysilane (HFIP-TMS) to treat DE particles and identified the minimum amount of HFIP-TMS required to make superhydrophobic surfaces. The fluorosilane treated DE particles (HFIP-DE) were used to prepare coatings with PS and PVAc binders. The development of superhydrophobicity with increasing amounts of treated DE was verified by contact angle measurements and scanning electron microscopy (SEM). Highly hydrophobic coatings prepared from DE and polymers may have important future practical applications.

3.3. MATERIALS AND METHODS

3.3.1. Materials

Untreated diatomaceous earth, Celtix DE, was obtained from Dry Surface Coatings (DSC) (Guthrie, OK). The specific surface area of the DE particles was determined to be 28 m^2/g using Brunner-Emmett-Teller (BET) methods on a NOVA 2200 (Quantachrome, Boynton Beach, FL). Polystyrene (PS) with number average molecular mass of 280,000 g/mol and *para*-toluenesufonic acid were obtained from SigmaAldrich (Saint Louis, MO). Poly(vinyl acetate) (PVAc) with molecular mass of 260,000 g/mol was purchased from Scientific Polymer Products, Inc.(Ontario, NY). 3-(heptafluoroisopropoxy)propyltrimethoxysilane (HFIP-TMS) was purchased from Gelest, Inc. (Morrisville, PA). Tetrahydrofuran (THF) was purchased from Fisher Scientific International Inc. (Pittsburgh, PA).

A series of treated DE samples were prepared in 25 ml plastic vials. Around 2 g of Celtix DE was placed in each vial and mixed with 20 mL of toluene. Approximately 1% of *para*-toluenesulfonic acid was added to the mixture.[62] Different amounts (0.01 to 1.0

mL) of HFIP-TMS were added to vials. The mixtures were heated to 50 °C and shaken in a mechanical shaker at 5000 rpm for 4 h. The samples were then centrifuged and the supernatants were discarded. The mixture in each vial was washed two times with 20 mL of hexane to remove excess of unreacted fluorosilane and the supernatant was discarded after centrifugation. The contents were then left overnight to dry in air. All samples were transferred to glass vials and heated to 140 °C for 4 h to remove the solvent and water. The treated DE samples for making coatings were prepared by scaling up the DE amounts to 20 g. The amounts of grafted fluorosilane coupling agents were determined by thermogravimetric analysis.

To measure the contact angles associated with the treated particles alone (in the absence of binder), a slurry made from treated DE was prepared by mixing 0.05 g of the treated DE in 0.5 mL of THF. The treated DE slurry (200 µL) in THF was used to coat a microscopic glass cover slip. The slurry was dried in air for 24 h to remove the excess solvent and water droplet contact angles were measured on the surface of treated DE.

Treated DE polymer coatings were prepared by mixing different amounts of HFIP-DE (0 to 70%) with high molecular mass PS or PVAc. The mixtures were dispersed in 3.5 mL THF solvent and were then shaken for 6 h at room temperature in a mechanical shaker. Aluminum pans (I.D. 5 cm x H 1.5 cm) were coated with 2 mL of the sample mixture, allowed to air dry, and used for contact angle measurements.

3.3.2. Characterization

The compositions of DE and fluorosilane coupling agent were analyzed by high-resolution thermogravimetric analysis (TA Q-50, TA instruments, New Castle, DE). The samples were heated with a rate of 20 °C/min from room temperature to 950 °C under 40 ml/min of continuous air flow.

The IR spectra of DE samples were collected using a Nicolet iS50 Spectrometer Thermo Scientific Inc. (Waltham, MA) equipped with a deuterated triglycine sulfate detector and a diamond crystal (45° angle) as an attenuated total reflection (ATR) accessory. Each sample was run using 64 scans versus the background that was also collected using 64 scans to generate a single beam spectrum at 4 cm^{-1} resolution in the range of 600 to 4000 cm^{-1}.

Scanning electron microscopy (SEM) was used to study the surface properties of DE/polymer coatings. The surface structure of the coatings was probed with an FEI Quanta 600 SEM with Evex EDS system (FEI, Hillsboro, OR). The SEM samples were prepared by mounting a piece of coating on an aluminum stub. Samples were then coated with a very thin layer of palladium/gold metal deposited using a MED 010 sputter coater (Balzers, Oberkochen, Germany) to make them conductive.

The water contact angle measurements were conducted using a home-built contact angle apparatus at ambient temperature.[63] The instrument had a moveable stage for the coated sample and the water droplet was added using a pipette. About 4 µL of water droplet was placed on the surface. Water droplet images were taken with a high-resolution Proscope camera capable of recoding 15 fps at a 640 × 480 resolution. The LB-ADSA technique was used to determine the contact angle of the water droplet images

on the surface.[64] The angle (θ) between the surface and the line tangent to the drop edge was measured using a drop analysis plugin in the ImageJ software. Three water droplet images were taken from different positions on the surfaces for each coating. The average contact angles for the coatings were plotted as a function of the amounts of grafted silane and treated DE in samples.

3.4. RESULTS

The amount of the grafted fluorosilane coupling agent in each sample was determined using TGA. The mass loss curves for DE and fluorosilane treated DE samples are shown in Fig. 3.1. The amount of fluorosilane coupling agent in the treated DE was obtained by subtracting result of the second mass loss (150 - 950 °C) of untreated DE from the second mass loss (150 - 950 °C) of treated DE.[49] The amount of fluorosilane in this particular sample shown in Figure 3b, based on the mass difference at 950 °C, was estimated to be 4.7%. For the type of DE sample used in this study, the adsorbed amount of fluorosilane was comparable to the amount added to the DE mixture, i.e., little material was washed off.

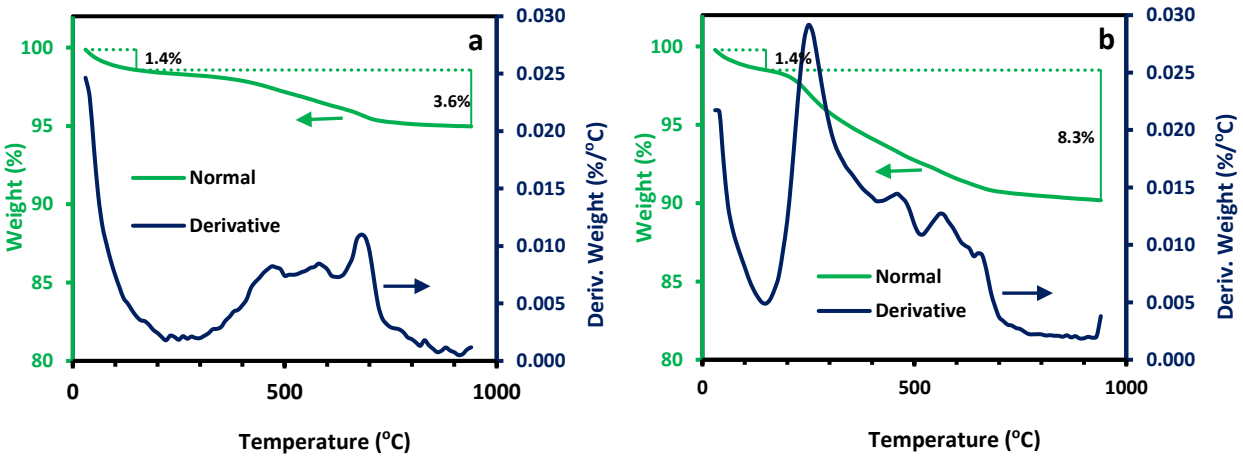

Fig. 3.1. TGA plots showing mass losses for (a) untreated and (b) treated DE in normal and derivative modes. Untreated and treated DE samples showed different decomposition patterns. The amounts of adsorbed coupling agents were determined by the differences between the mass losses of treated and untreated DE samples at 950 °C.

FTIR spectra of the DE samples were taken to confirm the grafting of silane coupling agent to the surface of DE particles. The IR spectra of untreated DE and HFIP-TMS treated DE samples are shown in two different regions, (2600 to 4000 cm^{-1} and 600 to 1600 cm^{-1}), for clarity, in Fig. 3.2. Two broad peaks in the range of 900 - 1300 cm^{-1} and 3000 - 3700 cm^{-1} were observed in both untreated and treated DE samples. Another intense peak was observed centered at 795 cm^{-1} in both samples. Additional peaks only found in treated DE samples were observed at 696, 732, 1200, 1328, 2934, 3624, and 3722 cm^{-1}.

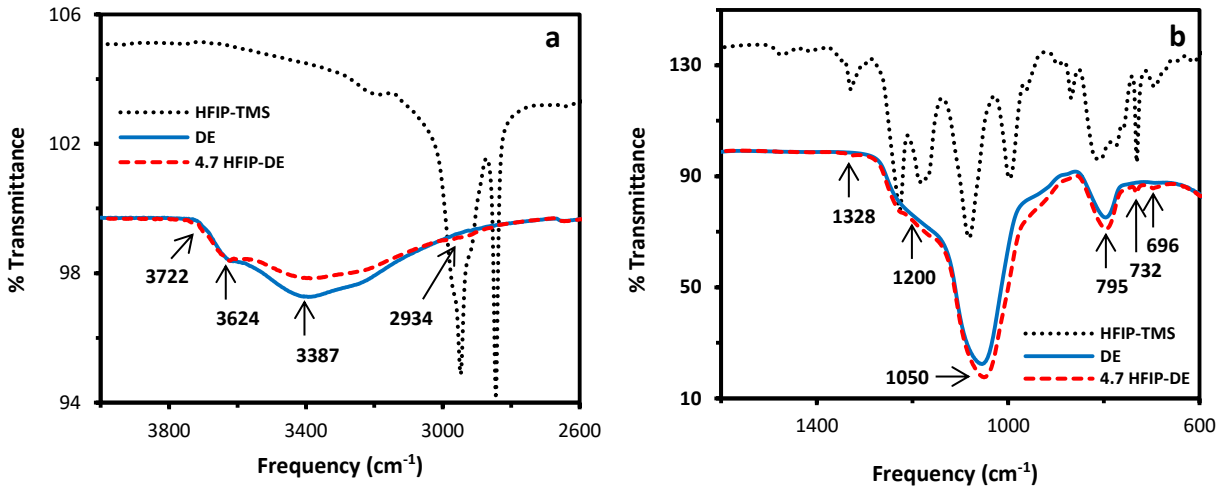

Fig. 3.2. FTIR spectra (ATR) of HFIP-TMS (black, upper), untreated DE (blue, lower in a and middle in b) and HFIP-TMS treated DE (red); a) 2600 – 4000 cm^{-1} range; b) 600 – 1600 cm^{-1} range. There was no difference in spectra in the range 1600 – 2600 cm^{-1}. The

Y-axis scale for HFIP-TMS spectrum (black, upper) was adjusted for comparison with other spectra.

A series of fluorosilane treated DE samples with different amounts of grafted HFIP-TMS were analyzed using TGA to calculate the adsorbed amount of fluorosilane on the surface. Then the water contact angle was measured for each sample for the bare particles without polymer binder. A plot of grafted amount of fluorosilane versus contact angle is shown in Fig. 3.3. The water contact angle increased with increasing amounts of grafted fluorosilane and then remained almost constant for grafted amounts larger than 2%. In this case, 2% fluorosilane corresponds to an average of 1.9 chains/nm^2 of DE surface.

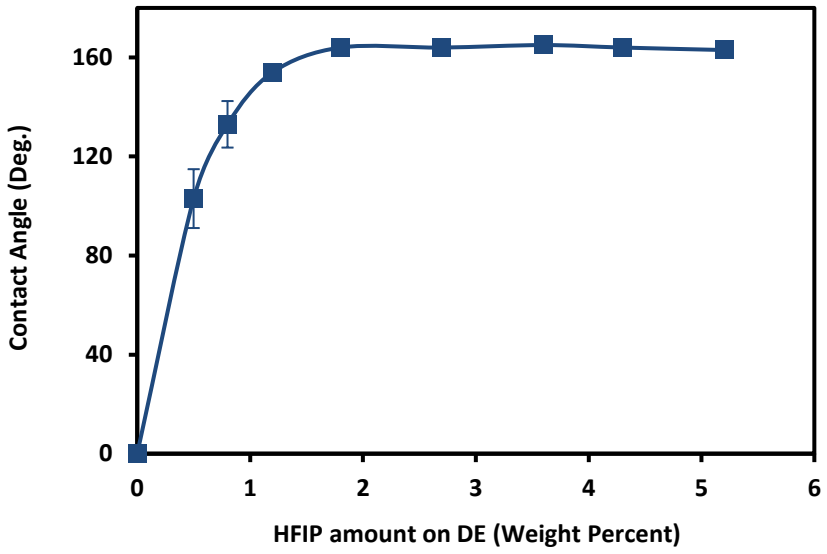

Fig. 3.3. Contact angle measurements of treated DE particles (alone) as a function of the amount of grafted fluorosilane on DE. The contact angle remained unchanged for samples with more than 2% mass fraction of coupling agent. In several cases, the

standard deviations of the measurements were smaller than the size of the symbols (between 0.4 to 1º).

SEM images of untreated Celtix DE particles at different magnifications were taken to observe their surface topography. Scanning electron micrographs of the untreated DE particles under high magnification are shown in Fig. 3.4. Intact DE particles have approximately 10 - 20 µm diameters as shown in Fig. 3.4a. The magnified view of a DE particle in Fig. 3.4b shows that the holes are of different shapes and sizes. The pores on the surfaces of the DE particles have diameters averaging about 250 nm.

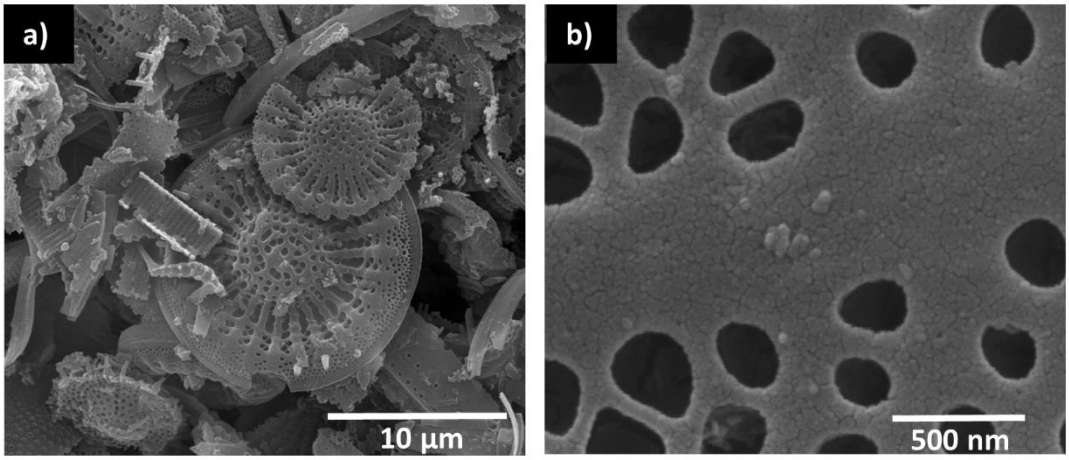

Fig. 3.4. SEM of DE particles under high resolution a) intact DE particles; the scale bar is 10 µm; b) magnified DE particle; the scale bar is 500 nm.

SEM images were taken to see the difference in the surface morphology of untreated and treated Celtix DE particles. SEM micrographs for untreated DE and treated DE with HFIP-TMS are shown in Fig. 3.5. The surface structures of both untreated and treated DE were found to be similar, which suggested that the structure of DE was largely preserved with the addition of fluorinated coupling agent.

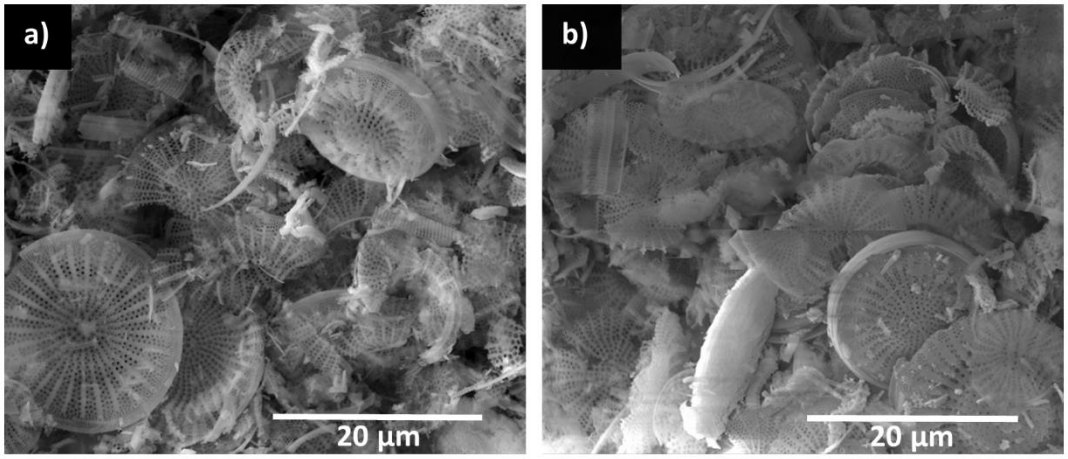

Fig. 3.5. SEM micrographs for a) untreated DE and b) treated DE; the scale bars are 20 µm. No significant difference was observed in morphology of untreated and treated DE surfaces.

SEM images of untreated DE and treated DE-polymer coatings were compared to observe the difference in their surface topography. Two coatings, one with untreated DE and one with treated DE were prepared and their SEM micrographs are shown in Fig. 3.6. The samples were made with polystyrene (50% by weight) binder and the treated DE contained 4.7% silane coupling agent (referred to as 4.7 HFIP-DE) to ensure superhydrophobic particles. In samples containing untreated DE, a mixture of DE and polymer was observed on the surface. Some particles were visible on the surface; however, they appeared to be largely covered by polymer. In contrast, there was no significant evidence of polymer on the surface in the coatings with treated DE.

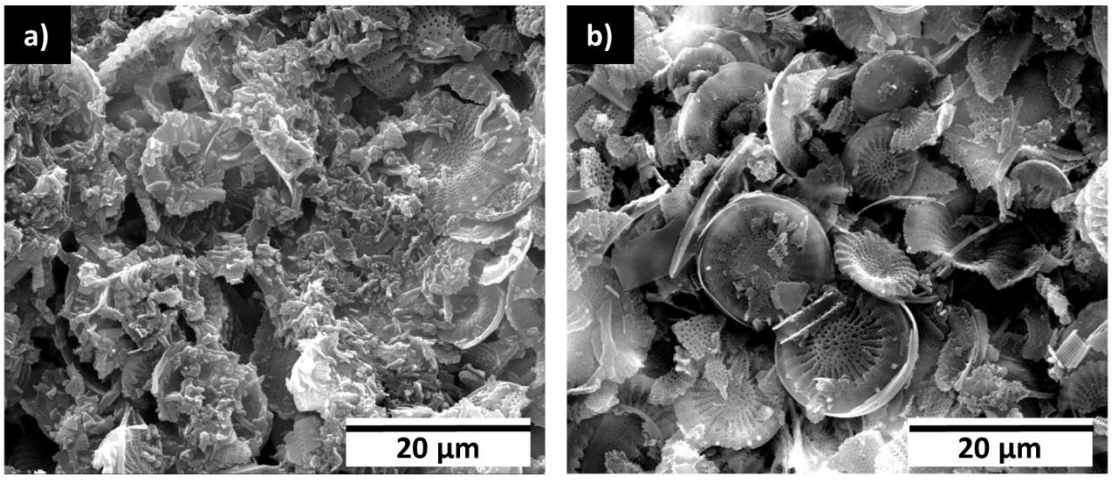

Fig. 3.6. SEM micrographs of top surfaces for coatings obtained from a) 50% untreated DE b) 50% treated DE with polystyrene as a binder; scale bars are 20 µm. The treated DE particles were more dominant on the surface than untreated DE particles. Similar results were observed in the PVAc binder system as well.

Surface topography of the high molecular mass PS with different loadings of 4.7 HFIP-DE particles were probed with SEM images and contact angle measurements. The water droplet and SEM images of the coating surfaces of samples with different amounts of treated DE (particle loadings) and PS as binder are shown in Fig. 3.7. The SEM micrographs showed that when a larger fraction of particles was included in the coatings, more DE particles were exposed on the surface. More particles resulted in enhanced hydrophobicity, leading to superhydrophobic surfaces. The largest contact angles of approximately 162° were achieved in this binder system when the composition of treated DE reached 40% or more. The SEM images and contact angle measurements on the surface of the coatings revealed that the coatings became superhydrophobic when the surface was completely covered with treated DE particles as in Fig 3.7d.

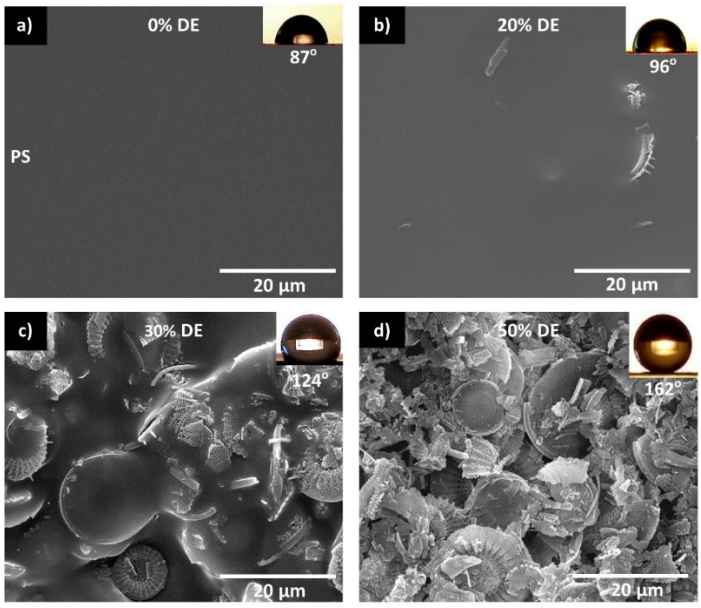

Fig. 3.7. SEM and water droplet images (insets) for PS samples with different particle loadings (amounts of 4.7 HFIP-DE): a) 0% b) 20% c) 30% and d) 50% DE with polystyrene binder. The scale bars are 20 µm.

The wetting behavior of PS and PVAc coatings with treated DE particles were investigated. The contact angles of the bulk polymers and treated DE coatings as a function of loading of the 4.7 HFIP-DE particles are shown in Fig. 3.8. The contact angles for the bulk PS and PVAc were 87° and 62°, respectively. The hydrophobicity increased with increased amounts of treated DE in the coatings. In both PS and PVAc binder systems, hydrophobic behavior of the coating surfaces increased gradually until about 40% of treated DE. There was no significant change in the contact angles (~162°) after 50% treated DE particles were included in the coatings for either system. Even though the two polymers had different contact angles for the bulk polymers, after about 40% of 4.7 HFIP-DE the contact angles were independent of the binder used.

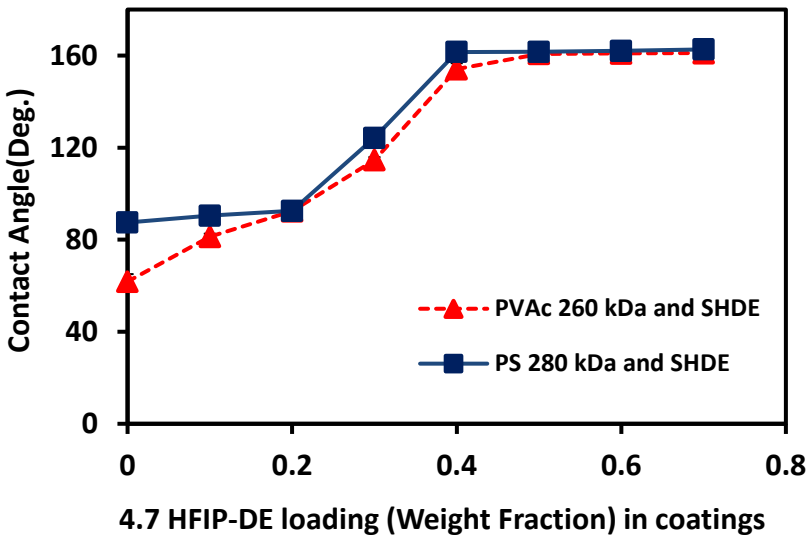

Fig. 3.8. Variation of contact angles with loading of 4.7 HFIP-DE particles loading in coatings prepared with PS and PVAc as binders. The contact angles increased with the mass fraction of treated DE and remained constant and similar for both systems at 50% mass fraction particles and beyond. The error bars are approximately the same size as the symbols.

The surface morphology of high molecular mass PVAc with different loadings of 4.7 HFIP-DE particles were analyzed by SEM images and contact angle measurements. The water droplets and SEM images of the coating surfaces prepared with treated DE and PVAc as the binder are shown in Fig. 3.9. These results indicated that the larger the percentage of the treated particles in the coatings, the more DE particles were exposed to the surface, and consequently, a larger contact angle was found. The highest contact angle of approximately 162° was achieved in this binder system when the composition of treated DE reached 40% or more. The SEM images and contact angle measurements on the surfaces of the coatings revealed that the coatings became superhydrophobic when the

surface was completely covered with treated DE particles, similar to the observations for PS surface.

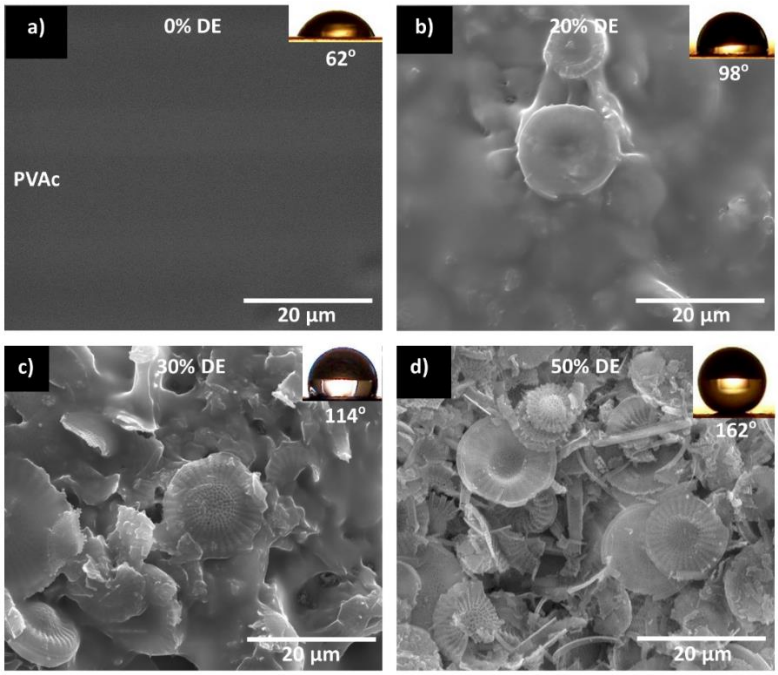

Fig. 3.9. SEM and water droplet images (insets) of coatings with varying particle loadings of: a) 0%; b) 20%; c) 30% and d) 50% treated 4.7 HFIP-DE particles with PVAc binder. The scale bars are 20 µm. The contact angle of water on the surfaces increased with the amount of treated DE on the surface, until about 40% particle loading, after which it was constant.

3.5. DISCUSSION

The TGA thermograms of untreated and treated DE particles showed mass losses in two different regions. The first mass loss, in the temperature range of 30 to 150 °C, in Fig. 3.1a and 3.1b was likely due to the loss of different types of physically-bound water

molecules and removal of some hydroxyl groups present in the silica surface of porous DE particles.[65] The second mass loss in the temperature range of 150 to 950 °C for untreated DE is expected due to the various inorganic substances present in DE particles. Natural frustules of DE contain several inorganic substances and the chemical analysis of DE has shown the main ingredients of SiO_2 (90.08%), Al_2O_3 (5.53%) and Fe_2O_3 (1.52%).[66, 67] The majority composition of SiO_2 means that the surface reactions of silica were likely active in our systems, including those of silane coupling agents.[68] The thermogram of DE treated with fluorosilane (Fig. 3.1b) showed a second mass loss (8.3%) in the temperature range of 150 to 950 °C. This mass loss was due to the decomposition of the fluorosilane plus the aforementioned inorganic substances in DE. The difference between the treated and untreated DE in the second mass loss represents the mass loss due to the fluorosilane coupling agent in the treated DE sample.

As expected, some differences between IR spectra of untreated DE and treated DE were observed. The IR spectra of untreated DE have previously been reported.[66, 69] The peaks centered at 1050 and 1200 cm^{-1} in Fig. 3.2 for untreated DE were assigned to the in-plane Si-O stretching mode. The intense peak at 795 cm^{-1} was due to symmetric Si-O stretching.[66] More intense peaks for the treated DE were observed at 1050 cm^{-1} and 1200 cm^{-1}, these peaks resulted from strong C-F symmetric and antisymmetric vibrations which indicated the presence of HFIP in the final product.[70] Additional peaks which exist only for treated DE at 696 cm^{-1} and 732 cm^{-1} were attributed to the vibration of C-F bond in polyfluorocarbon region of the fluorosilane.[71, 72] The spectrum of Celite DE shows only one broad band centered at approximately 3400 cm^{-1} in the hydroxyl region 3000 - 3750 cm^{-1} which is attributed to the -OH vibration of the physically adsorbed H_2O and -

OH from silanols of DE samples.[66] The IR spectrum of the HFIP-modified DE exhibits some new vibrations compared to those of the unmodified DE in Fig. 3.2, including CH_2 stretching (2934 cm^{-1}), and CH_2 deformation (1328 cm^{-1}). The decrease in the intensity of peaks for treated DE in the region 3000 – 3750 cm^{-1} is expected due to loss of some of the silanols –OH from the DE surface. Increased intensity of the peaks, at 1050 cm^{-1} and 795 cm^{-1} in treated DE as compared to untreated DE was considered due to the formation of new Si-O bonds in the treated samples between DE particles and silane coupling agent. The peaks at 3600-3750 cm^{-1} are attributed to the O-H stretching of the silanols in the hydrolyzed HFIP-TMS. These results confirm the success of the silane modification, i.e., the chemisorption of the coupling agent on the DE.

DE particles possess nano and meso-size pores[31, 32] and intact particles are a few microns in size. In treated DE particles, HFIP chains lower the surface energy of the particles and air remains trapped in the pores. Treated DE low energy surfaces interact with water through van der Waals forces. The wettability of such surfaces depend the outermost HFIP moieties, plus roughness present from the DE surface. The contact angles measured result from the DE particle surface asperities and air trapped (Cassie state) in the pores.[73]

Contact angle analysis of water droplets on the surface of treated DE particles with no binder, showed a rapid increased in hydrophobicity with increasing amounts of fluorosilane on the surface of DE particles (Fig. 3.3). The contact angles measured on the surface of the bare treated DE particles (prepared from the slurry in tetrahydrofuran) reached 163° with the grafted amount of fluorosilane of approximately 1.8%. The contact

angle remained constant at almost 164° with additional adsorbed silane. This result indicates that a relatively small amount of fluorosilane can result in a superhydrophobic surface.

The superhydrophobicity of the DE particles was the result of surface topography (DE) and the presence of low surface energy interfacial materials (fluorosilane). The leveling off of the contact angle at around 163° with adsorbed fluorosilane amount occurred because the surface of the particle, or perhaps more accurately, the surface of the adsorbed fluorosilane, was fairly constant above the minimum amount required (1.8%) for superhydrophobicity. It is known that silane coupling agents at moderate concentrations form oligomers after hydrolysis.[68] They then adsorb as oligomers and the structure of the oligomer away from the particle was roughly constant. Given the chemical structure of the fluorosilane used, a 2% fluorosilane-containing sample (2 molecules/nm^2) may roughly correspond to a fully covered DE surface.[68]

The SEM micrographs of DE particles under very high magnification (150,000 X) showed the presence of pores (Fig.3.4b). The pores in the DE particle have different shapes and sizes and are common to DE.[26, 34] These pores are in nanometer range with the average size of ~250 nm diameter. The treated DE coating surface SEM micrograph in Fig. 3.4a under 10,000 X magnification shows that the top surface of the coating was covered with both intact and broken pieces of DE particles. The intact DE particles have ~10-20 μm diameter. The presence of such particles on the surface contribute to surface roughness on the proper scales for superhydrophobicity. After about 40 – 50% of DE in coatings, the DE particles, without polymer, with micro- to nano-scale dimensions appear

on the surface and cover almost all the surface. Such micro- and nano-topography on the coating surface in combination with low surface energy coupling agent played important role in the development of superhydrophobicity in DE and polymer coatings.[49, 74-77]

Treated DE and untreated DE particles behaved differently in coatings prepared with polymer binders. The observation from SEM images, for coatings with 50% DE, in Fig. 3.6a (untreated DE) and Fig. 3.6b (treated DE) showed that for untreated DE/PS coatings, polymer coated particles (particles with clogged pores) were observed on the surface. In contrast, for treated DE and polymer coatings with PS, bare DE particles with open pores were observed. A similar situation was also found for coatings with PVAc. Untreated DE, without a low surface energy coating, did not move to the air interface. In these systems, the treated DE particles moved towards the air-surface interface and the top surface of the coating was completely covered with treated DE particles (Fig. 3.6b). The complete coverage of the surface with treated DE particles makes the surface superhydrophobic.

The observation of the top surface of coatings prepared from treated DE and with high molecular mass PS binder (Fig. 3.7) showed that the PS surface was flat and relatively featureless, as expected. Water droplet images on the surfaces of coatings without any DE (Fig. 3.7a) showed that coatings with bulk polystyrene had contact angle of 87°. With the addition of 20% treated DE, some SEM evidence of particles at the surface was found (Fig. 3.7b), but these particles were largely covered with polymer. The addition of more treated DE with (at 30%) resulted in more particles at the surface, but there was still a significant amount of polymer covering them (Fig. 3.7c). By 50% treated DE, the surface looked as if it was completely covered by particles with no polymer

covering their surface (Fig. 3.7d). The water contact angles of these surfaces were about 162° and the surfaces were superhydrophobic. In principle, a theoretical value of 180° for the contact angle would be found, however, DE is far from an ideal particle. As can be seen in the micrographs, the DE surfaces resulted in partial pieces of DE, pseudo-random orientations, the DE itself was somewhat non-uniform, and may not have the perfect configuration for superhydrophobicity. Consequently, due to the imperfections in the particle, perfect superhydrophobicity should not be expected. Water droplets did not stay on the surface and rolled off quickly. The water droplet images, SEM images and the contact angle values (Fig.3.7a-d) revealed that the presence of the treated DE on the surface was required to achieve superhydrophobicity. The contact angles increased with increasing fraction of treated DE and levelled off beyond 40% of treated DE particles in the coatings.

Behavior in the PVAc binder system with treated DE particles was observed in Fig. 3.9a-d and was similar to that in the PS system. The PVAc surface without treated DE particles showed a water droplet contact angle of 62° (Fig. 3.9a). As the percentage of treated DE increased, as shown in Fig. 3.9a-d, the surface topography also changed and water droplet images showed larger contact angles. In both binder systems, below 40% of treated DE particles in coatings, the hydrophobicity increased gradually with the fraction of particles introduced. After 50 % of treated DE particles in the coatings, the contact angles remained almost constant. These constant contact angles were also consistent with the SEM results (Fig.3.7d and 3.9d), where the surface morphology remained virtually unchanged after adding this amount of treated DE to coatings. The SEM images and the contact angles of the coatings with treated DE particles above 50%, particle loading

indicated that development of superhydrophobicity was independent of polymer used. The superhydrophobic surface from treated DE particles and polymer was easily obtained when the treated DE particles completely covered the surface of coatings.

These studies help to clarify under what conditions DE can be used to prepare superhydrophobic surfaces in a polymer-particle system. They demonstrate that a minimum amount of the fluorinated silane coupling agent needs to be on the particle and also that a minimum amount of treated particles need to be loaded in the coatings. In addition, this minimum loading needs to be such that the treated particles can move to the surface, for, in this case, a high molecular mass polymer binder system. It has not yet been demonstrated if transport to the surface is a factor in the determination of this minimum amount, but we have observed that particles are more likely to be found at the surface from more dilute binder solutions.

3.6. CONCLUSIONS

Diatomaceous earth treated with HFIP-TMS was used to prepare superhydrophobic coatings with polymeric binders. Superhydrophobic surfaces resulted when the amount of HFIP-TMS treated DE particles contained grafted silane amounts of 1.2% or more. Superhydrophobicity of the polymer coatings depended on the fraction of surface being covered with treated DE particles. DE particles having both micro and nano structures appeared on the top surface of the coating only when they were treated with the fluorinated silane coupling agent. With increasing the mass fraction of treated DE, the micro-nano hierarchical roughness also increased which made the coatings highly

hydrophobic. In the high molecular mass polymer solution binder systems, 40% or larger of treated 4.7 HFIP-DE particles in coatings made the surface superhydrophobic. The superhydrophobicity of the coated surface, after a certain minimum amount of treated DE particles on the surface, remained unchanged and was independent of the binder type.

Acknowledgement

The authors acknowledge the financial support of the Oklahoma State University, and Dry Surface Coatings (DSC), Guthrie, OK.

3.7. REFERENCES

1. Neinhuis, C.; Barthlott, W., Characterization and distribution of water-repellent, self-cleaning plant surfaces. *Ann. Bot.* **1997,** *79*, 667-677.
2. Nakajima, A.; Fujishima, A.; Hashimoto, K.; Watanabe, T., Preparation of transparent superhydrophobic boehmite and silica films by sublimation of aluminum acetylacetonate. *Adv. Mater.* **1999,** *11*, 1365-1368.
3. Zhang, X.; Shi, F.; Niu, J.; Jiang, Y.; Wang, Z., Superhydrophobic surfaces: from structural control to functional application. *J. Mater. Chem.* **2008,** *18*, 621-633.
4. Liu, H.; Szunerits, S.; Pisarek, M.; Xu, W.; Boukherroub, R., Preparation of superhydrophobic coatings on zinc, silicon, and steel by a solution-immersion technique. *ACS Appl. Mater. Interfaces* **2009,** *1*, 2086-2091.

5. Lundgren, M.; Allan, N. L.; Cosgrove, T., Modeling of wetting: a study of nanowetting at rough and heterogeneous surfaces. *Langmuir* **2007,** *23*, 1187-1194.

6. Cassie, A. B. D.; Baxter, S., Wettability of porous surfaces. *Trans. Faraday Soc.* **1944,** *40*, 546-551.

7. Wenzel, R. N., Resistance of solid surfaces to wetting by water. *Ind. Eng. Chem. Chem. Eng.* **1936,** *28*, 988-994.

8. Zheng, Y.; Zhang, W.; Gupta, M.; Kankanala, S.; Marks, C.; Carpenter, E.; Carroll, K.; Wynne, K. J., Poly (bis-2, 2, 2-trifluoroethoxymethyl oxetane): Multiple crystal phases, crystallization-induced surface topological complexity and enhanced hydrophobicity. *J. Polym. Sci., Part B: Polym. Phys.* **2010,** *48*, 1022-1034.

9. Feng, X. J.; Jiang, L., Design and creation of superwetting/antiwetting surfaces. *Adv. Mater.* **2006,** *18*, 3063-3078.

10. Minko, S.; Müller, M.; Motornov, M.; Nitschke, M.; Grundke, K.; Stamm, M., Two-level structured self-adaptive surfaces with reversibly tunable properties. *J. Am. Chem. Soc.* **2003,** *125*, 3896-3900.

11. Olde Riekerink, M.; Terlingen, J.; Engbers, G.; Feijen, J., Selective etching of semicrystalline polymers: CF4 gas plasma treatment of poly (ethylene). *Langmuir* **1999,** *15*, 4847-4856.

12. Shirtcliffe, N. J.; McHale, G.; Newton, M. I.; Perry, C. C., Wetting and wetting transitions on copper-based super-hydrophobic surfaces. *Langmuir* **2005,** *21*, 937-943.

13. Jennette, N. M.; Sukhada, S. K.; Lopamudra, D.; Saumil, B.; Gary, C. T.; Wynne, K. J.; Supriyo, B., Wetting behavior of polymer coated nanoporous anodic alumina

films: transition from super-hydrophilicity to super-hydrophobicity. *Nanotechnol.* **2011,** *22*, 35703-35713.

14. Zhao, Y.; Cao, X.; Jiang, L., Bio-mimic multichannel microtubes by a facile method. *J. Am. Chem. Soc.* **2007,** *129*, 764-765.

15. Khorasani, M.; Mirzadeh, H.; Kermani, Z., Wettability of porous polydimethylsiloxane surface: morphology study. *Appl. Surf. Sci.* **2005,** *242*, 339-345.

16. Thieme, M.; Frenzel, R.; Schmidt, S.; Simon, F.; Hennig, A.; Worch, H.; Lunkwitz, K.; Scharnweber, D., Generation of ultrahydrophobic properties of aluminium-a first step to self-cleaning transparently coated metal surfaces. *Adv. Eng. Mater.* **2001,** *3*, 691-695.

17. Qian, B.; Shen, Z., Fabrication of superhydrophobic surfaces by dislocation-selective chemical etching on aluminum, copper, and zinc substrates. *Langmuir* **2005,** *21*, 9007-9009.

18. Zhao, N.; Shi, F.; Wang, Z.; Zhang, X., Combining layer-by-layer assembly with electrodeposition of silver aggregates for fabricating superhydrophobic surfaces. *Langmuir* **2005,** *21*, 4713-4716.

19. Zhao, J.; Leng, B.; Shao, Z.; Ming, W., Triple-scale structured superhydrophobic and highly oleophobic surfaces. *RSC Adv.* **2013,** *3*, 22332-22339.

20. Shi, F.; Chen, X.; Wang, L.; Niu, J.; Yu, J.; Wang, Z.; Zhang, X., Roselike microstructures mormed by direct in situ hydrothermal synthesis: from superhydrophilicity to superhydrophobicity. *Chem. Mater.* **2005,** *17*, 6177-6180.

21. Gao, L.; McCarthy, T. J., A perfectly hydrophobic surface (θA/θR= 180/180). *J. Am. Chem. Soc.* **2006,** *128*, 9052-9053.

22. Lebeau, T.; Robert, J. M., Diatom cultivation and biotechnologically relevant products. Part I: Cultivation at various scales. *Appl. Microbiol. Biotechnol.* **2003,** *60*, 612-623.

23. Round, F. E.; Crawford, R. M.; Mann, D. G., *The diatoms: biology & morphology of the genera*. Cambridge University Press1990.

24. Martin-Jézéquel, V.; Hildebrand, M.; Brzezinski, M. A., Silicon metabolism in diatoms: implications for growth. *J. Phycol.* **2000,** *36*, 821-840.

25. Mann, S.; Ozin, G. A., Synthesis of inorganic materials with complex form. *Nature* **1996,** *382*, 313-318.

26. Crawford, S. A.; Higgins, M. J.; Mulvaney, P.; Wetherbee, R., Nanostructure of the diatom frustule as revealed by atomic force and scanning electron microscopy. *J. Phycol.* **2001,** *37*, 543-554.

27. Bäuerlein, E., Biomineralization of unicellular organisms: an unusual membrane biochemistry for the production of inorganic nano-and microstructures. *Angew. Chem. Int. Ed.* **2003,** *42*, 614-641.

28. Fuhrmann, T.; Landwehr, S.; Rharbi-Kucki, E.; Sumper, M., Diatoms as living photonic crystals. *Appl. Phys. B: Lasers Opt.* **2004,** *78*, 257-260.

29. Butcher, K.; Ferris, J.; Phillips, M.; Wintrebert-Fouquet, M.; Wah, J. J.; Jovanovic, N.; Vyverman, W.; Chepurnov, V., A luminescence study of porous diatoms. *Mater. Sci. Eng., C* **2005,** *25*, 658-663.

30. Hamm, C. E.; Merkel, R.; Springer, O.; Jurkojc, P.; Maier, C.; Prechtel, K.; Smetacek, V., Architecture and material properties of diatom shells provide effective mechanical protection. *Nature* **2003,** *421*, 841-843.

31. Losic, D.; Short, K.; Mitchell, J. G.; Lal, R.; Voelcker, N. H., AFM nanoindentations of diatom biosilica surfaces. *Langmuir* **2007,** *23*, 5014-5021.

32. Losic, D.; Rosengarten, G.; Mitchell, J. G.; Voelcker, N. H., Pore architecture of diatom frustules: potential nanostructured membranes for molecular and particle separations. *J. Nanosci. Nanotechnol.* **2006,** *6*, 982-989.

33. Toster, J.; Iyer, K. S.; Xiang, W.; Rosei, F.; Spiccia, L.; Raston, C. L., Diatom frustules as light traps enhance DSSC efficiency. *Nanoscale* **2013,** *5*, 873-876.

34. Fuhrmann, T.; Landwehr, S.; El Rharbi-Kucki, M.; Sumper, M., Diatoms as living photonic crystals. *Appl. Phys. B* **2004,** *78*, 257-260.

35. Rosi, N. L.; Thaxton, C. S.; Mirkin, C. A., Control of Nanoparticle Assembly by Using DNA-Modified Diatom Templates. *Angew. Chem. Int. Ed.* **2004,** *116*, 5616-5619.

36. De Stefano, L.; Rendina, I.; De Stefano, M.; Bismuto, A.; Maddalena, P., Marine diatoms as optical chemical sensors. *Appl. Phys. Lett.* **2005,** *87*, 233902.

37. Coradin, T.; Livage, J., Synthesis, characterization and diffusion properties of biomimetic silica-coated gelatine beads. *Mater. Sci. Eng., C* **2005,** *25*, 201-205.

38. Bariana, M.; Aw, M. S.; Losic, D., Tailoring morphological and interfacial properties of diatom silica microparticles for drug delivery applications. *Adv. Powder Technol.* **2013,** *24*, 757-763.

39. Aw, M. S.; Bariana, M.; Yu, Y.; Addai-Mensah, J.; Losic, D., Surface-functionalized diatom microcapsules for drug delivery of water-insoluble drugs. *J. Biomater. Appl.* **2013,** *28*, 163-174.

40. Li, B.; Huang, H.; Guo, Y.; Zhang, Y., Diatomite-immobilized BiOI hybrid photocatalyst: Facile deposition synthesis and enhanced photocatalytic activity. *Appl. Surf. Sci.* **2015,** *353*, 1179-1185.

41. Wang, B.; de Godoi, F. C.; Sun, Z.; Zeng, Q.; Zheng, S.; Frost, R. L., Synthesis, characterization and activity of an immobilized photocatalyst: Natural porous diatomite supported titania nanoparticles. *J. Colloid Interface Sci.* **2015,** *438*, 204-211.

42. Garcia, G.; Cardenas, E.; Cabrera, S.; Hedlund, J.; Mouzon, J., Synthesis of zeolite Y from diatomite as silica source. *Microporous Mesoporous Mater.* **2016,** *219*, 29-37.

43. Erdem, E.; Çölgeçen, G.; Donat, R., The removal of textile dyes by diatomite earth. *J. Colloid Interface Sci.* **2005,** *282*, 314-319.

44. Inchaurrondo, N.; Font, J.; Ramos, C.; Haure, P., Natural diatomites: Efficient green catalyst for Fenton-like oxidation of Orange II. *Appl. Catal., B* **2016,** *181*, 481-494.

45. Farrah, S.; Preston, D.; Toranzos, G.; Girard, M.; Erdos, G.; Vasuhdivan, V., Use of modified diatomaceous earth for removal and recovery of viruses in water. *Appl. Environ. Microbiol.* **1991,** *57*, 2502-2506.

46. Wu, J.; Yang, Y.; Lin, J., Advanced tertiary treatment of municipal wastewater using raw and modified diatomite. *J. Hazard. Mater.* **2005,** *127*, 196-203.

47. Yılmaz, B.; Ediz, N., The use of raw and calcined diatomite in cement production. *Cem. Concr. Compos.* **2008,** *30,* 202-211.

48. Osmanlioglu, A. E., Natural diatomite process for removal of radioactivity from liquid waste. *Appl. Radiat. Isot.* **2007,** *65*, 17-20.

49. Yu, Y.; Addai-Mensah, J.; Losic, D., Synthesis of self-supporting gold microstructures with three-dimensional morphologies by direct replication of diatom templates. *Langmuir* **2010,** *26*, 14068-14072.

50. Ergül, S.; Kadan, İ.; Savaşcı, Ş.; Ergül, S., Modified diatomaceous earth as a principal stationary phase component in TLC. *J. Chromatogr. Sci.* **2005,** *43*, 394-400.

51. Huttenloch, P.; Roehl, K. E.; Czurda, K., Sorption of nonpolar aromatic contaminants by chlorosilane surface modified natural minerals. *Environ. Sci. Technol.* **2001,** *35*, 4260-4264.

52. Li, X.; Li, X.; Wang, G., Surface modification of diatomite using polyaniline. *Mater. Chem. Phys.* **2007,** *102,* 140-143.

53. Hadjar, H.; Hamdi, B.; Jaber, M.; Brendlé, J.; Kessaïssia, Z.; Balard, H.; Donnet, J. B., Elaboration and characterisation of new mesoporous materials from diatomite and charcoal. *Microporous Mesoporous Mater.* **2008,** *107,* 219-226.

54. Li, X.; Bian, C.; Chen, W.; He, J.; Wang, Z.; Xu, N.; Xue, G., Polyaniline on surface modification of diatomite: a novel way to obtain conducting diatomite fillers. *Appl. Surf. Sci.* **2003,** *207,* 378-383.

55. Yu, Y.; Addai-Mensah, J.; Losic, D., Chemical functionalization of diatom silica microparticles for adsorption of gold (III) ions. *J. Nanosci. Nanotechnol.* **2011,** *11*, 10349-10356.

56. Yu, Y.; Addai-Mensah, J.; Losic, D., Functionalized diatom silica microparticles for removal of mercury ions. *Sci. Technol. Adv. Mater.* **2016**.

57. Simpson, J. T.; D'urso, B. R., Superhydrophobic diatomaceous earth. U.S. Patent No. 8,216,6742012.

58. Oliveira, N. M.; Reis, R. L.; Mano, J. o. F., Superhydrophobic surfaces engineered using diatomaceous earth. *ACS Appl. Mater. Interfaces* **2013,** *5*, 4202-4208.

59. Puretskiy, N.; Chanda, J.; Stoychev, G.; Synytska, A.; Ionov, L., Anti-icing superhydrophobic surfaces based on core-shell fossil particles. *Adv. Mater. Interfaces* **2015,** *2*, 1500124-1500131.

60. Nine, M. J.; Cole, M. A.; Johnson, L.; Tran, D. N.; Losic, D., Robust superhydrophobic graphene-based composite coatings with self-cleaning and corrosion barrier properties. *ACS Appl. Mater. Interfaces* **2015,** *7*, 28482-28493.

61. Polizos, G.; Winter, K.; Lance, M. J.; Meyer, H. M.; Armstrong, B. L.; Schaeffer, D. A.; Simpson, J. T.; Hunter, S. R.; Datskos, P. G., Scalable superhydrophobic coatings based on fluorinated diatomaceous earth: Abrasion resistance versus particle geometry. *Appl. Surf. Sci.* **2014,** *292*, 563-569.

62. García, N.; Benito, E.; Guzmán, J.; Tiemblo, P., Use of p-toluenesulfonic acid for the controlled grafting of alkoxysilanes onto silanol containing surfaces: preparation of tunable hydrophilic, hydrophobic, and super-hydrophobic silica. *J. Am. Chem. Soc.* **2007,** *129*, 5052-5060.

63. Wenzel, R. N., Surface roughness and contact angle. *J. Phys. Chem.* **1949,** *53*, 1466-1467.

64. Williams, D. L.; Kuhn, A. T.; Amann, M. A.; Hausinger, M. B.; Konarik, M. M.; Nesselrode, E. I., Computerised measurement of contact angles. *Galvanotechnik* **2010,** *101*, 2502-2512.

65. Zhuravlev, L., The surface chemistry of amorphous silica. Zhuravlev model. *Colloids Surf., A* **2000,** *173*, 1-38.

66. Yuan, P.; Liu, D.; Tan, D. Y.; Liu, K. K.; Yu, H. G.; Zhong, Y. H.; Yuan, A. H.; Yu, W. B.; He, H. P., Surface silylation of mesoporous/macroporous diatomite (diatomaceous earth) and its function in Cu (II) adsorption: the effects of heating pretreatment. *Microporous Mesoporous Mater.* **2013,** *170*, 9-19.

67. Gulturk, E.; Guden, M., Thermal and acid treatment of diatom frustules. *J. Achievements Mater. Manuf. Eng* **2011,** *46*, 196-203.

68. Blum, F. D.; Meesiri, W.; Kang, H. J.; Gambogi, J. E., Hydrolysis, adsorption, and dynamics of silane coupling agents on silica surfaces. *J. Adhes. Sci. Technol.* **1991,** *5*, 479-496.

69. Tsai, W. T.; Lai, C. W.; Hsien, K. J., Characterization and adsorption properties of diatomaceous earth modified by hydrofluoric acid etching. *J. Colloid Interface Sci.* **2006,** *297*, 749-754.

70. Liang, Z.; Chen, W.; Liu, J.; Wang, S.; Zhou, Z.; Li, W.; Sun, G.; Xin, Q., FT-IR study of the microstructure of Nafion® membrane. *J. Membr. Sci.* **2004,** *233*, 39-44.

71. Heitner-Wirguin, C., Infra-red spectra of perfluorinated cation-exchanged membranes. *Polymer* **1979,** *20*, 371-374.

72. Liang, C. Y.; Krimm, S., Infrared spectra of high polymers. III. Polytetrafluoroethylene and polychlorotrifluoroethylene. *J. Chem. Phys.* **1956,** *25*, 563-571.

73. Cassie, A.; Baxter, S., Wettability of porous surfaces. *Trans. Faraday Soc.* **1944,** *40*, 546-551.

74. Wu, J.; Xia, J.; Jing, C.; Lei, W.; Wang, B. P., Formation of hierarchical ZnO nanostructure on tinfoil substrate and the application on wetting repellency. *Appl. Phys. A* **2011,** *105*, 221-224.

75. Jin, M.; Feng, X.; Feng, L.; Sun, T.; Zhai, J.; Li, T.; Jiang, L., Superhydrophobic aligned polystyrene nanotube films with high adhesive force. *Adv. Mater.* **2005,** *17*, 1977-1981.

76. Sun, T.; Feng, L.; Gao, X.; Jiang, L., Bioinspired surfaces with special wettability. *Acc. Chem. Res.* **2005,** *38*, 644-652.

77. Erbil, H. Y.; Demirel, A. L.; Avcı, Y.; Mert, O., Transformation of a simple plastic into a superhydrophobic surface. *Science* **2003,** *299*, 1377-1380.

3.8. SUPPLEMENTARY INFORMATON

S3.1. SEM images of PS and treated DE coatings

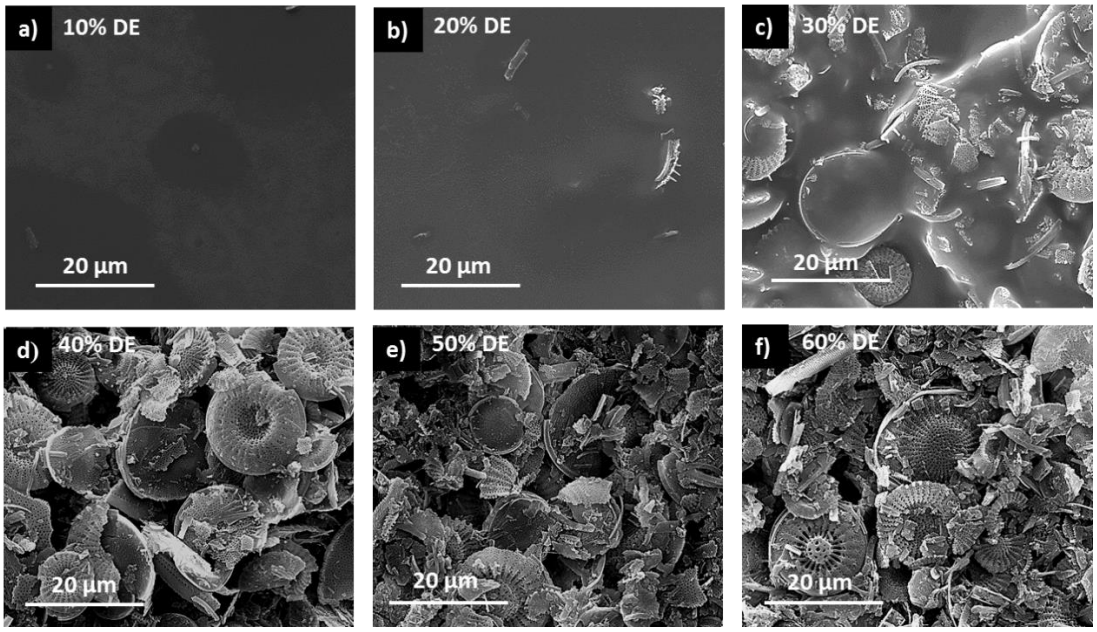

Fig. S3.1. SEM images of PS and treated DE coatings with: a) 10%; b) 20%; c) 30%; d) 40%; e) 50%; and f) 60% treated DE particle loadings. Below 30% particle loadings, top surface of coatings were significantly different. But, above 40% particle loadings in coatings, top surface of coatings were covered with treated DE particles and no significant difference was observed.

CHAPTER IV

PARTICLE MORPHOLOGY DEPENDENT SUPERHYDROPHOBICITY IN TREATED DIATOMACEOUS EARTH/POLYSTYRENE COATINGS

Note: This chapter has been prepared to submit in the Journal Microporous and Mesoporous Materials

Bhishma R. Sedai[a], Habib S. Alavi[b], Sandip S. Harimkar[b], Mark McCollum[c], Joseph F. Donoghue[c], and Frank D. Blum[a]*

[a]Department of Chemistry, Oklahoma State University, Stillwater, Oklahoma, 74078, USA

[b]Mechanical and Aerospace Engineering, Oklahoma State University, Stillwater, Oklahoma, 74078, USA

[c]Department of Geology, Oklahoma State Univeristy, Stillwater, Oklahoma, 74078, USA

4.1. ABSTRACT

Superhydrophobic surfaces have been prepared from three different types of diatomaceous earth (DE) particles treated with 3-(heptafluoroisopropoxy)-propyl-

trimethoxysilane (HFIP-TMS) and low molecular mass polystyrene. The untreated particles, consisting of CelTix DE (disk shape), DiaFil DE (rod shape) and EcoFlat DE (irregular), were studied using particle size analysis, bulk density, pore volume and surface area analysis (via Brunner-Emmett-Teller, BET, methods). The treated particles were characterized with thermogravimetric analysis (TGA), contact angles, scanning electron microscopy, profilometry, and FTIR spectroscopy. The minimum amount of silane coupling agent on the DE surfaces required to obtain superhydrophobicity of the particles was determined and found to be dependent on the particle morphology. In the coatings, the minimum amount of treated particle loadings with 2.4 wt% HFIP-TMS treated DE for superhydrophobicity was determined with the less dense CelTix (disks) DE requiring about 30 wt%, DiaFil (rods) DE requiring about 40 wt%, and EcoFlat (irreg.) DE each requiring about 60 wt% loading of treated particles.

4.2. INTRODUCTION

Diatomite is a light-colored sedimentary rock. It is obtained from the fossilized skeletons of diatoms. When diatomite is crushed into a powder, it is usually called "diatomaceous earth," or abbreviated DE.[1] Diatoms grow as single cells or form filaments and simple colonies in aquatic and moist environments. There are currently estimated to be over 100,000 different diatom species, classified by their unique frustule morphologies.[2] The cell walls of diatoms are known as frustules. Diatom frustules are highly ornamented, forming an amazing range of forms. The shapes of the diatom frustule are species specific. The frustules have a broad variety of delicate, lacy, perforated shapes, including rods, disks, feathers, ladders, needles, and spheres.[2] Diatoms

are usually classified in to two main groups based on the symmetry of their frustules; a) Centric Diatoms and b) Pennate Diatoms. Centric Diatoms are radially symmetrical, while Pennate Diatoms are elongated and generally have parallel striae (furrows or rows of holes in the silica) arranged normal to the long axis.[3]

DE particles have been used in various applications. A variety of unique frustule architectures are attractive materials for optical,[4] mechanical,[5, 6] and transport properties.[7] DE particles have also been used in the construction of advanced devices for applications such as light harvesting, photonics,[8] molecular separation,[7] sensing,[9, 10] and drug delivery,[11-16] DE and its modified forms have also been used in catalysis,[17, 18] removal of heavy metals[19-24] synthesis of zeolites,[25] removal of dyes,[26, 27] waste water treatment,[28-30] cement production,[31] nanotechnology[32] and chromatography.[33]

Treated-DE particles have been used to prepare superhydrophobic surfaces in different ways. Simpson and D'Urso made superhydrophobic powder using DE.[34] Superhydrophobic surfaces using DE particles were prepared by surface chemical modification through fluorosilanization and argon plasma treatment.[35] Superhydrophobic coatings with improved abrasion resistance were prepared using DE particles of different particle morphologies.[36] Leonid and coworkers have designed surfaces with superhydrophobic and ice-repellent properties using polymer-modified DE particles.[37] Nine, et al. have reported robust superhydrophobic graphene and DE based composite coatings with self-cleaning and corrosion barrier properties.[38] Perera, et al. have prepared superhydrophobic coatings using fluorosilane treated-DE particles and resin systems as binder.[39]

In our previous work, we have described the development of superhydrophobicity in 3-(heptafluoroisopropoxy)propyltrimethoxysilane (HFIP-TMS) treated CelTix diatomaceous earth (Disk DE) and simple high molecular mass polymer coatings. We have identified the minimum amount of HFIP-TMS required to make the CelTix DE (Disk DE) superhydrophobic.[40] In the present work, we have modified two additional morphologically different DE particles, DiaFil DE (Rod DE) and EcoFlat DE (Irreg DE), with HFIP-TMS and identified the minimum amounts of HFIP-TMS required to make those DE samples superhydrophobic. The HFIP treated-DE particles (HFIP-DE) were used to prepare coatings with low molecular mass polystyrene as the binder. We have also identified and compared the minimum amount of treated-DE particle loadings needed for each type of treated-DE sample to make those superhydrophobic coatings. The effects of DE particle morphologies and porosities on the development of superhydrophobicity in the DE/polymer coating have been further understood.

4.3. MATERIALS AND METHODS

4.3.1. Materials

Untreated diatomaceous earth, CelTix DE (Disk DE), DiaFil DE (Rod DE) and EcoFlat DE (Irreg DE) were obtained from Dry Surface Coatings (DSC) (Guthrie, OK). Polystyrene (PS) with number average molecular mass of 20,000 g/mol and *para*-toluenesufonic acid were obtained from Sigma Aldrich (Saint Louis, MO). 3-heptafluoro-isopropoxy-propyl-trimethoxysilane (HFIP-TMS) was purchased from Gelest, Inc. (Morrisville, PA). The chemical structure of HFIP-TMS is shown in Fig. 4.1.

Tetrahydrofuran (THF), toluene, hexane and methanol were purchased from Fisher Scientific International Inc. (Pittsburgh, PA) and used as received.

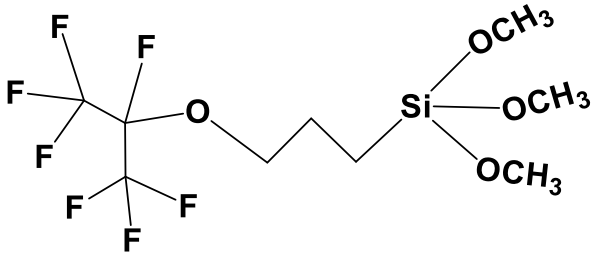

Fig. 4.1. Structure of HFIP-TMS with three hydrolysable methoxy groups on the silicon atom.

A series of treated-DE samples were prepared. Around 2 g of different DE samples were placed in 25 mL plastic vials and mixed with 20 mL of toluene. Approximately 1% of *para*-toluenesulfonic acid relative to DE was added to the mixture.[40] Different amounts of HFIP-TMS (0.001 to 1.0 mL) were added to the vials. The mixtures were heated to 50 °C and shaken in a mechanical shaker at 5000 rpm for 4 h. The samples were then centrifuged and the supernatants were discarded. The mixture in each vial was washed with 20 mL of hexane and then 20 mL of methanol to remove unreacted HFIP-TMS and the supernatant was discarded after centrifugation. The contents were then left overnight to dry in air. All samples were transferred to glass vials and heated to 140 °C for 4 h to remove the solvent and water. The amounts of grafted HFIP-TMS were determined by thermogravimetric analysis.

Particle size measurements were made using a CILAS 1180 particle-size-analyzer (Orleans, France). The CILAS 1180 particle-size-analyzer had integrated wet and dry

dispersion modes, built in video camera, and short optical path. A laser beam of known wavelength was passed through the suspension of the sample. Detectors measured the angular distribution of the intensity of the light diffracted by particles. Approximately 1.0 g of diatomaceous earth samples were dispersed in 50 mL of dispersant solution (5% sodium hexametaphosphate in deionized water). A magnetic stirrer was placed in the mixture and stirred avoiding excess turbulence and vortices. Stirring was continued with a magnetic stirrer to get good sample suspension. The sample (about 5 mL) to be analyzed was drawn from the beaker with a pipette while it was being stirred. The sample was transferred into the particle size analyzer and immediately, an additional 5 ml of deionized water was added using the same pipette. A background measurement was done before running each sample. The graphic mean grain size (θ) and the mean diameter of the DE particles were determined.

4.3.2. Characterization

BET surface area measurements and the pore size distributions of different types of DE samples were done using nitrogen adsorption with a Quantachrome NOVA 2200 instrument (Boynton Beach, FL). The samples were outgassed under vacuum at 100 ºC for 2 h prior to nitrogen gas adsorption. The BET specific surface area was determined using at least five pressures within the range of linearity of the physical adsorption theory ($0.05 < P/P_o < 0.35$) by means of the standard Brunauer-Emmett-Teller (BET) equation (using a molecular cross-sectional area of 0.162 nm^2 for N_2).[41] The pore size distributions were determined using density functional theory (DFT) in the relative pressure range

from 10^{-7} to 1. Prior to measurements, all of the samples were degassed at 373 K for 2 h and finally outgassed to 10^{-3} Torr.

The compositions and presence of DE and fluorosilane coupling agents were analyzed by thermogravimetric analysis and FTIR. High-resolution thermogravimetric analysis was done with a TA Q-50 (TA instruments, New Castle, DE). The samples were heated with a rate of 20 °C/min from room temperature to 950 °C under 40 mL/min of continuous air flow while the sample mass monitored. IR spectra were collected using a Nicolet iS50 Spectrometer from Thermo Scientific Inc. (Waltham, MA) equipped with a deuterated triglycine sulfate detector and a diamond crystal (45° angle) as an attenuated total reflection (ATR) accessory. Each sample was run using 64 scans versus the background that was also collected using 64 scans to generate a single beam spectrum at 4 cm^{-1} resolution in the range of 600 to 4000 cm^{-1}.

Scanning electron micrographs (SEM) were made on the surfaces of the coatings using a FEI Quanta 600 SEM with Evex EDS system (FEI, Hillsboro, OR). The SEM samples were prepared by mounting a piece of coating on an aluminum stub. Samples were then coated with a very thin layer of palladium/gold metal deposited using a MED 010 sputter coater (Balzers, Oberkochen, Germany) to make them conductive.

Treated-DE polymer coatings were prepared by mixing different amounts of HFIP-DE (0 to 70%) with low molecular mass PS with a molecular mass of 20 kDa. The mixtures were dispersed in 7.0 mL THF solvent and were then shaken for 6 h at room temperature in a mechanical shaker. Aluminum pans (I.D. 5 cm x H 1.5 cm) were coated

with 2 mL of the sample mixture, allowed to air dry, and used for contact angle measurements.

Water contact angle measurements were performed using a home-built contact angle apparatus at ambient temperature.[42] The instrument was equipped with a moveable stage for the coated sample and the water droplet added using a pipette. About 4 µL of water droplet was put on the surface. Water droplet images were taken with a high-resolution Proscope camera capable of recoding at 15 fps at a 640 x 480 resolution. The contact angle of the water droplet images on the surface was determined using LB-ADSA technique.[43] The angle (θ) was measured using a drop analysis plugin of the ImageJ software. Three water droplet images were taken on the surfaces for each coating from different positions. The average contact angles for the coatings were plotted against the amounts of grafted silane and treated DE in samples. To measure the contact angles associated with the treated particles alone (in the absence of binder), a slurry made from treated DE was prepared by mixing 0.05 g of the treated DE in 0.5 mL of THF in a scintillation vial. The treated-DE slurry (200 µL) in THF was used to coat a microscopic glass cover slip. The slurry was dried in air for 24 h to remove the excess solvent and water droplet contact angles were measured on the surface of treated DE.

Surface roughness of treated DE and polymer coatings was measured using a two dimensional stylus type profilometer, Mahr Perthometer (Mahr Federal Inc., Providence, RI, US) with a drive unit that was connected with pick-up and stylus. The drive unit moved in a straight line across the specimen surface during a measurement run at constant speed. During the measurement, the pick-up traveled in the longitudinal

direction on the sample surface. The pick-up had the ability to travel in the lateral, as well as upward, directions during the measurements. Vertical adjusters were used to connect the hand-held support for the adjustment of the pick-up height. The output of the profilometer provided the roughness parameters, R_a, R_z and R_{max}. Roughness measurements were made by scanning 1.7 mm lengths of the coating surfaces with the stylus of a profilometer. Scanning was performed at three different places on the same coating surface and the averages were calculated.

4.4. RESULTS

Properties of different DE particles

SEM images of different DE particles were taken to observe their surface topography. Scanning electron micrographs of the different DE particles are shown in Fig. 4.2. Intact DE particles of CelTix DE were disk shaped. Particles of DiaFil DE had cylindrical structures (rod like). Particles of EcoFlat DE were irregular in shape.

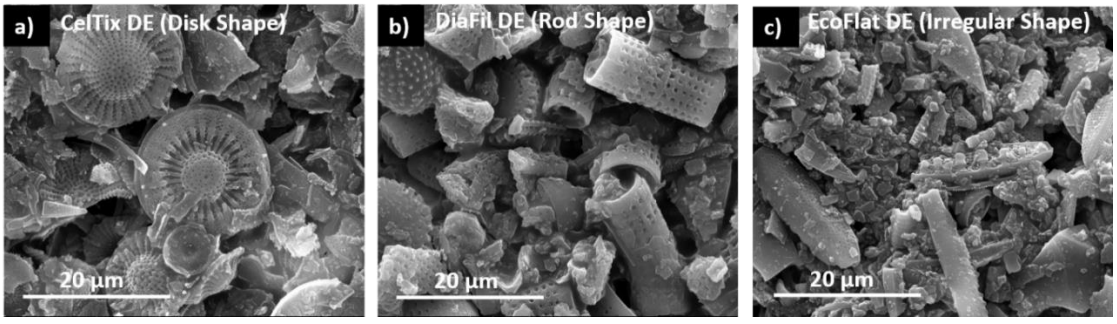

Fig. 4.2. SEMs of different DE particles: a) CelTix DE (Disk DE), b) DiaFil DE (Rod DE) and c) EcoFlat DE (Irreg DE).

Intact Disk DE particles had diameters less than 20 µm. Small broken fragments of DE particles were observed. The lengths of intact Rod DE particles were about15 µm (Fig. 2). SEM images showed many pores on the surface of Rod DE particles. Some broken DE particles were observed. The intact Irreg DE particle lengths were about 20 µm. Many fragmented irregular structures were observed on the surface (Fig. 4.2). Irreg DE particles did not show many pores on the surface of the particles.

The bulk densities of the different DE particles were determined. BET specific surface areas and average particle diameters were measured and shown in Table-4.1. The bulk density was found by simply pouring the samples into a 2 cm^3 pycnometer and measuring the mass of the sample.

Table 4.1. Bulk densities, Specific Surface Areas, Pore Volumes, and Average Particle Diameters of Untreated-DE Samples

DE Type	Bulk density (g/cm^3)	Specific Surface Area (m^2/g)	Average Particle Diameter (µm)	Average Pore Volume (cc/g)
Disk DE	0.11 ± 0.01	29.1 ± 1.2	11.4 ± 1.7	0.175 ± 0.008
Rod DE	0.31 ± 0.02	27.3 ± 0.7	13.5 ± 2.1	0.084 ± 0.019
Irreg DE	0.32 ± 0.01	8.2 ± 0.1	13.2 ± 2.4	0.029 ± 0.002

The bulk densities of Disk DE, Rod DE, and Irreg DE particles were 0.11, 0.31, and 0.32 g/cm^3, respectively. The specific surface areas of Disk DE, Rod DE, and Irreg DE were 29.1, 27.3, and 8.2 m^2/g, respectively, as shown in the table. Disk DE had both the

lowest bulk density and largest specific surface area. Irreg DE had a much smaller specific area than the other two.

Non-local density functional theory (NLDFT) was applied to characterize the pore sizes and pore volume distributions in both micro and mesopores. Pore size distribution curves from nitrogen sorption on different types of DE particles using the NLDFT model are shown in Fig. 4.3. NLDFT pore size distribution showed the presence of micropores with pore widths less than 2 nm diameter and mesopores in the range of 2 to 35 nm diameter in all types of DE samples. It is obvious from the pore size distribution plots that Disk DE particles were most porous and Irreg DE particles were least porous by far.

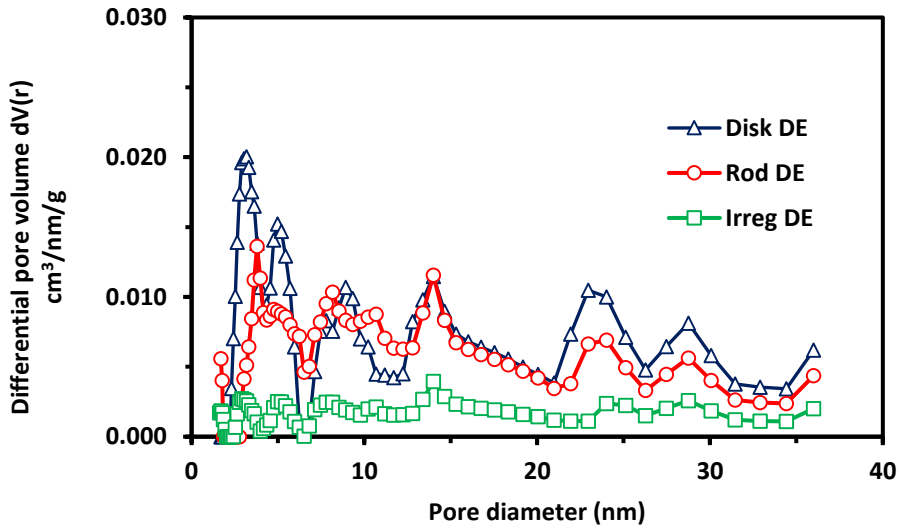

Fig. 4.3. NLDFT pore size distribution curves from nitrogen sorption for different types of DE samples. Disk DE particles were most porous.

Characterization of Treated DE Particles

The amounts of grafted HFIP- TMS in each sample were determined using TGA. The mass loss curves for DE and fluorosilane treated-DE samples are shown in Figs. 4.4-4.6. The amounts of fluorosilane coupling agents on the treated DE were obtained by subtracting the results of the second mass losses (150 - 950 °C) of untreated DE from the second mass losses (150 - 950 °C) of treated DE.[32]

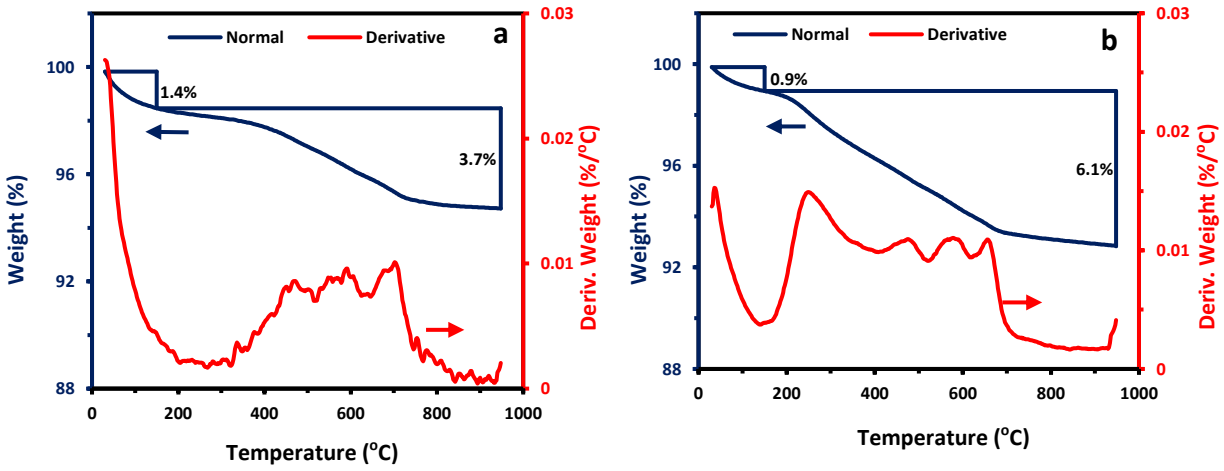

Fig. 4.4. TGA plots showing weight losses for: a) untreated and b) treated Disk DE in normal and derivative modes. Untreated and treated-DE samples showed different decomposition patterns. The amount of adsorbed coupling agent was determined by the difference between the mass losses of treated and untreated-DE samples at 950 °C.

The mass loss for untreated Disk DE in the temperature range of 30 to 150 °C (Fig.4.4a) was 1.4%. The mass loss in the same temperature range for treated Disk DE was 0.9 %. The mass loss for untreated Disk DE (Fig. 4.4b) in the temperature range 150 to 950 °C was 3.7%. The mass loss for HFIP-TMS treated Disk DE (Fig. 4.4b) in the temperature range 150 to 950 °C was 6.1%. The amount of HFIP-TMS grafted on the

surface of Disk DE was determined to be 2.4% by subtracting the mass loss of untreated DE from the mass loss of treated Disk DE at 950 °C.[40]

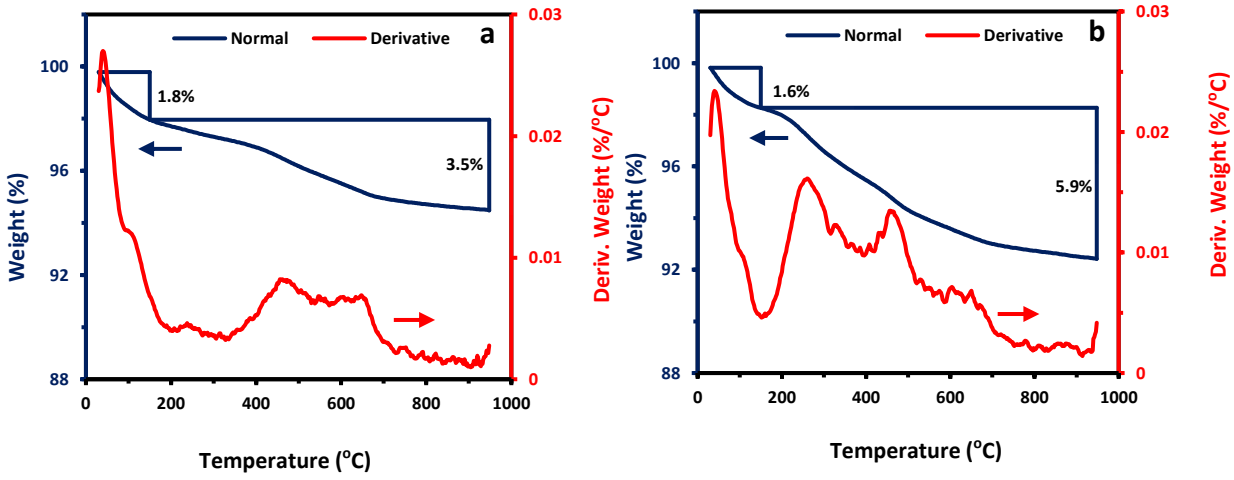

Fig. 4.5. TGA plots showing weight losses for: a) untreated and b) treated Rod DE in normal and derivative modes.

The TGA plots of untreated Rod DE (Fig. 4.5a) showed a mass loss of 1.8% in the temperature range 30 to 150 °C. The mass loss in the same temperature range for HFIP-TMS treated Rod DE was 1.6%. The mass loss for untreated Rod DE (Fig. 4.5a) in the temperature range 150 to 950 °C was 3.5%. The mass loss for HFIP-TMS treated Rod DE (Fig. 4.5b) in the same temperature range was 5.9%. The amount of HFIP-TMS grafted on the Rod DE was determined in the same way for treated Disk DE and found to be 2.4%.

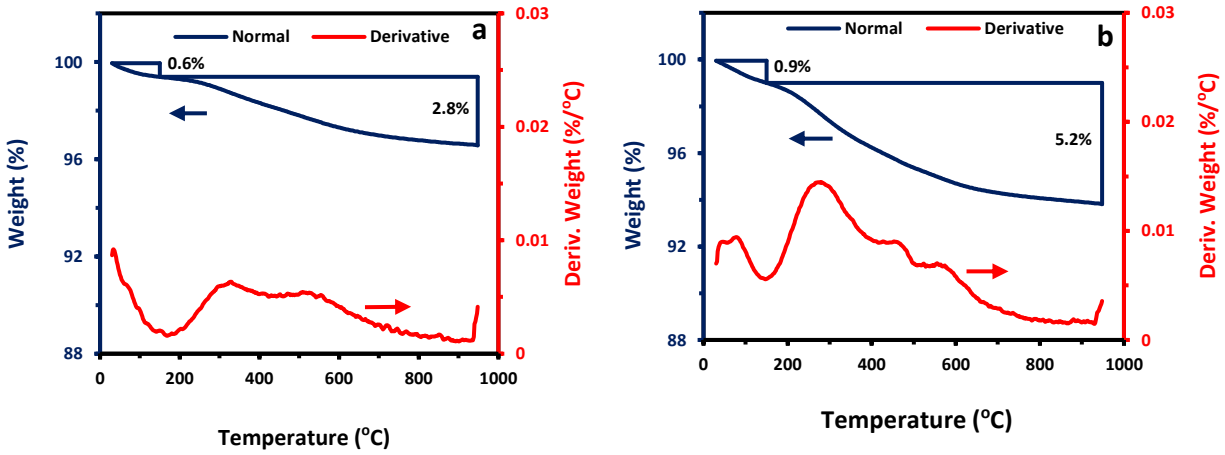

Fig. 4.6. TGA plots showing weight losses for: a) untreated and b) treated Irreg DE in normal and derivative modes.

Thermogravimetric plots for untreated and treated Irreg DE samples (Fig 4.6a-b) showed that the mass loss for treated Irreg DE compared to untreated DE in the temperature range 30 to 150 °C differed by 0.3%. The mass loss for untreated Irreg DE in the temperature range 150 to 950 °C (Fig. 4.6a) was 2.8% and for treated DE was 5.2%. The grafted HFIP-TMS on the surface of Irreg DE was determined to be 2.4% in the same way as of other treated-DE samples. The amounts of fluorosilane in all treated samples shown in Figs. 4.4-4.6, based on the mass differences at 950 °C, were estimated to each be 2.4%. The samples were prepared (selected) in this way for comparison.[40]

The FTIR spectra of untreated and treated DE samples were taken to confirm the presence of silane coupling agent on the DE particles. For reference, the spectrum of the neat coupling agent is shown in Fig. S4.1 of the Supplementary Information. The IR spectra of untreated DE and HFIP-TMS treated-DE samples are shown in the region, 600 to 1600 cm^{-1}, in Figs. 4.7 a-c. Two broad peaks in the range of 900 - 1300 cm^{-1} and

around 795 cm^{-1} were observed in all untreated and treated samples. Major peaks in all morphologically different DE samples were similar, but a slight variation in the peak position was observed as shown in Fig. S4.2 of Supplementary Information. Additional peaks only found in the treated-DE samples were observed at 731 cm^{-1} and 1200 cm^{-1}. These resonances were also found in the spectra of the neat HFIP-TMS as shown in Fig. S4.3 of the Supporting Information.

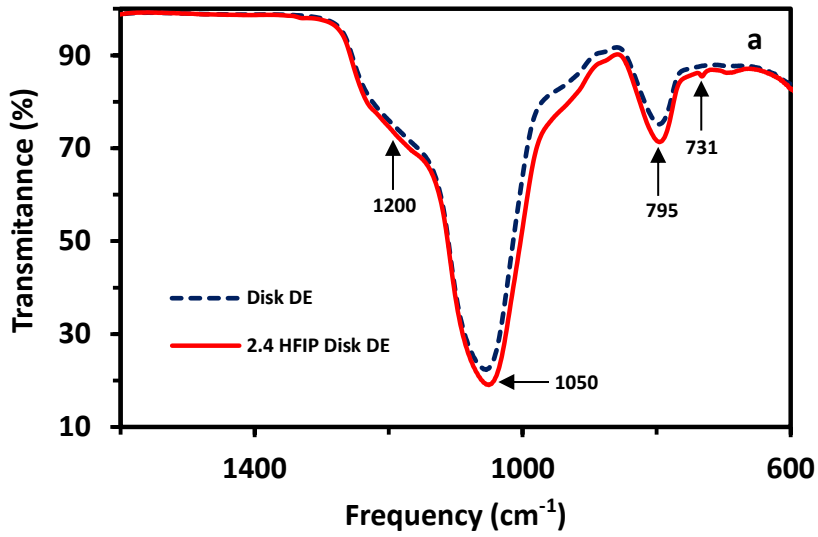

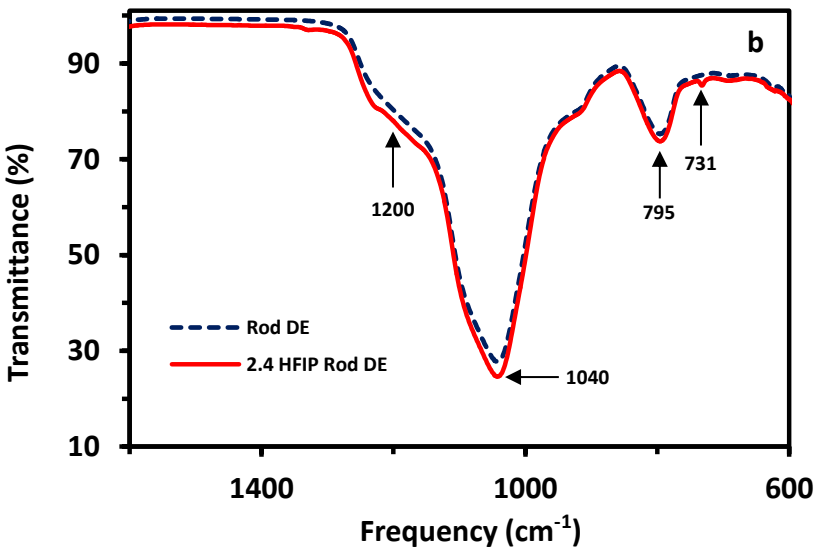

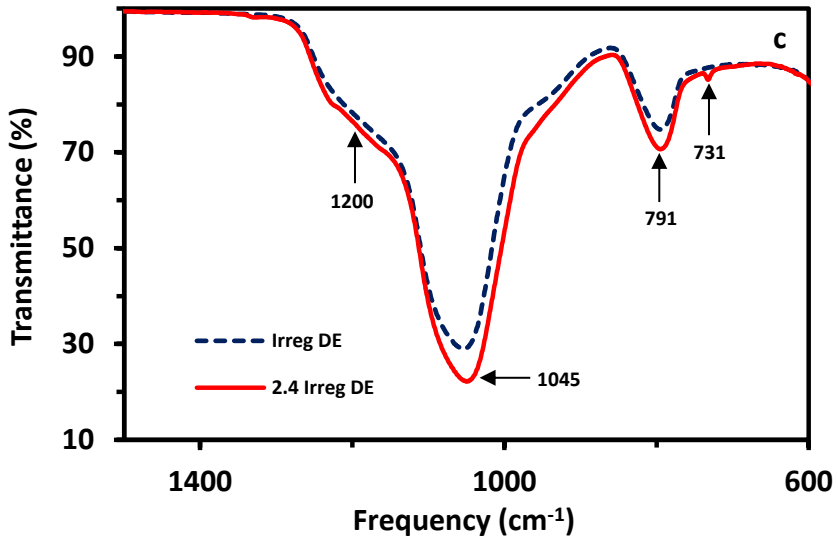

Fig. 4.7. FTIR Spectra (ATR) of untreated DE (blue) and HFIP-TMS treated DE (red); in 600 – 1600 cm^{-1} range; a) Disk DE, b) Rod DE and c) Irreg DE. All treated samples had 2.4 wt% of HFIP on the surface.

The amounts of silane coupling agent on the surface of the different DE samples were analyzed using TGA. The water contact angles were measured for each sample for the bulk treated-DE particles without polymer binder. Plots of adsorbed amount of HFIP on the surface of DE samples versus contact angle are shown in Figs. 4.8a and 4.8b for both mmol/g and mg/m^2, respectively. The water contact angle increased with increasing amounts of adsorbed fluorosilane and then remained almost constant for larger adsorbed amounts based on either mass or surface areas of the different particles. The error bars represent standard deviation of the measurements which ranged from ± 5.2 to ± 11.9° small-adsorbed amounts. For large silane-adsorbed amounts, the error bars sizes were smaller (± 0.1 to ± 2^o) than the size of symbols.

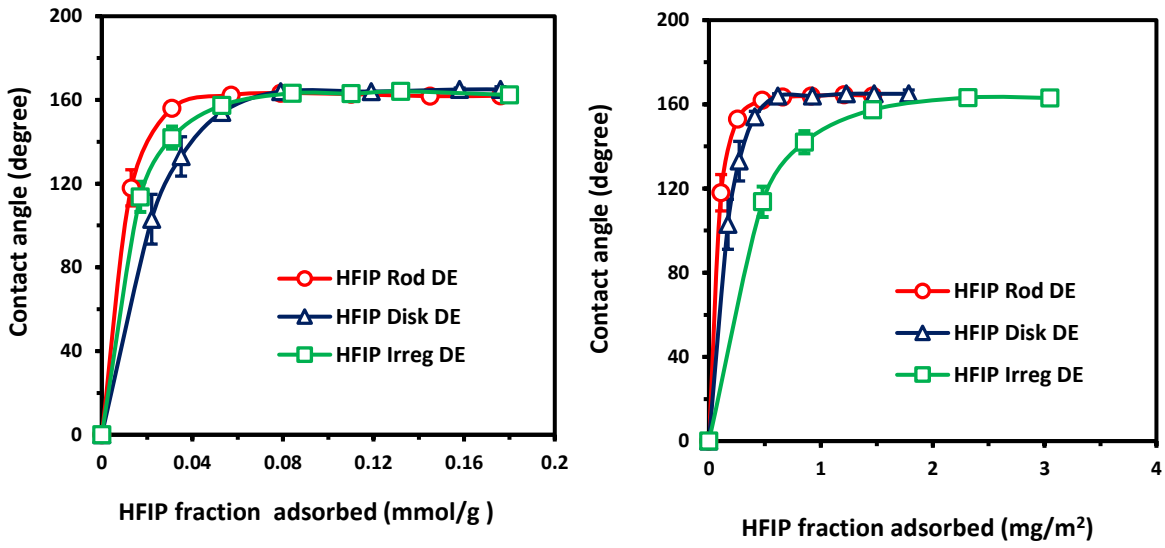

Fig. 4.8. Contact angle measurements of treated-DE particles (bare, no binder) as a function of HFIP adsorbed amount on different DE particles: a) adsorbed amounts in mmol of coupling agent per gram of DE sample and b) adsorbed amount in mg of coupling agent per m^2 of DE sample. Two different units in x-axis are chosen to clarify the effect of treated-DE particles morphology on their surface behavior.

The plots of contact angle versus HFIP-TMS amount (Fig. 4.8a) on the surface of morphologically different DE particles showed that at more than 0.08 mmol grafted silane coupling agent per gram of DE (1.9 wt%), the bulk treated-DE particles (without binder) for all DE samples behaved in the same way. The maximum water contact angles measured on the surface of bulk HFIP-TMS treated-DE particles were about 164°. The behavior of HFIP-TMS treated-DE particles for different DE samples with less than those grafted silane amounts was different. Based on the TGA and water contact angle results,

the bulk treated Disk DE coatings with 1.2% (0.05 mmol/g) of HFIP-TMS on the DE surface gave contact angle of about 155° as reported previously.[40]

A plot of contact angle versus adsorbed amount in milligrams of HFIP fraction per m^2 of DE samples (Fig. 4.8b) revealed that Rod DE particles developed superhydrophobicity with least amount of adsorbed fluorosilane (0.2 mg/m^2). The treated bare Disk DE particles surface exhibited superhydrophobicity at an adsorbed amount 0.4 mg/m^2. The treated bare Irreg DE particles required HFIP adsorbed amount 1.4 mg/m^2 on the surface to show superhydrophobicity.

Properties and wettability of treated DE/PS coatings

Water droplet images were taken and contact angles measured on the surface of the coatings prepared from different types and different amounts of treated-DE particles with PS with a molecular mass of 20 kDa. A plot of contact angle versus the weight fraction (particle loading) of treated-DE particles in the coatings is shown in Fig. 4.9. The figure shows that the contact angles of the coatings increased with increased loading of treated-DE particles. In most samples, the values of the standard deviation of the measurements were smaller than the size of the symbols (± 0.2 to ± 2^o). The large value of standard deviation of the measurements (± 12.7^o) for HFIP Irreg DE and PS coating at 50% particle loadings was because, in the transition region of surface from hydrophobic to superhydrophobic state, there is more variability in the samples produced due to local differences. After the transition, the contact angles leveled off with particle loadings. The leveling off, corresponded to greater than 30 wt% being superhydrophobic,

eventually reaching 160° for Disk DE samples. For Rod or Irreg DE, superhydrophobic behavior required at least 60 wt% particle loadings and leveled off around 150°.

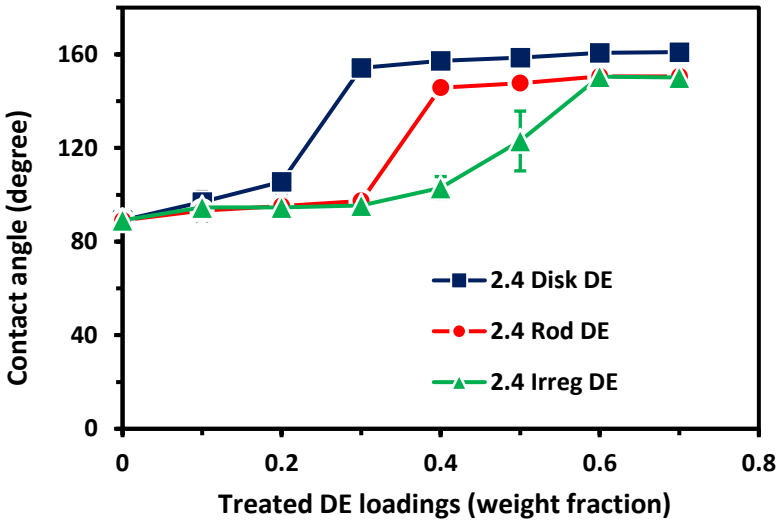

Fig. 4.9. Variation of the contact angles as a function of treated-DE particle loadings in coatings with 2.4 weight percent HFIP on Disk DE (blue squares), HFIP Rod DE (red circles) and HFIP Irreg DE (green triangles). For the different samples, 2.4 weight percent corresponded to HFIP adsorbed amounts of 0.8, 0.9 and 2.9 mg/m^2 for Disk DE, Rod DE and Irreg DE, respectively.

In order to correlate the contact angle studies with the surface structures, we examined electron micrographs of the coatings. SEM images of the coatings were taken to determine the differences in the structures of the surface with 30% particle loading of different types of HFIP treated DE with polystyrene in Fig. 4.10. For 30% treated Disk DE/PS coatings, more and clearer DE particles were observed at the surface which was

superhydrophobic. The other DE particles, for samples, which were only hydrophobic, appeared to be partially covered by polymer.

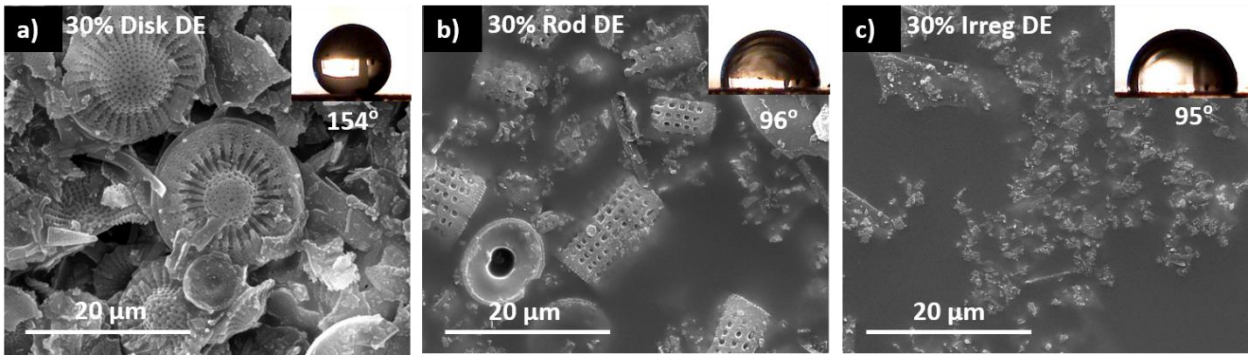

Fig. 4.10. SEM micrographs of the top (air) surfaces for coatings obtained from 30% of particle loadings of 2.4 HFIP on a) Disk DE, b) Rod DE, and c) Irreg DE with polystyrene as a binder. The scale bars are 20 µm. All the DE samples had 2.4 wt% of silane coupling agent on the surface.

To observe the effect of increased treated-DE particle loadings, SEM images of coatings with 40% of different treated DE and PS surfaces were taken and shown in Fig. 4.11. At 40% particle loadings, the top surface of the coating with treated Disk DE particles was similar to that at 30% loading. Many exposed treated-DE particles were now observed in the treated Rod DE/PS surface at 40% particle loading and this coating approached superhydrophobicity. For treated Irreg DE/ PS coatings, few clear particles were observed and the surface was hydrophobic only.

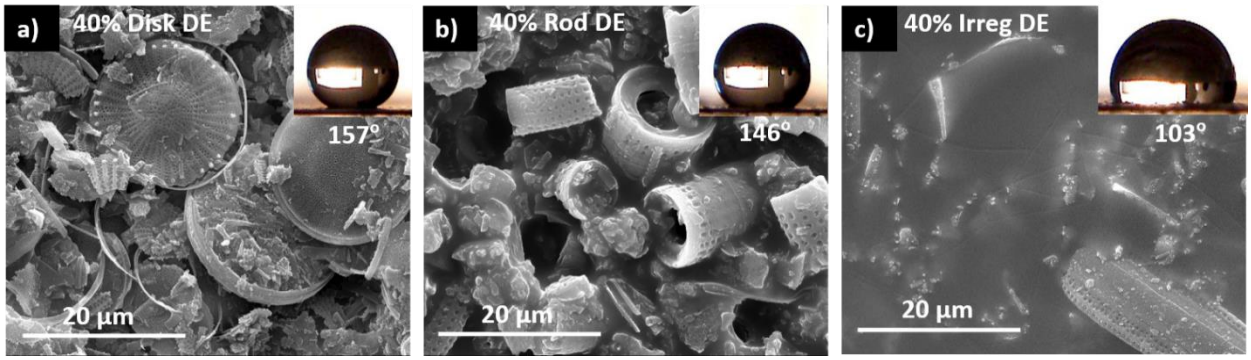

Fig. 4.11. SEM micrographs of the top (air) surfaces of the coatings obtained from 40% particle loading of 2.4 HFIP on a) Disk DE, b) Rod DE, and c) Irreg DE with polystyrene as a binder. The scale bars are 20 µm. All the DE samples had 2.4 wt% of silane coupling agent adsorbed on the surface.

The coatings with 60% particle loadings were all superhydrophobic. SEM images of three coatings were taken to observe and compare the surface structures of treated different types of DE and PS surfaces. The surface topography of these coatings are shown in Fig. 4.12. At 60% particles loadings, in all coatings the top surface was covered with treated-DE particles.

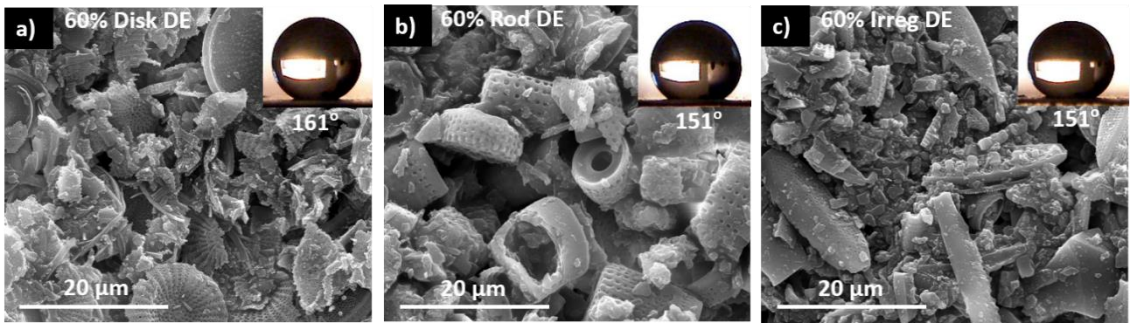

Fig. 4.12. SEM micrographs of the top (air) surfaces for coatings obtained from 60% particle loading of 2.4 HFIP on a) Disk DE, b) Rod DE and c) Irreg DE with polystyrene as a binder. The scale bars are 20 µm. All the DE samples had 2.4 wt% of silane coupling agent adsorbed on the surface.

Superhydrophobic coatings surfaces prepared from the three different types of DE with 60% particle loading were probed with the stylus of Mahr Perthometer (2-D profilometer). The output of the profilometer were roughness parameters, R_a (average height parameter), R_z (ten point height profile) and R_{max} (maximum height of the profile). The arithmetic average height parameter (R_a), is also known as center line average (CLA). It gives the average absolute deviation of the roughness irregularities from the mean line over one sampling length.[44] Ten point height (R_z) represents the difference in height between the average of the five highest peaks and the five lowest valleys along the assessment length of the profile.[44] Maximum height of the profile (R_{max}) which represents the vertical distance between the highest peak and the lowest valley along the assessment length of the profile.[44] The roughness parameters for three different coatings with the same percentage of particle loadings are shown in Fig. 4.13.

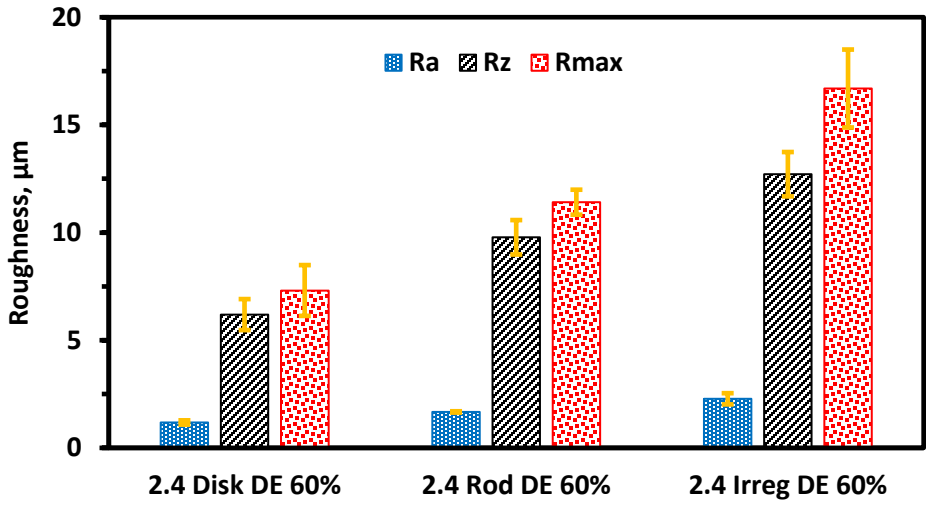

Fig. 4.13. Roughness parameters, R_a, R_z and R_{max} for superhydrophobic coatings. The coatings were prepared with the 60% of different types of treated-DE particle loadings with PS 20 kDa binder.

Average R_a values for coatings with 60 wt% of Disk DE, Rod DE and Irreg DE were 1.18, 1.67 and 2.28 µm, respectively. Average R_z values for coatings with 60% of Disk DE, Rod DE and Irreg DE were found to be 6.19, 9.79 and 12.71 µm, respectively. Similarly, average R_{max} values for coatings with 60% of Disk DE, Rod DE and Irreg DE were found to be 7.31, 11.41 and 16.69 µm, respectively.

To understand the effect of increased amount of particle loadings on the roughness, three more coating samples were scanned. The coating samples selected for roughness measurement were prepared from treated Irreg DE particles. A plot of averages of roughness parameters R_a, R_z and R_{max} for coatings prepared with 50, 60 and 70 wt% of treated Irreg DE particles is shown in Fig. 4.14.

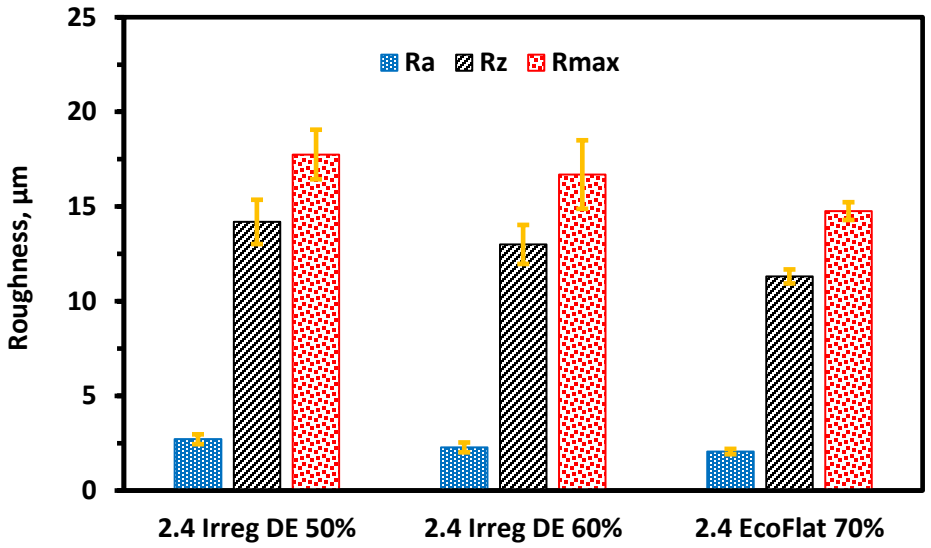

Fig. 4.14. A plot showing roughness parameters, R_a, R_z and R_{max} for the coatings prepared with the 50, 60 and 70 wt% of treated Irreg DE particle loadings with PS 20 kDa binder.

The average R_a values for coatings with 50, 60 and 70 wt% of Irreg DE were 2.71, 2.28 and 2.06 µm, respectively. The average R_z values for coatings with 50, 60 and 70 wt% of Irreg DE were found to be 14.19, 13.00 and 11.31µm, respectively. The average R_{max} values for coatings with 50%, 60% and 70% of Irreg DE were 17.75, 16.69 and 14.76 µm, respectively.

4.5. DISCUSSION

Diatomaceous earth contains various inorganic species. Chemical composition of DE from previous work has shown that it contains SiO_2, Fe_2O_3, CaO, MgO, TiO_2, and others.[45] Diatomaceous earth also contains physically bound water molecules on the surface of diatom-silica.[46, 47] For the thermal degradation shown in Figs. 4.4-4.6 for untreated and treated-DE samples, the removal of physically bound water molecules,

dehydration of surface silanols, and physically adsorbed silane coupling agents (if any) were expected to evaporate around 150 °C. The mass losses for each type of DE in the temperature range 30 to 150 °C were different probably due to different amount of water because of slightly different surface structures. The mass losses in the temperature range of 150 to 950 °C for all untreated-DE samples were due to the decomposition of various inorganic substances, plus dehydroxylation of surface silanol groups of DE silica. These mass losses were also different for the different types of untreated-DE samples because of different particle structures and possibly different amounts of water on the samples and small amounts contained in the solvents and PTSA. The mass losses for the treated-DE samples were comparable to those for the untreated samples of the same type. The additional mass losses for all HFIP-TMS treated-DE samples in the temperature range 150 to 950 °C were primarily due to the decomposition of grafted HFIP-TMS. The amounts of HFIP-TMS grafted on the surface the different DEs were determined by the difference of the mass losses of the untreated DE from the mass losses of treated DE samples at 950 °C.

FTIR spectroscopy using an ATR accessory was useful to characterize both the untreated and treated DEs. Only slight differences were found in the three different types of untreated DEs. The resonances around 1050 and 1200 cm^{-1} (Fig. 4.7 a-c) for untreated DE were due to the in-plane Si-O stretching modes and that around 795 cm^{-1}, was due to symmetric Si-O stretching.[48] The well-known covalent bonding of the silane coupling agents to silica surfaces has previously been previously been shown with solid state ^{29}Si NMR.[49] The presence of the coupling agents in the treated DE samples was verified by ATR-FTIR. We have previously reported[40] the FTIR spectra of HFIP and HFIP-treated

Disk DE. For all of the treated samples shown, the amount of HFIP was only 2.4 wt%, so the intensities of the silanes was small, but observable. Comparison of FTIR spectra of untreated-DE and treated-DE samples (Fig. 4.7 a-c) showed some resonances in all of the treated-DE samples that not present in the untreated-DE samples, and assignable to HFIP-TMS. Resonances for treated DE around 1050 and 1200 cm^{-1} were observed from C-F (symmetric and antisymmetric) stretches and formation of new Si-O bonds with HFIP-TMS.[50, 51] Additional resonances at 731cm^{-1} which, were present only in treated-DE samples, resulted due to the vibration (wagging) of C-F bond in polyfluorocarbon region of HFIP-TMS.[50, 51] FTIR results of treated DE indicated the presence of HFIP-TMS on the surface of all DE samples.

The plots of contact angle versus HFIP-TMS amount (Fig. 4.8 a-b) on the surface of morphologically different DE particles showed that among the three types of morphologically different DE particles, treated bulk Rod DE required least amount of HFIP-TMS on the surface to achieve superhydrophobicity. The similarity of Disk and Rod DE suggests that their similar porosities and surface areas play a role in the hydrophobicity of the bulk particles at similar amounts of coupling agent. The surface of slurry coatings prepared from 2.4 Rod DE particles (no binder) was rougher than Disk DE slurry coating (Fig. S4.3, Supplementary Information) and Rod DE particles were also porous. The synergistic effect of surface roughness and porous nature of particles made Rod DE particles superhydrophobic with a minimum amount of silane coupling agent on the surface.

The dependence of the hydrophobicities of the coatings samples as a function of the particle loadings (Fig. 4.9) showed the dependency of the superhydrophobicity on the DE particle morphology. For 2.4 HFIP-Disk DE 30% particle loading was required to achieve superhydrophobicity compared to double that for HFIP-Rod DE and HFIP-Irreg DE. At these amounts, the top surface was found to be covered with treated-DE particles (Fig. 4.12 a-c). All of the particles could be used to make superhydrophobic coatings, but Disk DE was most effective. At all compositions, the water contact angles of treated Disk DE/PS coatings were larger than those from treated Rod and Irreg DE, even in the superhydrophobic region (about 160° compared to 150°).

The average values of the roughness parameters for the three different DE coatings with polystyrene (Fig. 4.13) showed that the surface irregularities were largest for treated Irreg DE/PS followed by Rod DE/PS surfaces. This result suggested, though the surface structures overall were rough, this roughness on the 10-18 μm scale did not enhance superhydrophobicity.

Interestingly, for treated Irreg DE/PS coatings, all three-roughness parameters, R_a, R_z and R_{max} decreased with the increased loadings of treated-DE particles. This decrease in roughness coincided with an increase in water contact angles (Fig. 4.14) for the samples from 50 to 70% particle loading in the transition region from hydrophobic to superhydrophobic. The effect was also consistent with the roughness of the coatings from the different shaped DE/PS coatings, decreased surface roughness in the 10-18 μm scale increased water contact angles. These two roughness effects suggested that very rough surfaces with particles protruding extensively may not yield superhydrophobic surfaces.

In addition, the Irreg DE has less porosity than the other two samples. Porosity and sub-micron scale-roughness from the holes in the DE and trapped air in the pores seemed to be required for superhydrophobicity. In contrast, Disk DE/PS coatings, even at 30 wt% particle loading, contained suitable roughness and porosity. While these Disk-shaped particles must come to the surface for superhydrophobicity, they do not protrude into the air interface like the other samples with prolate-shape particles.

There are additional reasons for the differences in the development of superhydrophobicity in the different DEs. These differences are evident at large treated-DE particle loadings (60%) because of the inherent structures and porosity differences. On one hand, Rod DE and Irreg DE particles had larger densities (Table-4.1) than Disk DE particles, so at the same mass fraction, the number of Disk DE particles (less dense) were larger than the number Rod DE and Irreg DE particles. The smaller number of dense particles of Rod DE and Irreg DE were not sufficient, at small particle loadings, to make a rough porous structured surface required for superhydrophobicity. Another reason is the behavior of treated-DE particles just before drying of superhydrophobic DE particles from the polymer suspension. Our pervious results[40] have shown that when superhydrophobic Disk DE particles in polymer suspensions were poured on the flat aluminum substrate and allowed to dry, the solvent slowly evaporates and the polymer dispersion becomes viscous. Superhydrophobic DE particles move towards the hydrophobic air interface. The air-surface interface resulted from Disk DE/PS coating was relatively flat and half of the pores of flat disk shaped particle were exposed to the surface. Less dense and porous HFIP TMS treated particles (Disk DE) appear to find their way more easily to the air interface compared to more dense particles of Rod and

Irreg DE. Heavier particles remain more submersed in polymer and their pores are partially exposed as their top surfaces ware not flat compared to less dense particles Disk DE particles.

The different superhydrophobic behavior of different types of treated-DE particles with PS 20 kDa binder system also underscores that air trapped in the pores of DE particles and their surface roughness have a significant role in the development of superhydrophobicity. Irreg DE particles with PS 20 kDa binder system required 60% particle loading to achieve superhydrophobicity as they had fewer pores, consequently less trapped air in the pores, compared to other DEs. Rod DE and Irreg DE particles were heavier than Disk DE, and their pores were only partially exposed to the air interface in the coatings prepared with PS binder system. The water contact angle were about 10° less for treated Rod DE and Irreg DE (~151°), though their surfaces were very rough, compared to treated Disk DE coatings as the Disk DE particles had more trapped-air in pores at the air-coating interface.

4.6. CONCLUSIONS

The development of superhydrophobicity in coatings prepared with treated diatomaceous earth and a simple polymer as binder (polystyrene) was found to depend on the nature of the particles especially their morphologies as it affects density, surface area, and porosity.

The least dense (0.12 g/cm^3) and most porous Disk DE particles showed superhydrophobicity at 30% treated-DE particle loading with PS 20 kDa binder. Bulk treated Disk DE particles surface as well as coatings with PS binder showed the fewest

irregularities in surface roughness as the resulting air surface interface was relatively flat due to their inherent disk shaped structure. For these flat disk shaped particles and PS coatings, the pores present in the particles were exposed to the air surface interface and air trapped in their pores made Disk DE particles superior for superhydrophobicity. Bulk particle surface achieved superhydrophobicity with 0.4 mg/m^2 of fluorosilane on the surface.

Rod DE particles had surface area, and porosity comparable to Disk DE, but they a have larger bulk density (0.30 g/cm^3). Bulk treated Rod DE particles surface showed more irregularities in surface roughness compared to Disk DE particle surface. These bulk treated particles required least amount of fluorosilane coupling agent (0.2 mg/m^2) to achieve superhydrophobicityin bulk because the resulting surfaces were rough and porous. In PS coatings, treated Rod DE particle/PS coatings had fewer pores exposed on the top side of the particles due to their barrel shaped geometry. Although particles were porous, most of the pores had no access to air surface interface of coatings with polymer binder system.

Irreg DE particles were most dense (0.32 g/m^2), least porous and had the smallest surface area (8.2 m^2/g). Bulk treated particle surfaces of Irreg DE required largest amount (1.4 mg/m^2) of fluorosilane coupling agent as the least porous particles had no ability to trap much air.

The average values of the roughness parameters showed that the surface irregularities were largest for treated Irreg DE/PS and also large for Rod DE/PS surfaces. Both treated Irreg DE and Rod DE required 60% particle loadings with PS 20 kDa binder to achieve

superhydrophobicity Although the surface structures for Irreg DE/PS and Rod DE/PS at low particle loadings were rough, their roughness on the 50 - 100 μm scale did not enhance superhydrophobicity. The difference in superhydrophobicity observed for coatings prepared from bulk treated different DE particles and their suspensions with polymer were due to their difference in structure, surface roughness, surface area and porosities.

Acknowledgements

The authors acknowledge the financial support of the Oklahoma State University, and Dry Surface Coatings (DSC), Guthrie, OK.

4.7. REFERENCES

1. Yang, W.; Lopez, P. J.; Rosengarten, G., Diatoms: Self assembled silica nanostructures, and templates for bio/chemical sensors and biomimetic membranes. *Analyst* **2011,** *136*, 42-53.
2. Round, F. E.; Crawford, R. M.; Mann, D. G., *Diatoms: biology and morphology of the genera*. Cambridge University Press1990.
3. Parkinson, J.; Gordon, R., Beyond micromachining: the potential of diatoms. *Trends Biotechnol.* **1999,** *17*, 190-196.
4. Butcher, K.; Ferris, J.; Phillips, M.; Wintrebert-Fouquet, M.; Wah, J. J.; Jovanovic, N.; Vyverman, W.; Chepurnov, V., A luminescence study of porous diatoms. *Mater. Sci. Eng., C* **2005,** *25*, 658-663.

5. Hamm, C. E.; Merkel, R.; Springer, O.; Jurkojc, P.; Maier, C.; Prechtel, K.; Smetacek, V., Architecture and material properties of diatom shells provide effective mechanical protection. *Nature* **2003,** *421*, 841-843.

6. Losic, D.; Short, K.; Mitchell, J. G.; Lal, R.; Voelcker, N. H., AFM nanoindentations of diatom biosilica surfaces. *Langmuir* **2007,** *23*, 5014-5021.

7. Losic, D.; Rosengarten, G.; Mitchell, J. G.; Voelcker, N. H., Pore architecture of diatom frustules: potential nanostructured membranes for molecular and particle separations. *J. Nanosci. Nanotechnol.* **2006,** *6*, 982-989.

8. Fuhrmann, T.; Landwehr, S.; El Rharbi-Kucki, M.; Sumper, M., Diatoms as living photonic crystals. *Appl. Phys. B* **2004,** *78*, 257-260.

9. Rosi, N. L.; Thaxton, C. S.; Mirkin, C. A., Control of Nanoparticle Assembly by Using DNA-Modified Diatom Templates. *Angew. Chem. Int. Ed.* **2004,** *116*, 5616-5619.

10. De Stefano, L.; Rendina, I.; De Stefano, M.; Bismuto, A.; Maddalena, P., Marine diatoms as optical chemical sensors. *Appl. Phys. Lett.* **2005,** *87*, 233902.

11. Coradin, T.; Livage, J., Synthesis, characterization and diffusion properties of biomimetic silica-coated gelatine beads. *Mater. Sci. Eng., C* **2005,** *25*, 201-205.

12. Aw, M. S.; Simovic, S.; Yu, Y.; Addai-Mensah, J.; Losic, D., Porous silica microshells from diatoms as biocarrier for drug delivery applications. *Powder Technol.* **2012,** *223*, 52-58.

13. Aw, M. S.; Bariana, M.; Yu, Y.; Addai-Mensah, J.; Losic, D., Surface-functionalized diatom microcapsules for drug delivery of water-insoluble drugs. *J. Biomater. Appl.* **2013,** *28*, 163-174.

14. Bariana, M.; Aw, M. S.; Losic, D., Tailoring morphological and interfacial properties of diatom silica microparticles for drug delivery applications. *Adv. Powder Technol.* **2013,** *24*, 757-763.

15. Bariana, M.; Aw, M. S.; Kurkuri, M.; Losic, D., Tuning drug loading and release properties of diatom silica microparticles by surface modifications. *Int. J. Pharm.* **2013,** *443*, 230-241.

16. Maher, S.; Alsawat, M.; Kumeria, T.; Fathalla, D.; Fetih, G.; Santos, A.; Habib, F.; Losic, D., Luminescent silicon diatom replicas: self-reporting and degradable drug carriers with biologically derived shape for sustained delivery of therapeutics. *Adv. Funct. Mater.* **2015,** *25*, 5107-5116.

17. Tang, W.; Qiu, K.; Zhang, P.; Yuan, X., Synthesis and photocatalytic activity of ytterbium-doped titania/diatomite composite photocatalysts. *Appl. Surf. Sci.*

18. Hsien, K. J.; Tsai, W. T.; Su, T. Y., Preparation of diatomite-TiO2 composite for photodegradation of bisphenol-A in water. *J. Sol-Gel Sci. Technol.* **2009,** *51*, 63-69.

19. Yuan, P.; Liu, D.; Tan, D. Y.; Liu, K. K.; Yu, H. G.; Zhong, Y. H.; Yuan, A. H.; Yu, W. B.; He, H. P., Surface silylation of mesoporous/macroporous diatomite (diatomaceous earth) and its function in Cu (II) adsorption: the effects of heating pretreatment. *Microporous Mesoporous Mater.* **2013,** *170*, 9-19.

20. Khraisheh, M. A.; Al-degs, Y. S.; Mcminn, W. A., Remediation of wastewater containing heavy metals using raw and modified diatomite. *Chem. Eng. J.* **2004,** *99*, 177-184.

21. Sheng, G.; Hu, J.; Wang, X., Sorption properties of Th (IV) on the raw diatomite-effects of contact time, pH, ionic strength and temperature. *Appl. Radiat. Isot.* **2008,** *66*, 1313-1320.

22. Yu, Y.; Addai-Mensah, J.; Losic, D., Chemical functionalization of diatom silica microparticles for adsorption of gold (III) ions. *J. Nanosci. Nanotechnol.* **2011,** *11*, 10349-10356.

23. Branton, P.; Carrott, P.; Llewellyn, P.; Müller, E.; Flores-Cano, J.; Leyva-Ramos, R.; Padilla-Ortega, E.; Mendoza-Barron, J., Adsorption of heavy metals on diatomite: mechanism and effect of operating variables. *Adsorpt. Sci. Technol.* **2013,** *31*, 275-292.

24. Khraisheh, M. A. M.; Al-degs, Y. S.; McMinn, W. A. M., Remediation of wastewater containing heavy metals using raw and modified diatomite. *Chem. Eng. J.* **2004,** *99*, 177-184.

25. Garcia, G.; Cardenas, E.; Cabrera, S.; Hedlund, J.; Mouzon, J., Synthesis of zeolite Y from diatomite as silica source. *Microporous Mesoporous Mater.* **2016,** *219*, 29-37.

26. Maeda, H.; Ishida, E. H., Hydrothermal preparation of diatomaceous earth combined with calcium silicate hydrate gels. *J. Hazard. Mater.* **2011,** *185*, 858-861.

27. Erdem, E.; Çölgeçen, G.; Donat, R., The removal of textile dyes by diatomite earth. *J. Colloid Interface Sci.* **2005,** *282*, 314-319.

28. Farrah, S.; Preston, D.; Toranzos, G.; Girard, M.; Erdos, G.; Vasuhdivan, V., Use of modified diatomaceous earth for removal and recovery of viruses in water. *Appl. Environ. Microbiol.* **1991,** *57*, 2502-2506.

29. Hadjar, H.; Hamdi, B.; Jaber, M.; Brendlé, J.; Kessaïssia, Z.; Balard, H.; Donnet, J. B., Elaboration and characterisation of new mesoporous materials from diatomite and charcoal. *Microporous Mesoporous Mater.* **2008,** *107*, 219-226.

30. Xiong, W.; Peng, J., Development and characterization of ferrihydrite-modified diatomite as a phosphorus adsorbent. *Water Res.* **2008,** *42*, 4869-4877.

31. Yılmaz, B.; Ediz, N., The use of raw and calcined diatomite in cement production. *Cem. Concr. Compos.* **2008,** *30*, 202-211.

32. Yu, Y.; Addai-Mensah, J.; Losic, D., Synthesis of self-supporting gold microstructures with three-dimensional morphologies by direct replication of diatom templates. *Langmuir* **2010,** *26*, 14068-14072.

33. Ergül, S.; Kadan, İ.; Savaşcı, Ş.; Ergül, S., Modified diatomaceous earth as a principal stationary phase component in TLC. *J. Chromatogr. Sci.* **2005,** *43*, 394-400.

34. Simpson, J. T.; D'urso, B. R., Superhydrophobic diatomaceous earth. U.S. Patent No. 8,216,6742012.

35. Oliveira, N. M.; Reis, R. L.; Mano, J. F., Superhydrophobic surfaces engineered using diatomaceous earth. *ACS Appl. Mater. Interfaces* **2013,** *5*, 4202-4208.

36. Polizos, G.; Winter, K.; Lance, M. J.; Meyer, H. M.; Armstrong, B. L.; Schaeffer, D. A.; Simpson, J. T.; Hunter, S. R.; Datskos, P. G., Scalable superhydrophobic

coatings based on fluorinated diatomaceous earth: Abrasion resistance versus particle geometry. *Appl. Surf. Sci.* **2014,** *292*, 563-569.

37. Puretskiy, N.; Chanda, J.; Stoychev, G.; Synytska, A.; Ionov, L., Anti-icing superhydrophobic surfaces based on core-shell fossil particles. *Adv. Mater. Interfaces* **2015,** *2*, 1500124-1500131.

38. Nine, M. J.; Cole, M. A.; Johnson, L.; Tran, D. N.; Losic, D., Robust superhydrophobic graphene-based composite coatings with self-cleaning and corrosion barrier properties. *ACS Appl. Mater. Interfaces* **2015,** *7*, 28482-28493.

39. Perera, H. J.; Khatiwada, B. K.; Paul, A.; Mortazavian, H.; Blum, F. D., Superhydrophobic surfaces with silane-treated diatomaceous earth/resin systems. *J. Appl. Polym. Sci.* **2016,** *133*, 44072-44081.

40. Sedai, B. R.; Khatiwada, B. K.; Mortazavian, H.; Blum, F. D., Development of superhydrophobicity in fluorosilane-treated diatomaceous earth polymer coatings. *Appl. Surf. Sci.* **2016,** *386*, 178-186.

41. Brunauer, S.; Emmett, P. H.; Teller, E., Adsorption of gases in multimolecular layers. *J. Am. Chem. Soc.* **1938,** *60*, 309-319.

42. Wenzel, R. N., Surface roughness and contact angle. *J. Phys. Chem.* **1949,** *53*, 1466-1467.

43. Williams, D. L.; Kuhn, A. T.; Amann, M. A.; Hausinger, M. B.; Konarik, M. M.; Nesselrode, E. I., Computerised measurement of contact angles. *Galvanotechnik* **2010,** *101*, 2502-2512.

44. Gadelmawla, E.; Koura, M.; Maksoud, T.; Elewa, I.; Soliman, H., Roughness parameters. *J. Mater. Process. Technol.* **2002,** *123*, 133-145.

45. Yuan, P.; Yang, D.; Lin, Z.; He, H.; Wen, X.; Wang, L.; Deng, F., Influences of pretreatment temperature on the surface silylation of diatomaceous amorphous silica with trimethylchlorosilane. *J. Non-Cryst. Solids* **2006,** *352*, 3762-3771.

46. Ek, S.; Root, A.; Peussa, M.; Niinistö, L., Determination of the hydroxyl group content in silica by thermogravimetry and a comparison with 1H MAS NMR results. *Thermochim. Acta* **2001,** *379*, 201-212.

47. Vansant, E. F.; Van Der Voort, P.; Vrancken, K. C., *Characterization and chemical modification of the silica surface*. Elsevier1995; Vol. 93.

48. Yuan, P.; Liu, D.; Tan, D.-Y.; Liu, K.-K.; Yu, H.-G.; Zhong, Y.-H.; Yuan, A.-H.; Yu, W.-B.; He, H.-P., Surface silylation of mesoporous/macroporous diatomite (diatomaceous earth) and its function in Cu (II) adsorption: The effects of heating pretreatment. *Microporous Mesoporous Mater.* **2013,** *170*, 9-19.

49. Jo, H.; Blum, F. D., Structure and adsorption of 3-acryloxypropyltrimethoxysilane. *Langmuir* **1999,** *15*, 2444-2449.

50. Heitner-Wirguin, C., Infra-red spectra of perfluorinated cation-exchanged membranes. *Polymer* **1979,** *20*, 371-374.

51. Liang, C.; Krimm, S., Infrared spectra of high polymers. III. Polytetrafluoroethylene and polychlorotrifluoroethylene. *J. Chem. Phys.* **1956,** *25*, 563-571.

4.8. SUPPLEMENTARY INFORMATION

S4.1. FTIR spectra of HFIP-TMS

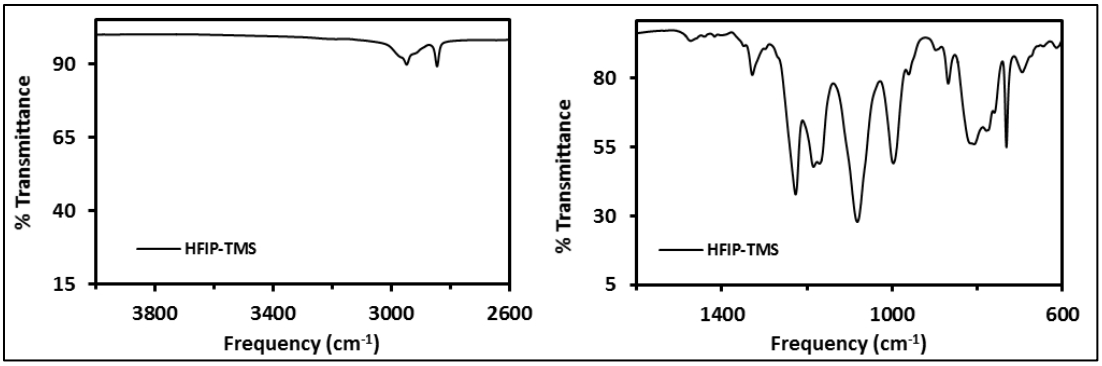

Fig. S4.1. FTIR spectra of HFIP-TMS in two different regions: a) 2600 to 4000 cm^{-1} and b) 600 to 1600 cm^{-1}

S4.2. FTIR spectra of untreated Disk DE, Rod DE and Irreg DE

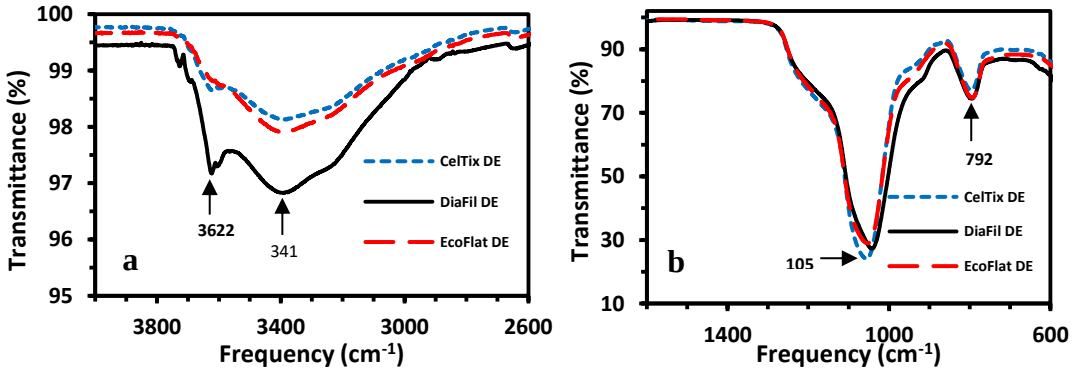

Fig. S4.2. FTIR spectra of different untreated DE samples: in the range a) 600 to 4000 cm^{-1}; b) 600 to 1600 cm^{-1}. The spectra in between 1600 to 2600 is not shown because there was no difference between the samples. The position of intense resonance at around 1050 cm^{-1} is found to be slightly different in DE sample

S4.3. Roughness of treated DE particles coatings

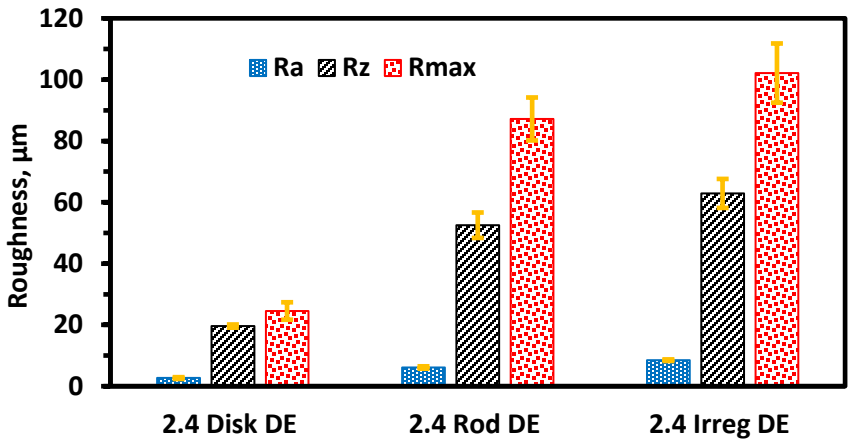

Fig. S4.3. A plot showing roughness parameters, R_a, R_z and R_{max} for bare particle superhydrophobic coatings. The coatings were prepared with the different types of treated DE particles slurry.

CHAPTER V

EFFECT OF VISCOSITY, SOLVENTS AND SONICATION FOR SILANE TREATED DIATOMACEOUS EARTH/POLYSTYRENE SURFACES

5.1. ABSTRACT

The effects of the viscosity of binder solutions, different solvents and sonication on surfaces prepared from treated diatomaceous earth (DE) particles and polystyrenes have been studied. Superhydrophobic DE particles were prepared by treating DE with 3-(heptafluoroisopropoxy)-propyl-trimethoxy-silane (HFIP-TMS). The amount of grafted silane coupling agent in treated DE samples was determined using thermogravimetric analysis (TGA). The presence of HFIP-TMS on the surface of DE was confirmed by Fourier transform infrared spectroscopy (FTIR). The effect of viscosity of the binder solution was observed in coatings prepared with polystyrene of two different number average molecular masses (M_n = 20,000 g/mol. and M_n =280,000 g/mol.) in tetrahydrofuran. For similar overall coating compositions, the coatings mixture with the less viscous binder solution developed superhydrophobicity with fewer treated DE particles. The treated DE particles and polystyrene dispersions in different

solvents; tetrahydrofuran, ethylacetate, dichloromethane and toluene, were also used to make coating mixtures. Treated DE/PS surfaces prepared using all four solvent systems were also subjected to sonication and the sonicated samples were used to make coatings. The sonicated samples also retained the topography required for superhydrophobicity. The coatings were characterized by contact angle measurements and scanning electron microscopy.

5.2. INTRODUCTION

The appropriate roughness of surfaces on the nano and microscale plus low surface energy are required to exhibit superhydrophobicity.[1, 2] The lotus plant, which is well-known for its unique self-cleaning properties, often serves as a natural model for the design of synthetic superhydrophobic surfaces.[3, 4] The surface structure of this plant has two levels of roughness (micro and nanoscales) that traps air under water droplets which has an important contribution to the rolling droplet effect, a well-known characteristic for superhydrophobic surfaces.[5, 6]

Artificial superhydrophobic surfaces inspired from the natural materials have been prepared using different methods. Various techniques such as plasma etching,[7] electrodeposition,[8] laser treatment,[9] sol-gel processing,[10] anionic oxidation,[11] and chemical etching,[12, 13] have been used to make artificial superhydrophobic surfaces. Most of these techniques require complicated multistage processes and several treatments to create artificial surface topography required for superhydrophobicity.

Inexpensive materials with micro- and nano- topography suitable for superhydrophobicity are in demand. One inexpensive material with micro- and nano-topography can be obtained from the skeletons of diatoms is diatomaceous earth (DE).[14] DE has also many unique physical and chemical characteristics,[15-18] such as highly developed mesoporosity and/or macroporosity, strong acid resistance, high mechanical strength and low thermal conductivity. Because of these properties, DE has been used in a variety of applications for high-performance technologies (e.g., microelectronics, chemo- and bio-sensors, and transducers) or as fillers, filters or supports, catalysts, adsorbents, drug delivery and mild abrasives.[19-26] A few applications of DE particles have been reported to prepare superhydrophobic surfaces. Simpson and D'Urso[27] have made superhydrophobic surfaces using perfluorosilane treated DE particles. Mano and coworkers[28] have produced superhydrophobic surfaces using DE by plasma treatment. I. Hejadi et al. have reported the superhydrophobic polypropylene surface prepared by the incorporation of ZnO nanoparticles using phase separation method via simple solution casting.[29] Leonid and coworkers have made superhydrophobic surfaces using polymer-modified DE particles.[30] In our previous work, we have reported the development of superhydrophobicity in HFIP-TMS treated diatomaceous earth particles and polymer coatings.[31] We have identified the minimum amount HFIP-TMS on the surface of DE particles required to achieve superhydrophobic surfaces for a simple polymer treated DE-system. We have also systematically determined the amount of treated DE particles required to make superhydrophobic surfaces.[31]

In this work, the effect of the viscosity of binder on surfaces prepared from treated DE and different molecular masses polystyrenes have been studied. Polystyrene with

different number average molecular masses (M_n = 20,000 and M_n = 280, 000 g/mol.) in THF have been used as binders. Different solvents, tetrahydrofuran (THF), toluene, ethyl acetate (EtOAc) and dichloromethane (DCM) have been used to make coating mixtures. The coating mixtures, prepared in two different solvent systems, were subjected to sonication. The effect of solvents and sonication on the surface topography and superhydrophobicity has also been described.

5.3. MATERIALS AND METHODS

5.3.1. Materials

Untreated diatomaceous earth, CelTix DE, was obtained from Dry Surface Coatings (DSC) (Guthrie, OK). The specific surface area of the DE particles was determined to be 28 m^2/g using Brunner-Emmett-Teller (BET) methods on a NOVA 2200 (Quantachrome, Boynton Beach, FL). 3-(heptafluoroisopropoxy)propyltrimethoxysilane was purchased from Gelest, Inc. (Morrisville, PA). Polystyrene (PS) with number average molecular mass of 20,000 and 280,000 g/mol and *para*-toluenesufonic acid were obtained from Sigma Aldrich (Saint Louis, MO). Tetrahydrofuran (THF), toluene, dichloromethane (DMC) and ethyl acetate (EtOAc) were purchased from Fisher Scientific International Inc. (Hampton, NH).

For the modification of DE, around 20 g of CelTix DE was placed in a plastic bottle; the DE sample was then mixed in 200 ml of toluene. Approximately 1% of *para*-toluenesulfonic acid relative to DE was added into the mixture.[32] With the aid of plastic syringe, 2 ml of HFIP-TMS was added. The mixture was heated to 50 °C and shaken in a mechanical shaker for 4 h. The sample was then centrifuged and the supernatant was

discarded. The mixture in the bottle was washed two times with 200 ml of hexane and methanol to remove excess unreacted fluorosilane and the supernatant was discarded after centrifugation. The content was then left overnight to dry in air. The sample was transferred to a glass bottle and heated to 140 °C for 4 h to remove the solvent and water. The amount of grafted fluorosilane coupling agent was calculated by thermogravimetric analysis using a TA Q-50 (TA Instruments, New Castle, DE).

For the preparation of treated DE-polystyrene surfaces, different amounts of HFIP-TMS treated DE (0 to 70%) were mixed with two different molecular mass polystyrene (M_n = 20,000 and M_n = 280,000 g/mol). Both dilute and concentrated dispersions were made. The concentrated mixtures were dispersed in 7 ml of THF. The mixtures were shaken for 6 h at room temperature. For concentrated (7 ml) coating mixtures, 2 ml of the mixture was used to coat aluminum dishes (I.D. 5 cm x H 1.5 cm). To further investigate the effect of viscosity on HFIP-DE and PS surfaces, the coating mixture of HFIP-DE and PS 280 kDa was diluted 5 times to make dilute dispersions so that the concentrated and dilute coatings would have the same dried mass of solid particles and polymer, the HFIP-DE/PS surfaces were prepared with 10 ml of coating mixtures (5 times more). The coated aluminum dishes were air dried for overnight at room temperature. The coated aluminum substrate was cut in to desired size with a scissors before subjecting them to water droplet and SEM analysis.

To understand the surface properties of treated DE in different solvent systems, treated DE-polystyrene coating mixtures were prepared in THF, toluene, EtOAc and DMC. The mixtures were shaken in mechanical shaker at 5000 rpm for 24 h. Each

coating mixture was prepared by mixing 50% of PS 20 kDa polymer and 50% HFIP-DE. The coatings were prepared by pouring 2 ml of mixtures on aluminum dishes (I.D. 5 cm x H 1.5 cm). The coated samples were dried overnight in air before analysis.

To observe the robustness and surface topography of treated DE particles in different solvent systems, the remaining treated DE-polymer coating mixtures (~ 5ml) prepared in two different solvents (THF and DCM) were diluted with respective solvents and subjected to sonication in an ultra-sonicator (Microson, Farmingdale, NY) for 5 h with output power of 20 watts in continuous mode. Finally, the volume of the coating mixtures were adjusted to an initial volume (~ 5 ml). The coatings were prepared in the same way using 2 ml of the coating mixture and dried well in air.

The relative viscosity of low molecular mass polystyrene (20,000 g/mole) and high molecular mass polystyrene (280,000 g/mole) was determined by using Canon Ubbelohde Viscometer (Col-Parmer Instrument Company, IL). Different percentages polymer solutions were prepared in THF. Time required to flow from upper level to lower level in viscometer was noted for solvent, THF. Then, the same procedure was repeated for the different solutions of polystyrenes. Laboratory temperature was constant (22 °C) throughout the experiments. Densities of the pure solvent, THF and different polymers solutions were calculated using a Pycnometer.

5.3.2. Characterization

High-resolution thermogravimetric analyzer (TA Q-50, TA instruments, New Castle, DE) was used to determine the amounts of HFIP-TMS grafted on the surface of DE. The

samples were heated with a rate of 20 °C/min from room temperature to 950 °C under 40 ml/min of continuous air flow.

A Nicolet iS50 Spectrometer from Thermo Scientific Inc. (Waltham, MA) equipped with a deuterated triglycine sulfate detector and a diamond crystal (45° angle) as an attenuated total reflection accessory was used to take IR spectra of the DE samples. Each spectrum was collected using 64 scans to generate a single beam spectrum at 4 cm^{-1} resolution in the range of 600 to 4000 cm^{-1}.

Scanning electron microscopy (SEM) was used to study the surface topography of treated DE/polystyrne surfaces. The surface topography of the coatings was probed with an FEI Quanta 600 SEM with Evex EDS system (FEI, Hillsboro, OR). The coated aluminum dishes were cut into desired sizes and mounted on aluminum stubs. MED 010 sputter coater (Balzers, Oberkochen, Germany) was used to deposit a very thin layer of palladium/gold metal on the surface of the coating.

A home-built contact angle instrument was used for the contact angle measurements at ambient temperature.[33] Coated samples were cut into desired sizes and about 4 µl of water droplet was placed on the surface. A high-resolution Proscope camera capable of recording 15 fps at a 640 × 480 resolution was used to take water droplet images. The contact angles of the water droplets were determined using LB-ADSA technique.[34] The angle (θ) between the surface and the line tangent to the drop edge was measured using a drop analysis plugin in the ImageJ software. Three water droplet images were taken from different positions on the surfaces for each coating and their average reported.

5.4. RESULTS

Thermogravimetric analysis

The amount of the grafted fluorosilane-coupling agent in the sample was analyzed using TGA. The decomposition thermograms for untreated DE sample and 3-(heptafluoroisopropoxy)-propyl-trimethoxysilane treated DE samples are shown in Fig. 3.1a-b.

The thermogram of an untreated and treated DE samples (Fig. 3.1a) showed the first mass loss of 1.3% in the temperature range of room temperature 30 to 150 ^{o}C. The second mass loss in the temperature range of 150 to 950 ^{o}C for untreated and treated samples (Fig. 3.1a and 3.1b) were 3.6% and 8.3% respectively. The amount of fluorosilane coupling agent in the treated diatomaceous earth is calculated (~ 4.7%) by subtracting the second mass loss of untreated diatomaceous earth from second mass loss of treated diatomaceous earth at 950 °C.

IR Spectra

The grafted fluorosilane silane coupling agents on the surface of DE particles were further confirmed by FTIR spectroscopy as in our previous report.[31] The IR spectra of both untreated and treated sample are shown in two separate regions, 2600 to 4000 cm^{-1} and 600 to 1600 cm^{-1} (Fig. 3.2). Both untreated and treated DE showed broad peaks in the range of 900 - 1300 cm^{-1} and 3000 - 3700 cm^{-1}. In both DE samples, another distinct peak was observed at 795 cm^{-1}. Additional peaks at 696 cm^{-1}, 732 cm^{-1}, 1200 cm^{-1}, 1328 cm^{-1}, 2934 cm^{-1}, 3624 cm^{-1}, and 3722 cm^{-1} were observed only for treated DE samples.[31]

Relative viscosities of polystyrene solutions

The relative viscosities of PS solutions were calculated using the following relation,

$$\eta_r = \frac{\eta}{\eta_\circ} = \frac{t\rho}{t_\circ \rho_\circ}$$

where, η_r = relative viscosity; η = viscosity of polymer solution; η_o = viscosity of pure solvent; t = time of flow for polymer solution; t_o= time of flow for pure solvent; ρ = density of polymer solution; ρ_o = density of pure solvent

The average time of flow, relative and dynamic viscosities of the two different polymer solutions with the same concentration were determined and shown in Table 1.

Table 5.1
Relative viscosities of polystyrene solutions

Samples	Concentration (w/v) % in THF	Average time of flow (sec.)	Densities of Solutions (g/cc)	Relative viscosity (η_r)	Viscosity, η (cP)
PS 20 kDa	2.5	47	0.881	1.4	0.70
	5.0	65	0.883	1.9	0.95
	7.1	77	0.886	2.3	1.15
PS 280 kDa	2.5	132	0.878	3.9	1.95
	5.0	314	0.876	9.3	4.65
	7.1	698	0.888	20.9	10.45

Note: The units for w/v.was g/mL

Contact angle measurements

The wetting behavior of the treated DE (HFIP-DE) and PS coatings was investigated.

The variation of contact angle with increased loadings of HFIP-DE particles in coatings prepared using polystyrene of different viscosities is shown in Fig. 5.1. The hydrophobicity of the coatings increased with increased loading of treated DE particles in the coatings. PS 20 kDa and diluted PS 280 kDa binder systems (low viscosity binders) exhibited almost the same behavior. The surfaces became superhydrophobic at 30% HFIP-DE particle loading for those binder-systems. PS 280 kDa concentrated-binder system showed superhydrophobicity only when HFIP-DE particle loadings exceeded 40%. Past 40% treated DE particle loadings, there was no difference in superhydrophobicity (~ 162°) in all three binder systems.

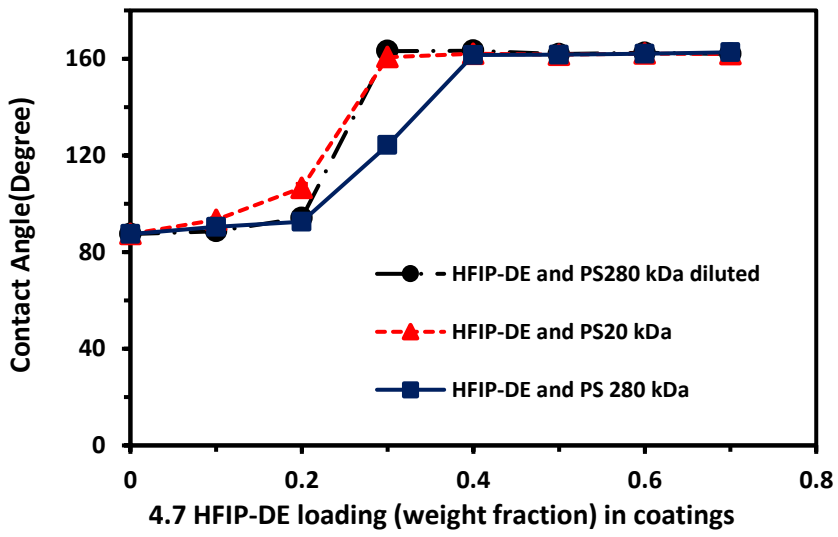

Fig. 5.1. Variation of contact angle as a function of treated DE particle loadings in coatings for different solutions.

Surface structures of coatings with PS 20 kDa and PS 280 kDa in 7 ml (concentrated) coatings mixture

SEM images were taken to observe the differences in the surface topography of HFIP-DE/PS 20 kDa and HFIP-DE/PS 280 kDa surfaces (Fig. 5.2). SEM images of HFIP-DE/PS 20 kDa surfaces with different percentages of particle loadings (20% and 30%) are shown in Fig. 5.2a-b. HFIP-DE/PS 280 kDa surfaces with different percentages of particle loadings (20% and 30%) HFIP-DE are shown in Fig. 5.2c-d. In both binder-systems, at 10% particles loadings, top surface was mostly covered with polymer (Fig. S5.1 Supplementary Information). Coatings with 20% of DE particles and PS 20 kDa, showed more treated particles on the top surface as compared to HFIP-DE/PS 280 kDa surfaces. In coatings with 30% DE particles and PS 20 kDa, there was no visible polystyrene on the top surfaces, but for the coatings prepared with the same amount of HFIP-DE and PS 280 kDa, the DE particles covered with polystyrenes were observed on the top surface. In both binder systems, at 40% DE particle loadings, the surface structures appeared similar, top surfaces were covered with DE particles and no polystyrene was observed (Fig. S5.1).

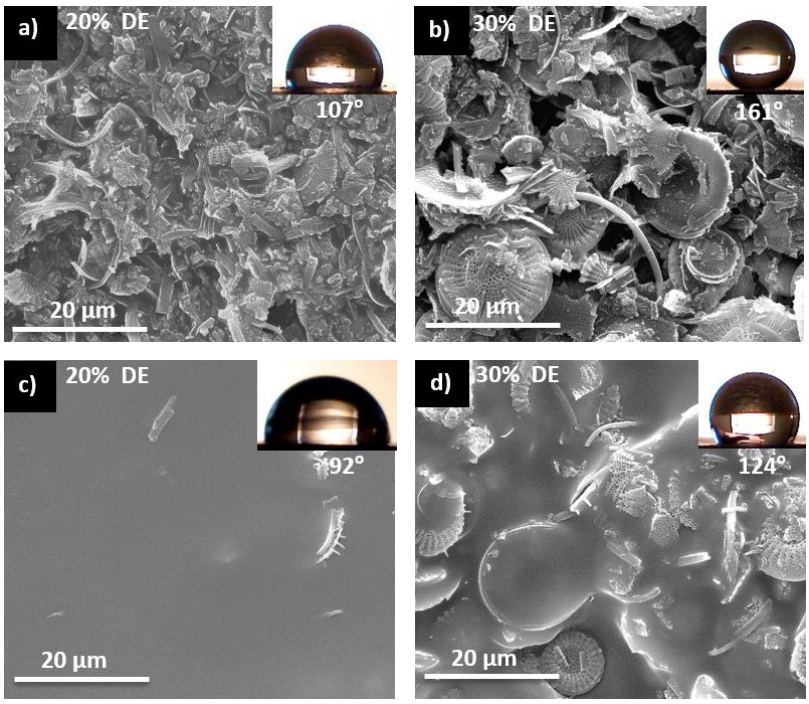

Fig. 5.2. SEM images for PS 20 kDa and HFIP-DE a) 20%, b) 30% surfaces; for PS 280 kDa and HFIP-DE c) 20%, d) 30% surfaces; scale bars are 20 µm. The coating mixtures were prepared in 7 ml THF.

Surface structures of coatings with PS 280 kDa in dilute coatings mixtures

To understand the effect of viscosity, the PS 280 kDa binder system was diluted 5 times. The surface structures of coatings prepared with different percentages of HFIP-DE (20 and 30 %) and PS 280 kDa in dilute (35 ml) coating mixtures are shown in Fig. 5.3. At 20% DE particle loading, mostly polystyrene was observed on the top surfaces and DE particles can be hardly seen. At 30% particle loading, lighter fragments of DE particles were observed on the top surface and at 40 % DE particles in coatings (Fig. S5.2 in Supporting Information), top surfaces in both coatings were completely covered with HFIP-DE particles and surfaces exhibited contact angles ~163^{o}.

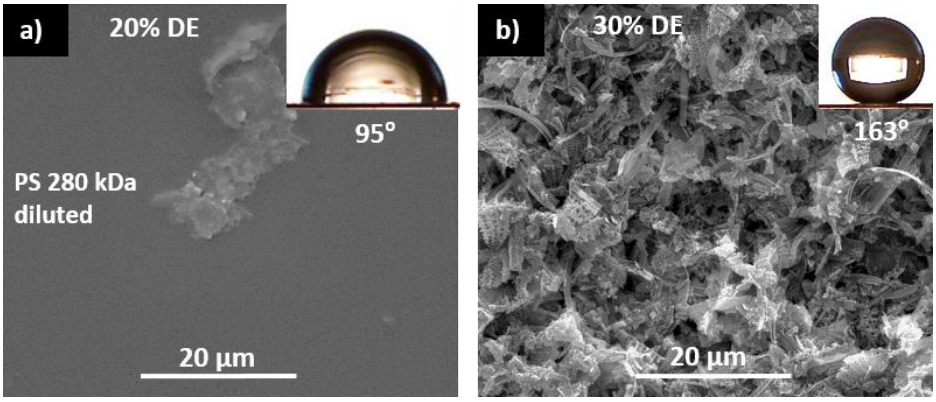

Fig. 5.3. SEM images for PS 280 kDa and HFIP-DE at furfaces a) 20%, b) 30% particle loadings. The coating mixtures were prepared with 35 ml of THF. Surfaces with diluted coating mixtures showed more particles on the top surfaces. The scale bars are 20 µm.

Effect of solvents on the surface topography and superhydrophobicity of coatings

To observe the effect of solvents on the HFIP-DE particles, four different solvents were chosen to make coating mixtures of HFIP-DE and PS 20 kDa. The surface structures and superhydrophobicity of HFIP-DE/PS 20 kDa coatings are shown in Fig. 5.6a-d. The top surface of all coatings showed some broken and intact DE particles. The contact angles on the surfaces were approximately 162º.

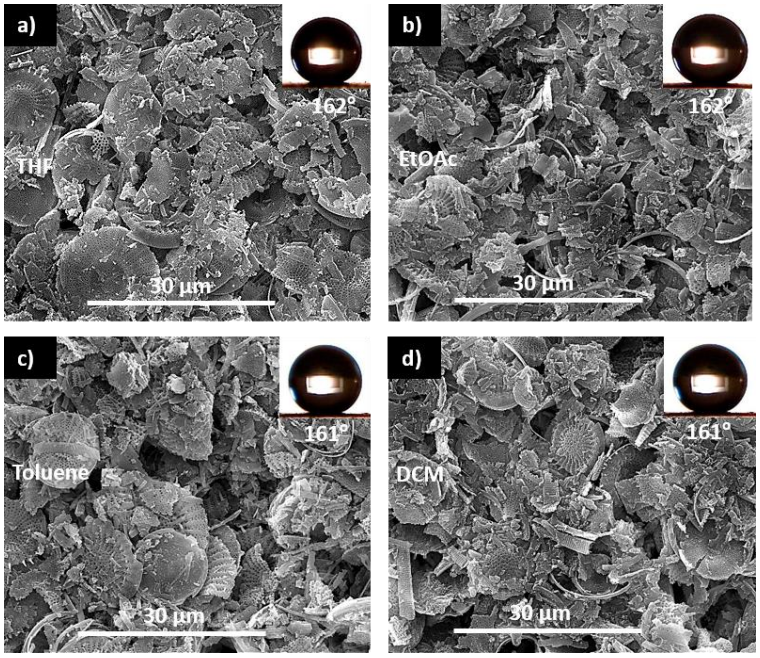

Fig. 5.4. Coatings prepared using different solvents: a) THF, b) EtOAc, c) toluene and d) DMC. The scale bars are 30 µm. Fragmented treated DE particles were observed on the top surface. With all solvent systems surface topography and water contact angles were almost same.

Effect of sonication on surface topography and superhydrophobicity

To understand the effect of sonication, HFIP-DE particles mixtures with PS 20 kDa in two different solvents, THF and DCM, were subjected to ultrasonic disruption for 5 h. The top view of HFIP-DE/polystyrene surfaces prepared with sonicated coating mixtures are shown in Fig. 5.5a-b. Both surfaces exhibited superhydrophobicity with contact angle of ~150^{o}. Contact angles were approximately 10^{o} less than surfaces prepared from mixtures without sonication.

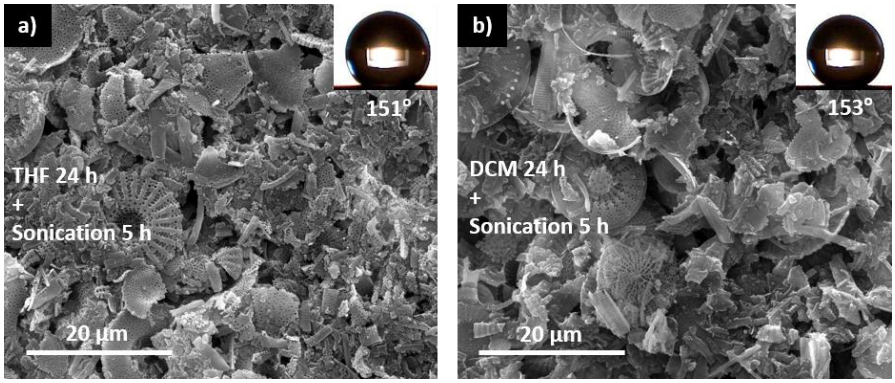

Fig. 5.5. Effect of sonication on the surface structure and superhydrophobicity a) for coating mixture in THF; b) coating mixture in DCM. Both samplaes were shaken for 24 h and sonicated for 5 h. The scale bars are 20 µm. Even after 5 h of sonication, in both solvents, intact DE particles were observed.

5.5. DISCUSSION

Thermogravimetric analysis

DE particles contain some extent of physically bound water molecules. The first mass loss in the temperature range of 30 to 150 ^{o}C in Fig. 3.1 was expected due to the loss of different types of physically bound water molecules and removal of some hydroxyl groups present in the silica surface of porous diatomaceous earth particles.[35] The first mass loss for untreated DE and the treated DE sample were same. Some water molecules bound on the surface of the DE particles were involved in the hydrolysis of HFIP-TMS because there was no external water added during the reaction of DE. The treated DE samples were washed two times with organic solvents (hexane and methanol). So, the remaining negligible amount of unbound hydrolyzed HFIP-TMS (boiling point = 147 °C)

and physically adsorbed water molecules are expected to come off around 150 °C. The untreated DE contains various inorganic substances and the chemical analysis of DE particles in previous works have shown that the main ingredients are SiO_2 90.08%, Al_2O_3 5.53% and Fe_2O_3 1.52%.[26, 36] The second mass loss for untreated DE was 3.6% (Fig. 3.1a), this mass loss was due to decomposition of the inorganic substances present in the DE. The thermograms of HFIP-DE (Fig. 3.1) showed the second mass loss (8.4%) in the temperature range of 150 to 950 ºC. This mass loss represents the decomposition of fluorosilane plus inorganic substances in DE. The amount of fluorosilane coupling agent grafted on the surface of DE particles was calculated by subtracting the second mass loss of untreated DE from second mass loss of HFIP-DE at 950 °C.

FTIR of DE samples

The IR spectra of untreated DE have previously been reported.[26, 37] The peaks at 1050 and 1200 cm^{-1} in Fig. 3.2 for untreated DE were assigned to the in-plane Si-O stretching mode. The intense peak at 795 cm^{-1} was due to symmetric Si-O stretching.[26] Additional peaks which exist only for treated DE at 696 cm^{-1} and 732 cm^{-1} were attributed to the vibration of C-F bond in polyfluorocarbon region of the fluorosilane.[38, 39] The spectrum of CelTix DE shows only one broad band centered at approximately 3400 cm^{-1} in the hydroxyl region 3000 - 3750 cm^{-1} which is attributed to the -OH vibration of the physically adsorbed H_2O and -OH from silanols of DE samples.[26] The IR spectrum of the HFIP-modified DE exhibits some new vibrations compared to those of the unmodified DE in Fig. 3.2, including CH_2 stretching (2934 cm^{-1}), and CH_2 deformation (1328 cm^{-1}). The decrease in the intensity of peaks for treated DE in the region 3000 – 3750 cm^{-1} was

expected due to loss of some of the silanols –OH from the DE surface. Increased intensity of the resonances, at 1050 cm^{-1} and 795 cm^{-1} in treated DE as compared to untreated DE was considered due to the formation of new Si-O bonds in the treated samples between DE particles and silane coupling agent. The peaks at 3600-3750 cm^{-1} were attributed to the O-H stretching of the silanols in the hydrolyzed HFIP-TMS. These results confirm the presense of silane in the particles..

Effect of viscosity on HFIP-DE/PS surfaces

To understand the effect of viscosity, HFIP-DE/polystyrene surfaces prepared using coating mixtures with polystyrenes of different viscosities were compared. The relative viscosity results (Table. 1) showed that at the same percentage (w/v) solution of PS20 kDa in THF was much less viscous than the PS280 kDa. Viscosity of polymer solutions obviously depends on chain lengths. At the same composition by mass, a solution of high molecular weight polystyrene is much more viscous than low molecular weight polystyrene solution.[40-42]

For less viscous polymer binder systems, more treated DE particles were observed at the air-surface interface (Fig.5.2a and 5.2c). At 20% HFIP-DE particle loading, HFIP-DE/PS 20kDa surfaces had more exposed DE particles and was more hydrophobic 107^{o} (Fig. 5.2a) compared to HFIP-DE/PS280 kDa surface (Fig. 5.2c). At 30% HFIP-DE particle loadings, Fig. 5.2b and 5.2d, clearly revealed that in the PS 20 kDa binder-system, the HFIP-DE particles moved easily to air-surface interface as compared to PS 280 kDa binder-system. For the PS 20 kDa binder-system, at 30% DE particle loading, the top surface of the coatings were completely covered with HFIP-DE particles and

polymer molecules were not visible. So, surface was superhydrophobic and water droplet contact angle was ~162^{o}. In contrast, the top view of HFIP-DE/PS280 kDa surface at 30% particles loading, showed the visible polystyrene on the surface. The surface was not superhydrophobic. The water droplet contact angle on that surface was 124^{o}. The HFIP-DE/PS surfaces, for both binder systems, at 10% and 40% particle loadings, showed no visible difference in both surface structure and hydrophobicity (Fig. S5.1 in Supplementaty Information).

The effect of viscosity was also observed on HFIP-DE and PS surfaces prepared from the diluted coating mixture of HFIP-DE and PS 280kDa. Diluted PS 280 kDa binder-system in Fig. 5.3a and 5.3b compared with the concentrated PS 280 kDa binder-system (Fig. 5.2c and 5.2d) showed more treated DE particles exposed at 20% DE particles for diluted binder-system. At 30% particles in the coatings, for diluted binder-system the top surface was covered with treated DE particles and the surface was superhydrophobic but for concentrated binder-system treated HFIP-DE particles were with polymer and surface was not superhydrophobic.

Effect of solvents on the surface topography and superhydrophobicity

The effect of solvents was observed on the HFIP-DE/PS surfaces which were prepared by mixing the HFIP-DE particles with different solvents and PS 20kDa in a mechanical shaker for 24 h. 4.7 HFIP-DE/PS 20 kDa surfaces (Fig. 5.4a-d) prepared with treated DE particles and 50% PS 20 kDa in different solvents clearly showed that treated DE particles behaved in the same way in different solvent systems. HFIP-DE/PS 20 kDa surfaces in all solvents were superhydrophobic. SEM images of those surfaces (Fig. 5.4a-

d) showed most of the DE particles were broken and few DE particles were intact. Although treated DE particles were shaken in a mechanical shaker for 24 h at 5000 rpm in different solvents, there was no significant difference in the water droplet contact angles and the surface topography. Results showed that DE particles were not affected much by solvents and shaking in a mechanical shaker for 24 h.

Effect of sonication on surface topography and superhydrophobicity

The robustness of HFIP-DE particles were observed by subjecting the HFIP-DE particles to sonication for 5 h in two different solvents. Water droplet contact angle analysis of the surfaces prepared from sonicated HFIP-DE particles in THF and DCM for 5 h (Fig. 5.5a-b) showed that the coating surfaces were superhydrophobic. Although the contact angles were around 150^{o}, which was less than the surface prepared from mixtures without sonication, SEM images revealed that the surfaces were covered with mostly broken and few intact DE particles. The broken pieces of DE were more on coating mixtures prepared in THF than in DCM. But in both surfaces, intact DE particles were present. This result indicated that DE particles were robust. Treated DE particles can tolerate extreme physical condition like sonication for 5 h in different solvents and exhibit the topography required for superhydrophobicity.

5.6. CONCLUSIONS

The viscosity of the binders used to prepare coating mixture was found to affect the development of superhydrophobicity on HFIP-DE/PS surfaces. The less viscous the coating mixtures, the more easily the HFIP-DE move towards the air-coating interface.

Superhydrophobic surfaces resulted with fewer HFIP-DE particles in less viscous coating mixtures. All the solvent systems showed the similar topographies and similar superhydrophobicity. We believe that almost any solvent system which is compatible with treated DE particles and the polymer can be used to prepare superhydrophobic surfaces. The sonicated coating mixture showed the topography required for the superhydophobic surfaces which indicated that HFIP-DE particles can tolerate extreme physical condition without losing their inherent micro-nano morphology.

5.7. REFERENCES

1. Michael, N.; Bhushan, B., Hierarchical roughness makes superhydrophobic states stable. *Microelectron. Eng.* **2007,** *84*, 382-386.
2. Öner, D.; McCarthy, T. J., Ultrahydrophobic surfaces. Effects of topography length scales on wettability. *Langmuir* **2000,** *16*, 7777-7782.
3. Patankar, N. A., Mimicking the lotus effect: influence of double roughness structures and slender pillars. *Langmuir* **2004,** *20*, 8209-8213.
4. Barthlott, W.; Neinhuis, C., Purity of the sacred lotus, or escape from contamination in biological surfaces. *Planta* **1997,** *202*, 1-8.
5. Zhang, L.; Li, Y.; Sun, J.; Shen, J., Layer-by-layer fabrication of broad-band superhydrophobic antireflection coatings in near-infrared region. *J. Colloid Interface Sci.* **2008,** *319*, 302-308.

6. Ma, M.; Hill, R. M., Superhydrophobic surfaces. *Curr. Opin. Colloid Interface Sci.* **2006,** *11*, 193-202.

7. Olde Riekerink, M.; Terlingen, J.; Engbers, G.; Feijen, J., Selective etching of semicrystalline polymers: CF4 gas plasma treatment of poly (ethylene). *Langmuir* **1999,** *15*, 4847-4856.

8. Shirtcliffe, N. J.; McHale, G.; Newton, M. I.; Perry, C. C., Wetting and wetting transitions on copper-based super-hydrophobic surfaces. *Langmuir* **2005,** *21*, 937-943.

9. Khorasani, M.; Mirzadeh, H.; Kermani, Z., Wettability of porous polydimethylsiloxane surface: morphology study. *Appl. Surf. Sci.* **2005,** *242*, 339-345.

10. Nakajima, A.; Fujishima, A.; Hashimoto, K.; Watanabe, T., Preparation of transparent superhydrophobic boehmite and silica films by sublimation of aluminum acetylacetonate. *Adv. Mater.* **1999,** *11*, 1365-1368.

11. Masuda, H.; Yada, K.; Osaka, A., Self-ordering of cell configuration of anodic porous alumina with large-size pores in phosphoric acid solution. *Jpn. J. Appl. Phys.* **1998,** *37*, L1340.

12. Thieme, M.; Frenzel, R.; Schmidt, S.; Simon, F.; Hennig, A.; Worch, H.; Lunkwitz, K.; Scharnweber, D., Generation of ultrahydrophobic properties of aluminium-a first step to self-cleaning transparently coated metal surfaces. *Adv. Eng. Mater.* **2001,** *3*, 691-695.

13. Qian, B.; Shen, Z., Fabrication of superhydrophobic surfaces by dislocation-selective chemical etching on aluminum, copper, and zinc substrates. *Langmuir* **2005,** *21*, 9007-9009.

14. Fuhrmann, T.; Landwehr, S.; El Rharbi-Kucki, M.; Sumper, M., Diatoms as living photonic crystals. *Appl. Phys. B* **2004,** *78*, 257-260.

15. Yu, Y.; Addai-Mensah, J.; Losic, D., Synthesis of self-supporting gold microstructures with three-dimensional morphologies by direct replication of diatom templates. *Langmuir* **2010,** *26*, 14068-14072.

16. van Garderen, N.; Clemens, F. J.; Kaufmann, J.; Urbanek, M.; Binkowski, M.; Graule, T.; Aneziris, C. G., Pore analyses of highly porous diatomite and clay based materials for fluidized bed reactors. *Microporous Mesoporous Mater.* **2012,** *151*, 255-263.

17. Yuan, P.; Liu, D.; Fan, M.; Yang, D.; Zhu, R.; Ge, F.; Zhu, J.; He, H., Removal of hexavalent chromium [Cr (VI)] from aqueous solutions by the diatomite-supported/unsupported magnetite nanoparticles. *J. Hazard. Mater.* **2010,** *173*, 614-621.

18. Skubiszewska-Zięba, J.; Charmas, B.; Leboda, R.; Gun'ko, V., Carbon-mineral adsorbents with a diatomaceous earth/perlite matrix modified by carbon deposits. *Microporous Mesoporous Mater.* **2012,** *156*, 209-216.

19. Ivanov, S.; Belyakov, A., Diatomite and its applications. *Glass Ceram.* **2008,** *65*, 48-51.

20. Lopez, P. J.; Descles, J.; Allen, A. E.; Bowler, C., Prospects in diatom research. *Curr. Opin. Biotechnol.* **2005,** *16*, 180-186.

21. Aw, M. S.; Simovic, S.; Yu, Y.; Addai-Mensah, J.; Losic, D., Porous silica microshells from diatoms as biocarrier for drug delivery applications. *Powder Technol.* **2012,** *223*, 52-58.

22. Aw, M. S.; Bariana, M.; Yu, Y.; Addai-Mensah, J.; Losic, D., Surface-functionalized diatom microcapsules for drug delivery of water-insoluble drugs. *J. Biomater. Appl.* **2013,** *28*, 163-174.

23. Bariana, M.; Aw, M. S.; Kurkuri, M.; Losic, D., Tuning drug loading and release properties of diatom silica microparticles by surface modifications. *Int. J. Pharm.* **2013,** *443*, 230-241.

24. Li, X.; Li, X.; Wang, G., Surface modification of diatomite using polyaniline. *Mater. Chem. Phys.* **2007,** *102*, 140-143.

25. Wang, B.; Smith, T. R., Performance of a diatomite-based sorbent in removing mercury from aqueous and oil matrices. *J. Environ. Eng. Sci.* **2007,** *6*, 469-476.

26. Yuan, P.; Liu, D.; Tan, D. Y.; Liu, K. K.; Yu, H. G.; Zhong, Y. H.; Yuan, A. H.; Yu, W. B.; He, H. P., Surface silylation of mesoporous/macroporous diatomite (diatomaceous earth) and its function in Cu (II) adsorption: the effects of heating pretreatment. *Microporous Mesoporous Mater.* **2013,** *170*, 9-19.

27. Simpson, J. T.; D'urso, B. R., Superhydrophobic diatomaceous earth. U.S. Patent No. 8,216,6742012.

28. Oliveira, N. M.; Reis, R. L.; Mano, J. F., Superhydrophobic surfaces engineered using diatomaceous earth. *ACS Appl. Mater. Interfaces* **2013,** *5*, 4202-4208.

29. Hejazi, I.; Hajalizadeh, B.; Seyfi, J.; Sadeghi, G. M. M.; Jafari, S.-H.; Khonakdar, H. A., Role of nanoparticles in phase separation and final morphology of

superhydrophobic polypropylene/zinc oxide nanocomposite surfaces. *Appl. Surf. Sci.* **2014,** *293*, 116-123.

30. Puretskiy, N.; Chanda, J.; Stoychev, G.; Synytska, A.; Ionov, L., Anti-icing superhydrophobic surfaces based on core-shell fossil particles. *Adv. Mater. Interfaces* **2015,** *2*, 1500124-1500131.

31. Sedai, B. R.; Khatiwada, B. K.; Mortazavian, H.; Blum, F. D., Development of superhydrophobicity in fluorosilane-treated diatomaceous earth polymer coatings. *Appl. Surf. Sci.* **2016,** *386*, 178-186.

32. García, N.; Benito, E.; Guzmán, J.; Tiemblo, P., Use of p-toluenesulfonic acid for the controlled grafting of alkoxysilanes onto silanol containing surfaces: preparation of tunable hydrophilic, hydrophobic, and super-hydrophobic silica. *J. Am. Chem. Soc.* **2007,** *129*, 5052-5060.

33. Wenzel, R. N., Surface roughness and contact angle. *J. Phys. Chem.* **1949,** *53*, 1466-1467.

34. Williams, D. L.; Kuhn, A. T.; Amann, M. A.; Hausinger, M. B.; Konarik, M. M.; Nesselrode, E. I., Computerised measurement of contact angles. *Galvanotechnik* **2010,** *101*, 2502-2512.

35. Zhuravlev, L., The surface chemistry of amorphous silica. Zhuravlev model. *Colloids Surf., A* **2000,** *173*, 1-38.

36. Gulturk, E.; Guden, M., Thermal and acid treatment of diatom frustules. *J. Achievements Mater. Manuf. Eng* **2011,** *46*, 196-203.

37. Tsai, W. T.; Lai, C. W.; Hsien, K. J., Characterization and adsorption properties of diatomaceous earth modified by hydrofluoric acid etching. *J. Colloid Interface Sci.* **2006,** *297*, 749-754.

38. Heitner-Wirguin, C., Infra-red spectra of perfluorinated cation-exchanged membranes. *Polymer* **1979,** *20*, 371-374.

39. Liang, C. Y.; Krimm, S., Infrared spectra of high polymers. III. Polytetrafluoroethylene and polychlorotrifluoroethylene. *J. Chem. Phys.* **1956,** *25*, 563-571.

40. Fox Jr, T. G.; Flory, P. J., Viscosity molecular weight and viscosity temperature relationships for polystyrene and polyisobutylene1, 2. *J. Am. Chem. Soc.* **1948,** *70*, 2384-2395.

41. Bueche, F., Viscosity, self-diffusion, and allied effects in solid polymers. *J. Chem. Phys.* **1952,** *20*, 1959-1964.

42. Fox, T.; Loshaek, S., Isothermal viscosity-molecular weight dependence for long polymer chains. *J. Appl. Phys.* **1955,** *26*, 1080-1082.

5.8. SUPPLEMENTARY INFORMATION

S5.1. DE and PS 20 (kDa and PS 280 kDa) coatings

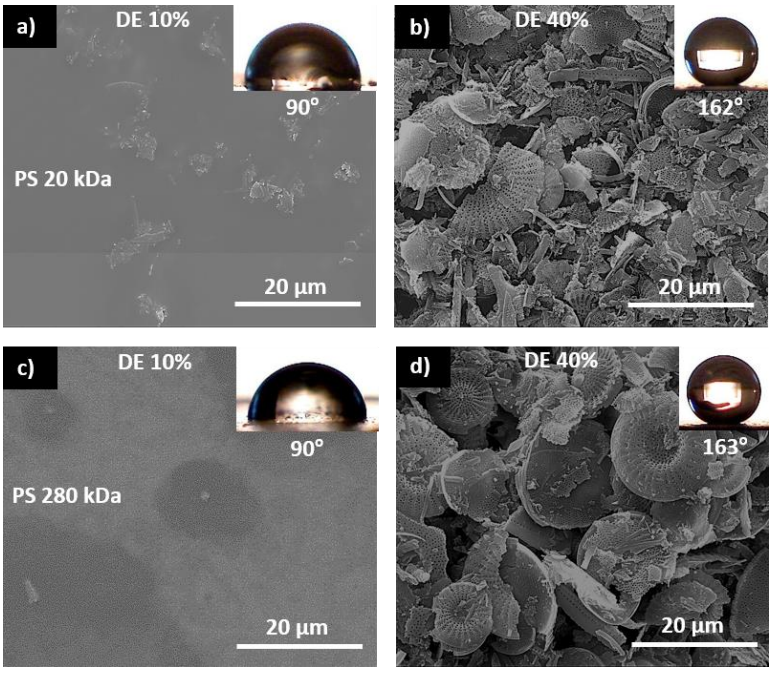

Fig. S5.1. SEM images for PS 20 kDa and HFIP-DE a) 10% b) 40%; for PS 280 kDa c) 10% and d) 40% coatings. Scale bars are 20 µm. The coating mixtures were prepared in 7 ml THF

S5.2. PS280 kDa and HFIP-DE coatings in dilute solution

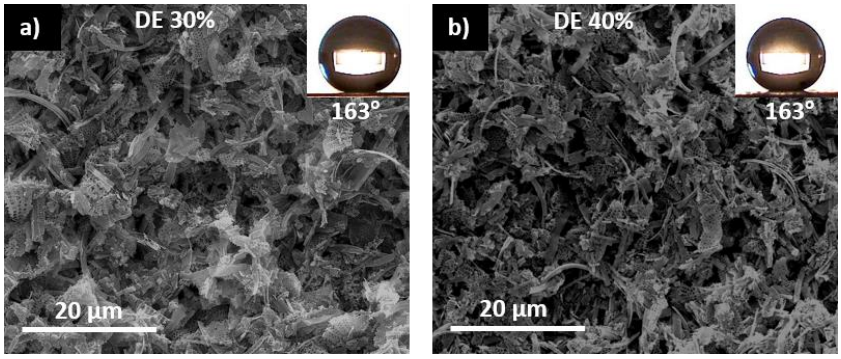

Fig. S5.2. SEM images for PS 280 KDa and HFIP-DE a) 30% and b) 40%; scale bars are 20 µm. The coating mixtures were prepared in 35 ml of THF.

CHAPTER VI

THERMAL AND DYNAMIC MECHANICAL ANALYSIS OF TREATED DIATOMACEOUS EARTH AND EPOXY COMPOSITES

6.1. ABSTRACT

Thermal and dynamic mechanical analysis of composites prepared from untreated diatomaceous earth (DE) (circular), treated diatomaceous earth (DE), and epoxy resin have been studied. Untreated diatomaceous earth is a superhydrophilic material. Treatment of diatomaceous earth with fluorosilane and non-fluorosilane silane coupling agents converts it into a superhydrophobic material. The amount of grafted silane coupling agent on the surface of DE particles was determined by thermogravimetric analysis (TGA). Superhydrophobic DE has potential application in preparation of hydrophobic and corrosion resistant coatings. Untreated DE/epoxy, fluorosilane treated DE/epoxy and non-fluorosilane treated DE/epoxy composites were prepared. The composite materials were prepared using 15 wt% of untreated and treated DE filler. The amount of filler in the composites were confirmed with thermogravimetric analysis. The storage modulus of the composites was found to increase with the incorporation of untreated and treated DE particles in an epoxy matrix. A shift in tan δ peak was observed in the DE/epoxy composites which indicated increase in the glass transition temperature of the composite as compared to bulk epoxy. The thermal properties of those composites

have also been studied using thermogravimetric analysis and differential scanning calorimetry.

6.2. INTRODUCTION

Materials with potential application for making superhydrophobic coatings can consist of skeletons from diatoms.[1] Diatoms are single-celled algae and the fossilized cell diatoms skeletons are called diatomite or diatomaceous earth (DE) or kieselguhr. The dimensions of amorphous silica skeletons range from about 1 to 500 μm. The regular features distributed on the frustules walls possess characteristic dimensions of 10 to 200 nm.[1, 2] DE is an abundant, inexpensive material and extensively used in many applications like: sound and heat insulation; chemical reactions as catalysts; sensor components; dynamite; pool water, beer and wine filtration; absorption; and gel filtration.[3-6] DE and its modified forms have been used in various other applications such as adsorption of heavy metals,[7-12] synthesis of zeolites,[13] removal of dyes,[14-16] waste water treatment,[17-19] cement production,[20] drug delivery,[21] nanotechnology,[22] chromatography[23] and fabrication of superhydrophobic surfaces.[1, 24-27]

Many reports are available related to the reinforcement of epoxy matrix with the incorporation of particle fillers and fibers. Researchers have reported the reinforcement of epoxy matrix with improved mechanical properties after the incorporation of natural fiber.[28, 29] Researchers have also shown that nanoparticles incorporated epoxy composite materials exhibits superior mechanical properties compared to neat matrix polymer or epoxy composites with micro-size fillers.[30-32] According to Lee et al.,[33] epoxy resin

matrix filled with carbon black exhibits improvement in electrical and flexural properties of composites. Papanicolau and coworkers have studied the effect of nanotube dispersion on the dynamic mechanical properties of epoxy nanocomposites.[34] Amendola et. al, have performed dynamic mechanical analysis of ceramic-reinforced epoxy nanocomposites and showed their use in electrical insulation.[35] The thermo-mechanical properties of epoxy/MWCNT composite samples containing various amounts of multi-walled carbon nanotubes (MWCNT) have been studied.[36] Tasdemirci and coworkers[37,38] have reported the use of rod shaped diatom frustules as reinforcements and fillers in polymeric materials. They have noted that 15% diatom frustule filling increases both modulus and yield strength of the epoxy matrix. Treatment of DE with ~4% of silane coupling agent changes its water repellent properties dramatically.[39] However, the effect of superhydrophobic treated DE particles on the mechanical properties of polymeric materials has not known yet been reported.

We have previously reported the development of superhydrophobicity in coatings prepared from diatomaceous earth and simple polymers as binder system.[39] In this work, composites of untreated DE, non-fluorosilane treated DE and fluorosilane treated DE have been prepared. The dynamic mechanical analysis of treated DE/epoxy and untreated DE/epoxy composites has been performed. The thermal properties of the composites have also been studied using differential scanning calorimetry.

6.3. MATERIALS AND METHODS

6.3.1. Materials

Untreated diatomaceous earth, Celtix DE, and fluorosilane (FS) treated diatomaceous earth (FS DE) were received from Dry Surface Coatings, Guthrie, OK. Epon resin 828 was from Momentive, USA. Ancamine 2280 curing agent was obtained from Air Products, USA. Octadecyltrimethoxysilane was purchased from, Gelest Inc., USA. *para*-toluene sulfonic acid, tetrahydrofuran, acetone and toluene were purchased from Sigma Aldrich, USA. All these materials were used as received.

Treatment of DE with non-fluorosilane

Non-fluorosilane treated samples were prepared in our laboratory. 20 g of the DE sample was dispersed in 200 mL toluene in a plastic bottle and then 0.2 g (1 wt%) of *para*-toluene sulfonic acid was added to the mixture. 2 g of octadecyltrimethoxysilane was added. The whole contents in the plastic bottle were shaken in mechanical shaker at 50 ^{o}C for 4 h. The solvent was removed after centrifugation. The mixture contents were washed two times with 200 ml of hexane. The contents were then dried in air for 24 h. The mixture was again heated at 140 ^{o}C for 4h to remove water, solvent and other volatile impurities.

The treated and untreated bulk DE samples were tested for their hydrophobicity. For the hydrophobicity test, both treated and untreated DE samples (0.05 g) were dispersed in 0.5 ml of THF. The resulting slurry was used to coat the surface of microscopic glass coverslips and dried in air. The contact angle for water reported were the average of three measurements on the surface of DE sample.

Epoxy and DE composites preparations

Treated and untreated diatomaceous earth samples 9.0 g (15 wt%) were dispersed in a minimum amount of acetone and 10 ml tetrahydrofuran was added. Epon 828 (54.4 wt%) and ancamine 2280 (30.6 wt.%) in the ratio 1.8:1 was added to the mixture. The mixtures were mixed well with a magnetic stirrer for 1 h and the contents were then degassed to remove air bubbles for 2 h. The mixture was poured in to a steel mold and allowed to cure at room temperature for 4 days. The samples were detached carefully from the mold and further cured at 140 ^{o}C for 24 h. All the cure samples had dimensions of 50 mm x 12 mm x 2 mm.

6.3.2. Characterization

The compositions of treated DE and epoxy-DE composites were analyzed by high-resolution thermogravimetric analysis (TA Q-50, TA instruments, New Castle, DE). The samples were heated with a rate of 20 °C/min from room temperature to 950 °C under 40 ml/min of continuous nitrogen flow.

The IR spectra of DE samples were collected using a Nicolet iS50 Spectrometer Thermo Scientific Inc. (Waltham, MA) equipped with a deuterated triglycine sulfate detector and a diamond crystal (45° angle) as an attenuated total reflection (ATR) accessory. Each sample was run using 64 scans versus the background that was also collected using 64 scans to generate a single beam spectrum at 4 cm^{-1} resolution in the range of 600 to 4000 cm^{-1}.

The water contact angle measurements were conducted using a home-built contact angle apparatus at ambient temperature.[40] The instrument had a moveable stage for the coated sample and the water droplet was added using a pipette. About 4 µl of water droplet was placed on the surface. Water droplet images were taken with a high-resolution Proscope camera capable of recoding 15 fps at a 640 × 480 resolution. The LB-ADSA technique was used to determine the contact angle of the water droplet images on the surface.[41] The angle (θ) between the surface and the line tangent to the drop edge was measured using a drop analysis plugin in the ImageJ software. Three water droplet images were taken from different positions on the surfaces for each coating.

Scanning electron microscopy (SEM) was used to study the surface properties of diatomaceous earth particles. The surface morphology of the prepared DE sample was probed with FEI Quanta 600 SEM with Evex EDS system (FEI, Hillsboro, OR, USA). The SEM samples were prepared by mounting a piece of coating on an aluminum stub with the help of two-sided sticky graphite tape. The samples were coated with very thin layer of palladium/gold metal with the help of MED 010 sputter coater (Balzers, Oberkochen, Germany) to make them conductive.

A dual cantilever clamp of the dynamic mechanical analyzer, DMA Q800 (TA Instruments) was used for dynamic mechanic analysis. The specimen dimension used was 50 x 12 x 2 mm^3. The temperature range over which these properties measured were 35-250 ^oC at a heating rate of 5 ^oC/min. The tests were carried out at frequencies of 1, 10 and 30 Hz under tensile mode.

Differential scanning calorimetry (DSC) was performed in standard mode with a DSC instrument (Q2000, TA Instruments) attached with RCS 90 as a cooling unit. About 5-10 mg of sample was prepared in an aluminum pan. The sample was placed in the DSC cell, referenced against an empty pan and heated from 35 °C to 250 °C with heating rate of 5 °C/min under nitrogen atmosphere.

6.4. RESULTS

Thermogravimetric analysis of DE samples

The amount of the grafted silane coupling agent in the samples was analyzed using thermogravimetric analysis (TGA). The decomposition thermograms for DE and fluorosilane and non-fluorosilane treated DE samples are shown in Figs. 6.1, 6.2 and 6.3.

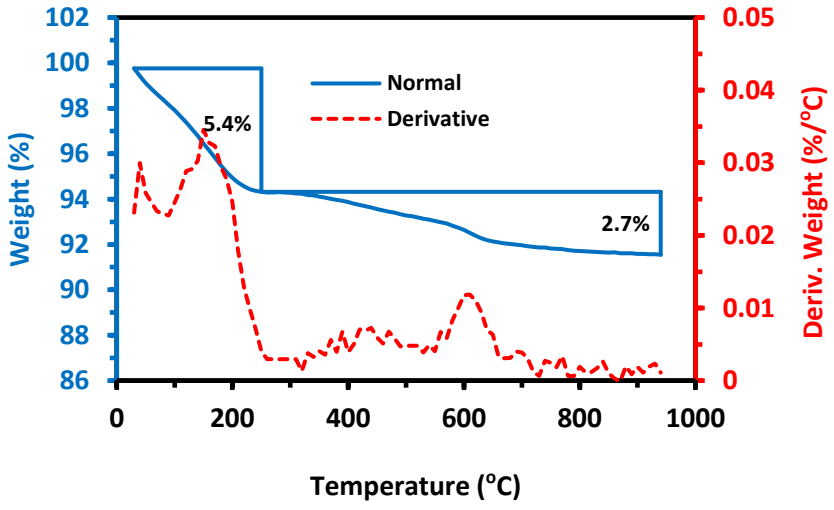

Fig. 6.1. TGA plots showing weight loss for untreated DE in normal and derivative modes for untreated DE.

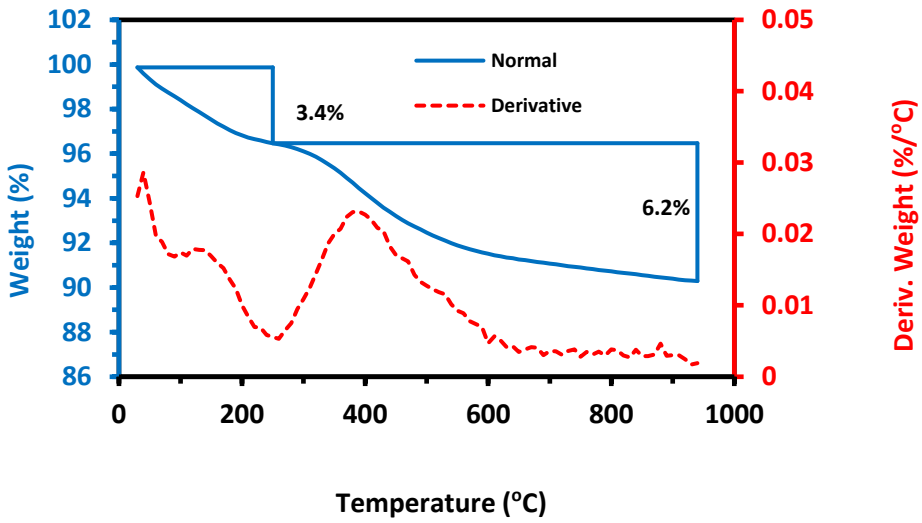

Fig. 6.2. TGA plots showing weight loss for fluorosilane treated DE (FS DE) in normal and derivative modes. Weight loss for fluorosilane treated DE sample was 6.1% in the temperature range 250 to 950 °C.

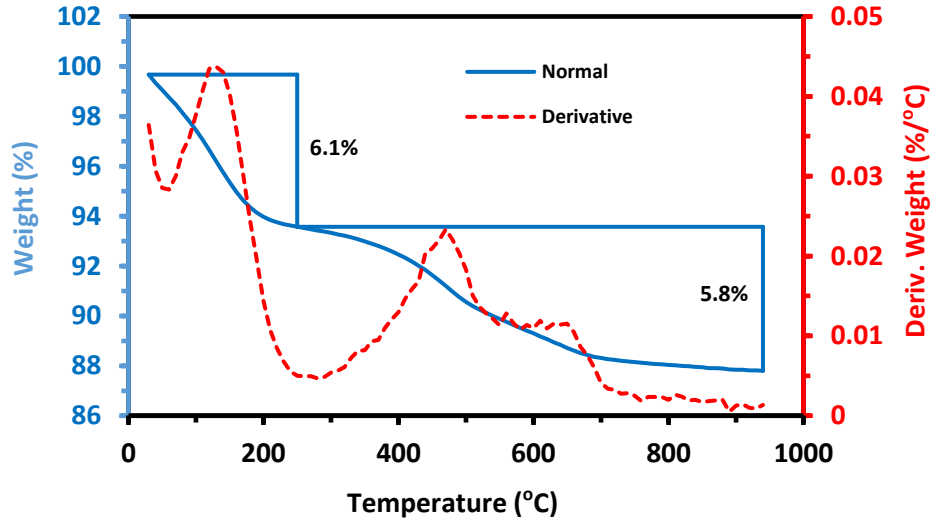

Fig. 6.3. TGA plots showing weight loss for non-fluorosilane treated DE in normal and derivative modes. Weight loss for ODTMS treated DE sample was 5.8% in the temperature range 250 to 950 °C.

FTIR of DE and treated DE samples

The presence of ODTMS and fluorosilane (FS) on the surface of DE samples was confirmed by FTIR experiments. The IR spectra of untreated DE and ODTMS treated DE samples (OD DE) are shown in the region 2700 to 4000 cm^{-1} (Fig. 6.4a). Similarly, the IR spectra of FS treated DE samples (FS DE) has been shown in the region 600 to 1600 cm^{-1} (Fig. 6.4b) for clarity. Two distinct peaks which were not in untreated DE samples were observed for OD DE samples at 2917 and 2849 cm^{-1}. Similarly, three more additional resonances were observed at 1190, 791 and 685 cm^{-1} for FS DE samples compared to untreated DE samples.

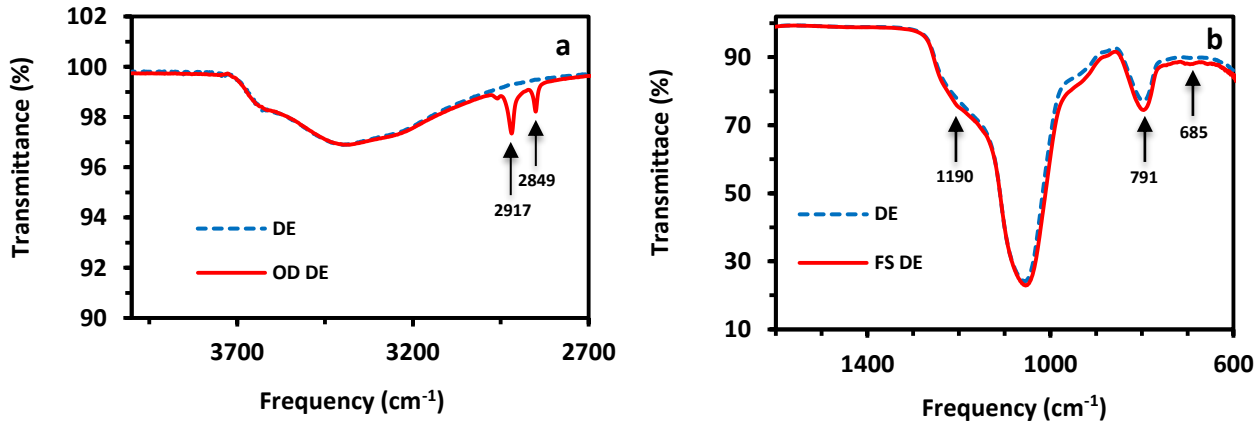

Fig. 6.4. FTIR of: a) untreated DE (blue) and non-fluorosilane treated DE (OD DE) (red); b) untreated DE (blue) and fluorosilane treated DE (FS DE) (red). For OD DE and untreated DE, FTIR spectra were the same in the region (600 - 2600 cm^{-1}). Similarly, for FS DE and untreated DE samples FTIR spectra were the same in the region (1600 - 4000 cm^{-1}).

Thermogravimetric analysis of DE and epoxy composites

The amounts of untreated and treated DE filler in the epoxy DE composites were analyzed by thermogravimetric analysis. The result of thermogravimetric analysis is shown in Fig. 6.5. for the determination of amount of filler in the composites.

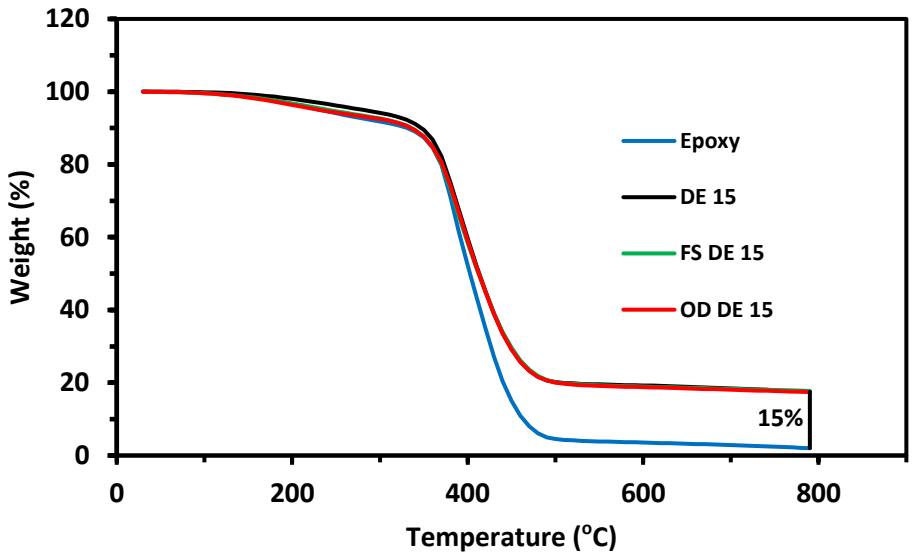

Fig. 6.5. TGA plots showing weight loss for pure epoxy (blue), untreated DE epoxy composite (black), fluorosilane treated DE epoxy composite (FS DE) (green) and non-fluorosilane treated DE epoxy composites (OD DE) (red). In all samples, the amount of filler was approximately 15%. The thermograms for the treated samples were all nearly the same.

Test of hydrophobicity of DE samples

Hydrophobicity tests was performed by putting water droplets on the surface of coatings prepared from bare untreated and treated DE particles (without binder). Water

droplet images were taken on the surface of those coatings. Contact angles of water droplets on the surfaces were measured and shown in Fig. 6.6a-c.

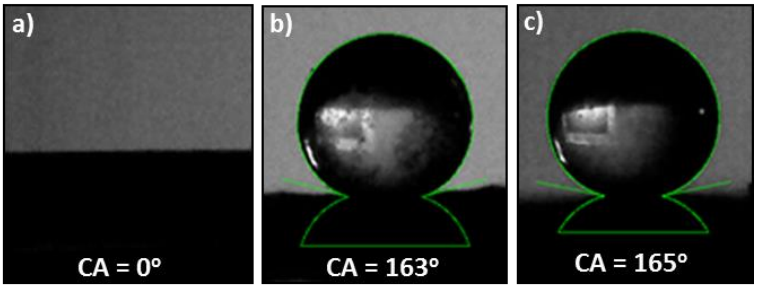

Fig. 6.6. Coatings prepared from slurry of: a) untreated DE; b) OD DE and c) FS DE particles. CA refers to contact angle of water droplets on the surface of bare particles.

Surface structure of DE particles

Scanning electron micrographs of DE particles Fig. 6.7a shows that intact DE particles were disc shaped with diameter of ~15 µm. The DE particle at higher magnification in Fig. 6.7b showed pores of different shapes with diameters of ~250 nm.

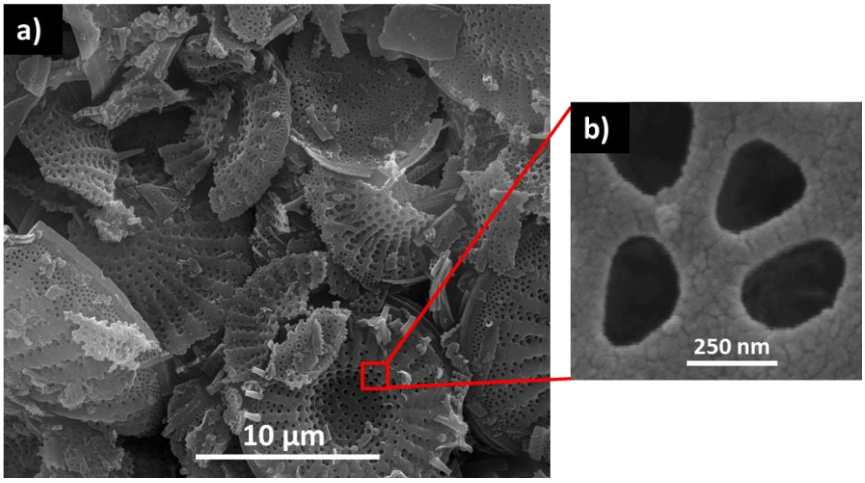

Fig. 6.7. Scanning electron micrograph of: a) DE particles; b) magnified view of a DE particle showing the smaller pores.

Dynamic Mechanical Properties

The effect of untreated and treated DE filler on the storage modulus, E', of epoxy matrix was studied by using dynamic mechanical analysis. The effects of DE filler as a function of temperature on the storage modulus values of bulk epoxy and DE/epoxy composites at 1 and 30 Hz frequencies are shown in Fig 6.8a and 6.8b.

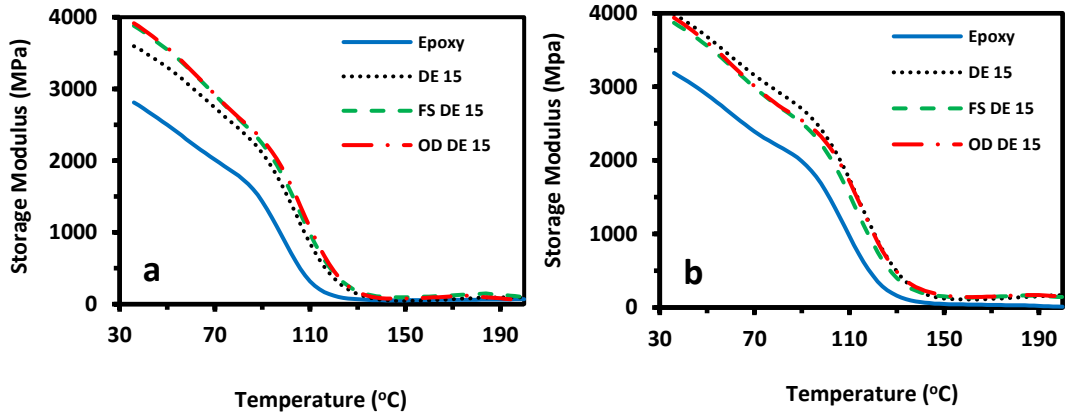

Fig. 6.8. Storage moduli, E', for: bulk epoxy (blue), DE epoxy composite (DE 15) (black), fluorosilane treated DE epoxy composite (FS DE 15) (green) and non-fluorosilane treated DE epoxy composite (OD DE 15) (red); a) at 1 Hz; b) at 30 Hz.

Three samples for bulk epoxy and DE/epoxy composites were run at each frequency to determine the storage moduli. The average values of storage moduli at frequencies 1, 10 and 30 Hz were taken for pure epoxy and DE/epoxy composites. The effect of

frequencies on the values of storage modulus of the pure epoxy and DE/epoxy composites are shown in Fig. 6.9

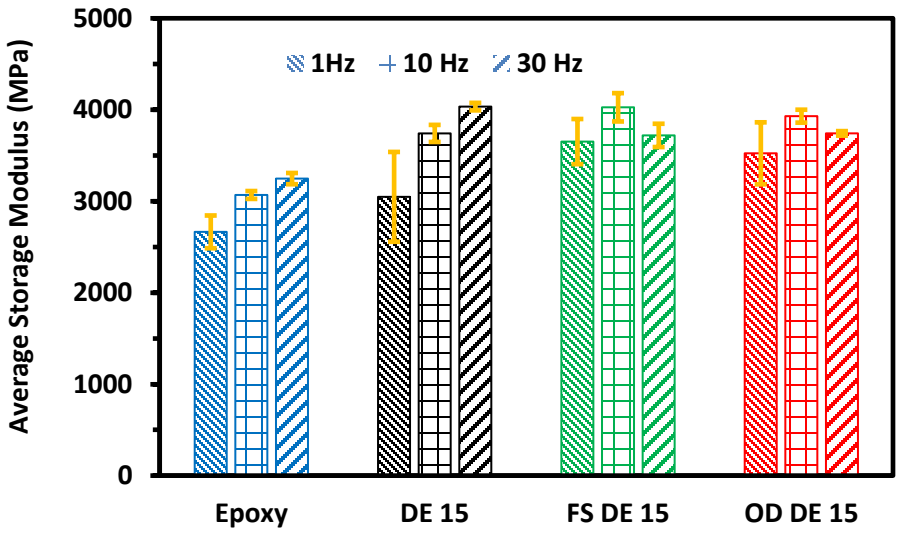

Fig. 6.9. Average of storage moduli values for: pure epoxy (blue), DE epoxy composites (DE 15) (Black), fluorosilane treated DE epoxy composites (FS DE 15) (green) and non-fluorosilane treated DE epoxy composites (OD DE 15) (red). Average storage moduli of all composites were larger than that of bulk epoxy.

The variation of loss modulus as a function of temperature for pure epoxy and DE/epoxy composites are shown Fig. 6.10a and 6.10b. The temperature of the maxima in the loss modulus curve increased with the addition of treated or untreated filler.

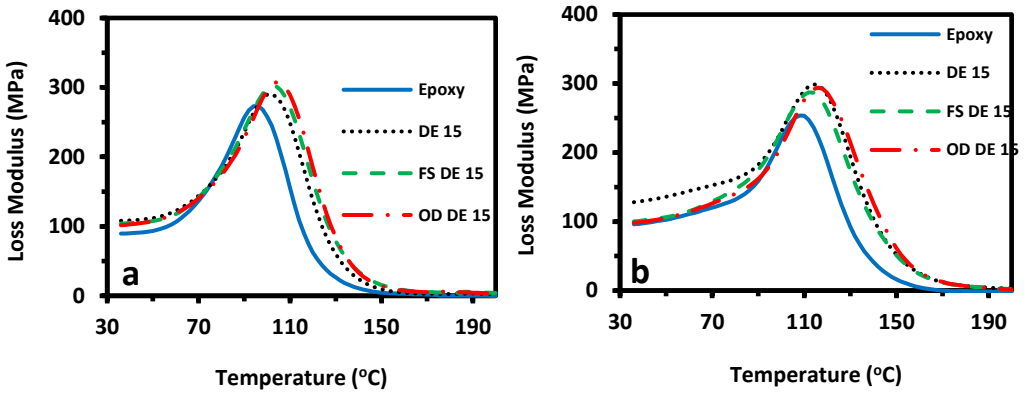

Fig. 6.10. Loss moduli for: pure epoxy (blue), untreated DE epoxy composite (DE 15) (black), flurosilane treated DE epoxy composite (FS DE 15) (green) and non fluorosilane treated DE epoxy composites (OD DE 15) (red); a) at 1 Hz and b) at 30 Hz

Damping properties (Tan δ)

The effect of damping properties as the function of temperature at two frequencies is shown in Figs. 6.11a and 6.11b. Again, the maxima (due to loss modulus) increased with addition of filler. The figures indicate that the incorporation of fillers in the matrix has considerably increased the damping property of the matrix.

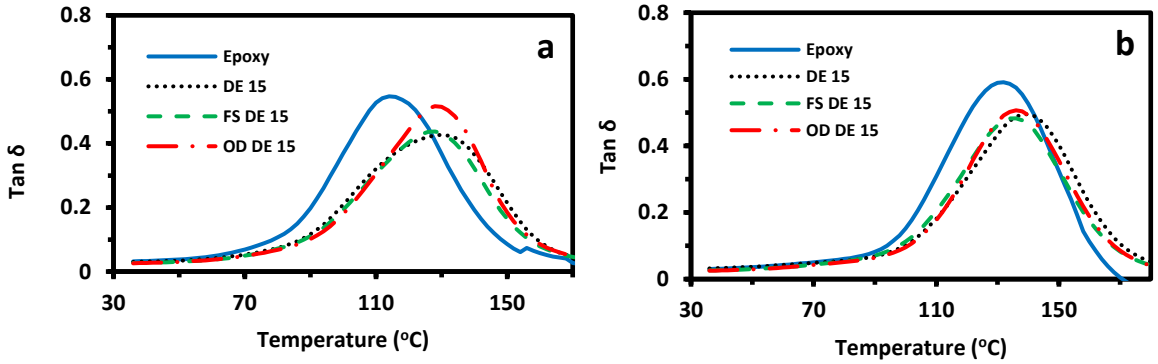

Fig. 6.11. Tan δ plots for: bulk epoxy (blue), untreated DE epoxy composite (DE 15) (black), fluorosilane treated DE epoxy (FS DE 15) (green), non-fluorosilane treated DE epoxy composite (OD DE) (red); a) at 1 Hz and b) at 30 Hz

Tan δ values of all samples were determined three times at different frequencies. Average values of tan δ from the maxima of the peaks for bulk epoxy and DE/epoxy composites at frequencies 1, 10 and 30 Hz were taken. A plot of average tan δ values of different samples at 1, 10 and 30 Hz are shown in Fig. 6.12. So, tan δ, and for that matter, loss modulus varies as a function of temperature.

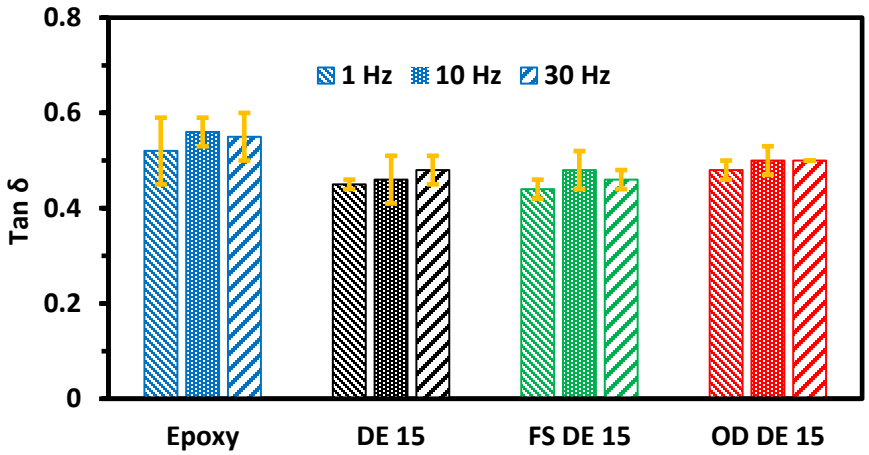

Fig. 6.12. Averages of tan δ values for different DE/epoxy composites samples as different frequencies. The average values of tan δ has decreased in all composites. There was no significant effect of frequency on tan δ values for all samples.

Glass transition temperatures (T_g)

The glass transition temperature of bulk epoxy and DE/epoxy composites were determined for each measurement at different frequencies from the mechanical data. Average values of the three measurements were taken. A plot of average glass transition temperature for bulk epoxy and all composites at 1, 10 and 30 Hz are shown in Fig. 6.13.

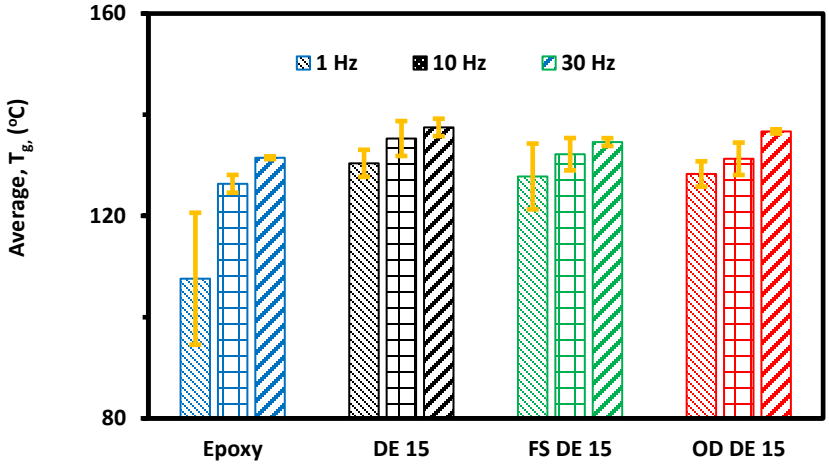

Fig. 6.13. Average of glass transition temperatures (T_g) of bulk epoxy and DE/epoxy composites at different frequencies. The average values of T_g was larger for all composites compared to bulk epoxy. The T_g was found to increase with increases in the frequency of oscillation as expected.

Differential scanning calorimetry (DSC)

DSC scans of the pure epoxy and DE/epoxy composites were taken in standard mode at ramp rate of 5 ^oC/min under N_2 atmosphere. A typical plot of DSC scan results for bulk epoxy and DE/epoxy composites is shown in Fig. 6.14.

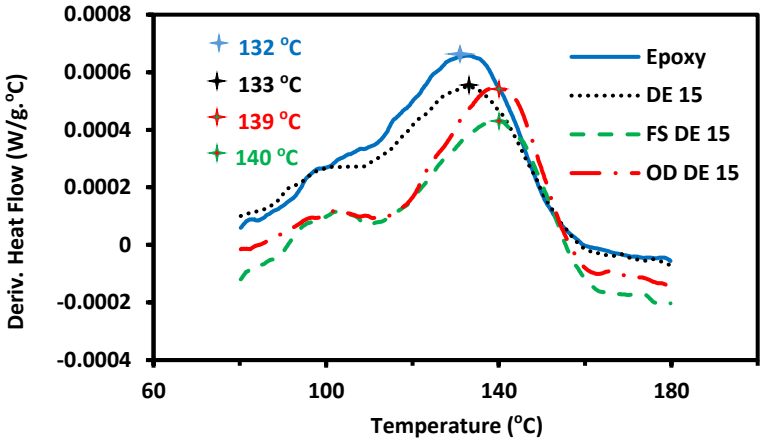

Fig. 6.14. DSC scans for epoxy and epoxy-DE composites. T_g values were larger for composites.

Average values of glass transition temperatures (T_g) of the bulk epoxy and composites determined from three different calorimetry results. A plot of average T_g of bulk and composites samples is shown in Fig. 6.15.

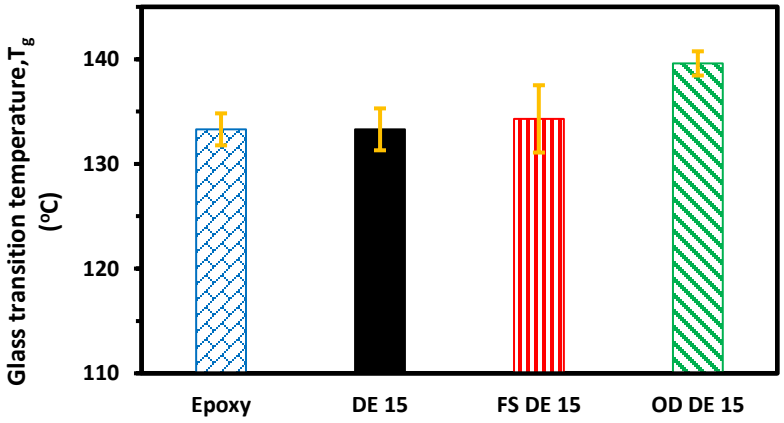

Fig. 6.15. A plot showing average glass transition temperature determined from DSC. Average T_g values of the composites were larger than that of bulk epoxy samples.

Cole-Cole Plot

This method is used to study the structural behavior of the matrix due to the addition of filler in it. Cole-Cole plot is represented by equation (1) given below

$$\mathbf{E''} = \mathbf{f}(\mathbf{E'}) \qquad (1)$$

The Cole-Cole plot, in which the loss modulus values (E") are plotted against storage moduli (E') is shown in Fig. 7.16.

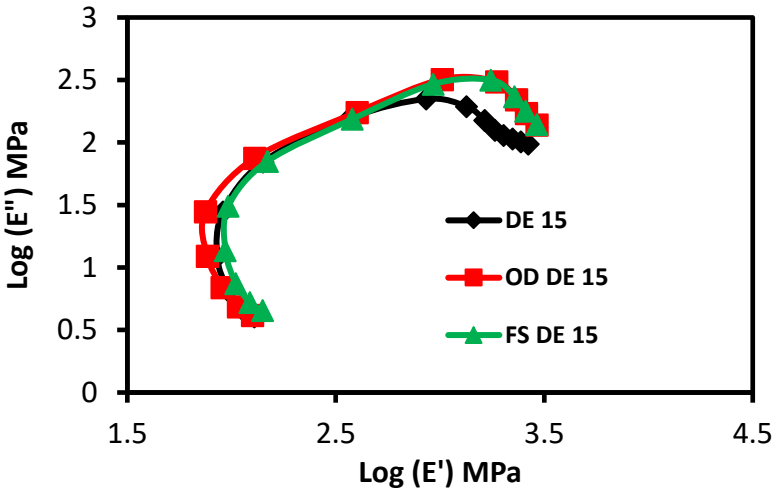

Fig. 6.16. Cole-Cole plot of the composite at 1 Hz frequency.

6.5. DISCUSSION

Thermogravimetric analysis

The mass losses of DE and DE composites were more complicated than those with pure silica because of the complication of DE.[42] Diatomaceous earth contains various

inorganic substances and its major chemical component is amorphous silica. It also contains physically bound water molecules. The decomposition of untreated DE (Fig. 6.1) showed a mass loss of 5.4% in the temperature range of 30 to 250 ^{o}C. This mass loss is considered due to the removal of physically adsorbed water molecules, evaporation of volatile impurities and partial dihydroxylation of silanol groups on the surface of DE. The mass loss in the temperature range of 250 to 950 °C was 2.7%. This mass loss is expected due to the decomposition of inorganic substances and dehydroxylation of silanols groups on the surface of DE.[43]

The TGA thermogram of FS treated DE sample (Fig. 6.2) showed a mass loss of 3.4 % in the temperature range of 30 to 250 °C. This mass loss was expected due to the removal of physically bound water molecules, unbound silane coupling agents and partial removal of surface silanol groups. The mass loss observed for FS treated DE in the temperature range of 250 to 950 ^{o}C was 6.2%. This mass loss resulted from the decomposition of silane coupling agent, decomposition of inorganic substances and dihydroxylation of silanols from DE. The amount of FS on the surface of DE was determined by subtracting the mass loss of untreated DE from mass loss of FS treated DE at 950 °C and it was found to be 3.5%.

The TGA thermal plots for ODTMS treated DE (Fig. 6.3) showed mass loss of 6.1% in the temperature range of 30 to 250 °C. This mass loss resulted from removal of water molecules, removal of unbound silane coupling agents and partial dehydroxylation of silanols on the DE surface. The mass loss in the temperature range of 250 to 950 °C for ODTMS treated DE was 5.8% corresponding to the decomposition of grafted silane,

inorganic substances and dihydroxylation of silanols from DE silica. The amount of non-fluorosilane chain grafted on the DE surface was determined by subtracting the mass loss of untreated DE sample from treated DE samples at 950 °C and it was found to be 3.1%.

The presence of ODTMS and FS on the surface of treated DE was confirmed from the results of FTIR experiments Fig. 6.4a and 6.4b. We have previously reported the FTIR spectra of HFIP treated Celtix DE.[39] Comparison of FTIR spectra of untreated DE samples and treated DE samples (Fig. 6.4a and 6.4b) showed additional distinct peaks in treated DE samples. The peaks around 1050 and 1200 cm^{-1} (Fig. 6.4a and 6.4b) for untreated DE were from the in-plane Si-O stretching mode. Another peak around 795 cm^{-1} was resulted from symmetric Si-O stretching.[44] More intense peaks for PF DE seen around 1190 cm^{-1} were expected due to C-F (symmetric and antisymmetric) vibrations.[45] Additional resonances at 791 and 685 cm^{-1} which, were present only in treated DE samples, resulted due to the vibration of C-F bond in polyfluorocarbon region of PFS.[46, 47] FTIR results of OD DE indicated additional peaks at 2917 and 2849 cm^{-1} and these peaks were due to the symmetric C-H_2 stretching of hydrocarbon chain.[48]

TGA plots of DE and epoxy composites (Fig. 6.5) showed the mass loss of ~98% for pure epoxy samples. The decomposition of epoxy matrix occurred mostly around 400 °C. The decomposition was almost complete around 800 °C. The thermograms of DE and epoxy composites showed the mass loss of 83% at 800 °C. This mass loss resulted due to the decomposition of epoxy matrix and volatile component of the DE and untreated DE filler. The amount of the filler in the composites was determined by subtracting the mass loss of DE-epoxy composites from mass loss of pure epoxy at 800 °C and it was found to be ~15% in all composites samples.

The contact angle results on the surface of coatings prepared from bulk particles (without binder) showed that ODTMS and FS treated DE particles were in the superhydrophobic range. OD DE particles surface showed water contact angle ~163^{o} and FS DE particles surfaces exhibited water contact angle ~165^{o}. The coatings prepared from untreated DE particles absorbed water droplets showing its superhydrophilic nature.

Mechanical properties

The storage modulus values (Fig. 6.8a and 6.8b) of the composite decreased with increased temperature. The addition of DE fillers (Fig. 6.8a and 6.8b) increased the storage modulus of the composite as compared to bulk epoxy resin. The comparison of average values of storage moduli for all samples (Fig. 6.9) at different frequencies (1, 10 and 30 Hz) showed that the storage moduli have increased compared to bulk epoxy with the incorporation of untreated and treated DE particles in the epoxy matrix. Average values of storage moduli of untreated DE/epoxy composites and treated DE/epoxy composites were almost similar. Treatment of DE samples with small amounts (<4 wt%) of fluoro and non-fluorosilane coupling agents did not change the storage moduli of the epoxy composites much. These increases in storage moduli of untreated DE/epoxy composites and treated DE/epoxy composites are expected due to better filler/matrix adhesion and greater degree of stress transfer at the interface. Incorporation of filler in the epoxy matrix probably increases the stiffness of the matrix with the reinforcing effect. The thermal stability of the bulk epoxy matrix increased with the addition of DE fillers. The storage moduli for untreated DE and epoxy composites was found to increase with increased applied frequency (Fig. 6.9). In cases of both treated DE/epoxy composites, the

average storage moduli of DE/epoxy composites at 30 Hz was found to be smaller than at 10 Hz. These results suggest that both OD DE/epoxy and FS DE/epoxy composites behaved in the same way at all frequencies.

The peak of the loss modulus curve (Fig. 6.10a and 6.10b) almost occurred at the same temperature i.e. glass transition temperature (T_g) for all DE/ epoxy composites. If we compare T_g of the resin at higher frequencies, there is a shift as the frequency of the experiment increased. At low frequency (1 Hz), the T_g of the resin occurred around 90 °C, as the frequency increased, T_g shifted to 110 °C. This increase in T_g occurred due to the low mobility of molecules at larger frequency. The drop in modulus on passing through the T_g occurred at higher temperature for all DE/epoxy composites compared to bulk epoxy matrix. The combination of hydrodynamic effects of the particles embedded in the viscoelastic medium and the mechanical restraints introduced by the filler particles has probably reduced the mobility and the deformability of matrix. This gives rise to the filler having a larger effect on the moduli above T_g than below it. The deviation in moduli of the bulk epoxy samples from the composites is greater at higher temperatures.[49]

The variation of tan δ as a function of temperature at 1 Hz and 30 Hz frequencies Fig. 6.11a and 6.11b showed that the tan δ values increased slowly at first with increased in temperature and reached a maximum value at glass transition temperature and again it started to decrease. A plot of average values of tan δ for bulk epoxy and DE/epoxy composites at 1, 10 and 30 Hz frequencies (Fig. 6.12) revealed the decreased damping peaks with the incorporation of both untreated and treated DE particles in the epoxy matrix. Lowering of damping peak was expected due to an improved filler matrix

bonding and the fillers carry a greater extent of stress and allows only a small part of it to strain the interface. Therefore, a stronger filler matrix interface results and less energy dissipation occurs in the stronger polymer matrix and filler interface.[50] The tan δ values of all samples were not affected much by the increases in the applied frequencies. Less damping of OD DE/epoxy and FS DE/epoxy composites indicated that the composites absorbed more amount of energy compared to bulk epoxy.

Glass transition temperature (T_g)

A plot of average glass transition temperature (T_g) values of epoxy and DE/epoxy composites in Fig. 6.13 showed that T_g of all composites were larger than the T_g of bulk epoxy sample. The average T_g values of DE/epoxy, OD DE/epoxy and FS DE/epoxy samples were found to be similar. The T_g values of all samples (bulk epoxy, DE/epoxy, OD DE/epoxy and FS DE/epoxy) were found to increase with increased applied frequency. The glass transition temperature of all the three types of composites were higher than that of pure epoxy. This indicated that there was the good filler/matrix interface in all DE-epoxy composites.

Differential Scanning Calorimetry (DSC)

DSC scans (Fig. 6.14) showed that the glass transition temperature of the DE and epoxy composites were higher than that of the pure epoxy. The treated DE epoxy composite glass temperature was higher than the DE and epoxy composites. This results points out that treated DE acts as stronger reinforcing filler than untreated DE.

The Cole-Cole plot is expected to be a perfect semi-circle for a homogenous system.[51, 52] However, for untreated DE, treated DE and epoxy composites, the points plotted did not form perfect semi-circles but the shape of curves were almost semi-circle which indicates the significant DE filler-matrix interaction. The nature of the curves for treated DE and epoxy composites are similar which suggests that fluorosilane and non-fluorosilane treated DE interacts with epoxy matrix in the similar way.

Microscopic images of DE particle in Fig. 6.7a revealed that Celtix DE particles were circular in shape and intact DE particles had ~15 μm diameter. The magnified view of the image (Fig. 6.7b) showed many pores in it with diameter of ~250 nm.[39] AFM studies of a *C. granii* diatom frustule wall surface by Noll and coworkers have revealed the presence of 100-200 nm spherical SiO_2 particles. These particles were responsible for forming granular nanostructure with roughness depths of 70 nm^2. Previous work by Tasdemirci and coworkers have mentioned the rod shaped DE particles reinforcing characteristics arises from a strong frustule adhesion to the epoxy matrix as well as extensive mechanical interlocking. The interlocking occurs due to the epoxy infiltration partly into the pores parallel to the frustule tube axis and partly in to the pores located at the back surface of the frustule tube as well.[37] So, the reinforcing properties of Celtix DE (circular) is expected from the filling of the pores with epoxy matrix and interlocking of the particles in the matrix. The mechanical interlocking between the frustule and matrix is expected to occur on the nanometer-scale, as effect similar like that in non-uniform carbon nano-tube reinforced polymers,[53] which require extra energy to deform the matrix. The larger average values of storage modulus and glass transition temperature of the FS DE/epoxy composites and OD DE/epoxy composites indicates that there was better

interaction between the treated DE particles and epoxy matrix compared to untreated DE. Treatment of DE with small amount (< 4%) of fluorosilane and non-fluorosilane coupling agents promotes the infiltration of the epoxy matrix it to the nano-size pores of Celtix DE particles and the interlocking of the DE particles perhaps occurs better than in untreated DE particles. The reason for this not yet fully understood.

6.6. CONCLUSIONS

Dynamic mechanical analysis of bulk epoxy, DE/epoxy composites and treated DE/epoxy composites revealed a shift in tan δ peak in all epoxy-DE composites an increase in the glass transition temperature (T_g) of all composites compared to bulk epoxy. The average storage modulus of the composites was found to increase with the incorporation of untreated and treated DE particles in an epoxy matrix. Increases in the frequency of oscillation during DMA has increased the glass transition temperature of the sample significantly in all samples. The DSC results of all composites showed that the glass transition temperature of all composites has increased and confirmed that superhydrophobic DE particles also interacts well with epoxy matrix. All these results suggested that fluorosilane and non-fluorosilane treated DE particles act as reinforcing filler and enhances the mechanical properties of epoxy matrix.

Acknowlegements

The authors acknowledge the financial support of the Oklahoma State University, and Dry Surface Coatings (DSC), Guthrie, OK.

6.7. REFERENCES

1. Simpson, J. T.; D'urso, B. R., Superhydrophobic diatomaceous earth. U.S. Patent No. 8,216,6742012.
2. Noll, F.; Sumper, M.; Hampp, N., Nanostructure of diatom silica surfaces and of biomimetic analogues. *Nano Lett.* **2002,** *2*, 91-95.
3. Cai, Y.; Allan, S. M.; Sandhage, K. H.; Zalar, F. M., Three-dimensional magnesia-based nanocrystal assemblies via low-temperature magnesiothermic reaction of diatom microshells. *J. Am. Ceram. Soc.* **2005,** *88*, 2005-2010.
4. Scala, S.; Bowler, C., Molecular insights into the novel aspects of diatom biology. *Cell Mol. Life Sci.* **2001,** *58*, 1666-1673.
5. Barlow, N., The Diatoms: Applications for the Environmental and Earth Sciences. Pergamon2011.
6. Ongerth, J. E.; Hutton, P., DE filtration to remove Cryptosporidium. *J. Am. Water Works Ass.* **1997,** *89*, 39-46.
7. Yuan, P.; Liu, D.; Tan, D. Y.; Liu, K. K.; Yu, H. G.; Zhong, Y. H.; Yuan, A. H.; Yu, W. B.; He, H. P., Surface silylation of mesoporous/macroporous diatomite (diatomaceous earth) and its function in Cu (II) adsorption: the effects of heating pretreatment. *Microporous Mesoporous Mater.* **2013,** *170*, 9-19.
8. Sheng, G.; Yang, S.; Sheng, J.; Hu, J.; Tan, X.; Wang, X., Macroscopic and microscopic investigation of Ni (II) sequestration on diatomite by batch, XPS, and EXAFS techniques. *Environ. Sci. Technol.* **2011,** *45*, 7718-7726.

9. Dantas, T. D. C.; Neto, A. D.; Moura, M. D. A., Removal of chromium from aqueous solutions by diatomite treated with microemulsion. *Water Res.* **2001,** *35*, 2219-2224.

10. Khraisheh, M. A.; Al-degs, Y. S.; Mcminn, W. A., Remediation of wastewater containing heavy metals using raw and modified diatomite. *Chem. Eng. J.* **2004,** *99*, 177-184.

11. Sheng, G.; Hu, J.; Wang, X., Sorption properties of Th (IV) on the raw diatomite-effects of contact time, pH, ionic strength and temperature. *Appl. Radiat. Isot.* **2008,** *66*, 1313-1320.

12. Yu, Y.; Addai-Mensah, J.; Losic, D., Chemical functionalization of diatom silica microparticles for adsorption of gold (III) ions. *J. Nanosci. Nanotechnol.* **2011,** *11*, 10349-10356.

13. Garcia, G.; Cardenas, E.; Cabrera, S.; Hedlund, J.; Mouzon, J., Synthesis of zeolite Y from diatomite as silica source. *Microporous Mesoporous Mater.* **2016,** *219*, 29-37.

14. Maeda, H.; Ishida, E. H., Hydrothermal preparation of diatomaceous earth combined with calcium silicate hydrate gels. *J. Hazard. Mater.* **2011,** *185*, 858-861.

15. Inchaurrondo, N.; Font, J.; Ramos, C. P.; Haure, P., Natural diatomites: Efficient green catalyst for Fenton-like oxidation of Orange II. *Appl. Catal., B* **2016,** *181*, 481-494.

16. Erdem, E.; Çölgeçen, G.; Donat, R., The removal of textile dyes by diatomite earth. *J. Colloid Interface Sci.* **2005,** *282*, 314-319.

17. Farrah, S.; Preston, D.; Toranzos, G.; Girard, M.; Erdos, G.; Vasuhdivan, V., Use of modified diatomaceous earth for removal and recovery of viruses in water. *Appl. Environ. Microbiol.* **1991,** *57,* 2502-2506.

18. Hadjar, H.; Hamdi, B.; Jaber, M.; Brendlé, J.; Kessaïssia, Z.; Balard, H.; Donnet, J. B., Elaboration and characterisation of new mesoporous materials from diatomite and charcoal. *Microporous Mesoporous Mater.* **2008,** *107,* 219-226.

19. Xiong, W.; Peng, J., Development and characterization of ferrihydrite-modified diatomite as a phosphorus adsorbent. *Water Res.* **2008,** *42,* 4869-4877.

20. Yılmaz, B.; Ediz, N., The use of raw and calcined diatomite in cement production. *Cem. Concr. Compos.* **2008,** *30,* 202-211.

21. Li, X.; Bian, C.; Chen, W.; He, J.; Wang, Z.; Xu, N.; Xue, G., Polyaniline on surface modification of diatomite: a novel way to obtain conducting diatomite fillers. *Appl. Surf. Sci.* **2003,** *207,* 378-383.

22. Yu, Y.; Addai-Mensah, J.; Losic, D., Synthesis of self-supporting gold microstructures with three-dimensional morphologies by direct replication of diatom templates. *Langmuir* **2010,** *26,* 14068-14072.

23. Ergül, S.; Kadan, İ.; Savaşcı, Ş.; Ergül, S., Modified diatomaceous earth as a principal stationary phase component in TLC. *J. Chromatogr. Sci.* **2005,** *43,* 394-400.

24. Oliveira, N. M.; Reis, R. L.; Mano, J. F., Superhydrophobic surfaces engineered using diatomaceous earth. *ACS Appl. Mater. Interfaces* **2013,** *5,* 4202-4208.

25. Polizos, G.; Winter, K.; Lance, M. J.; Meyer, H. M.; Armstrong, B. L.; Schaeffer, D. A.; Simpson, J. T.; Hunter, S. R.; Datskos, P. G., Scalable superhydrophobic

coatings based on fluorinated diatomaceous earth: Abrasion resistance versus particle geometry. *Appl. Surf. Sci.* **2014,** *292*, 563-569.

26. Puretskiy, N.; Chanda, J.; Stoychev, G.; Synytska, A.; Ionov, L., Anti-icing superhydrophobic surfaces based on core-shell fossil particles. *Adv. Mater. Interfaces* **2015,** *2*, 1500124-1500131.

27. Nine, M. J.; Cole, M. A.; Johnson, L.; Tran, D. N.; Losic, D., Robust superhydrophobic graphene-based composite coatings with self-cleaning and corrosion barrier properties. *ACS Appl. Mater. Interfaces* **2015,** *7*, 28482-28493.

28. Ellis, B. L.; Lee, K. T.; Nazar, L. F., Positive electrode materials for Li-ion and Li-batteries. *Chem. Mater.* **2010,** *22*, 691-714.

29. Jawaid, M.; Khalil, H. A., Effect of layering pattern on the dynamic mechanical properties and thermal degradation of oil palm-jute fibers reinforced epoxy hybrid composite. *BioResources* **2011,** *6*, 2309-2322.

30. Zabihi, O.; Ghasemlou, S., Nano-CuO/epoxy composites: thermal characterization and thermo-oxidative degradation. *Int. J. Polym. Anal.* **2012,** *17*, 108-121.

31. Mirmohseni, A.; Zavareh, S., Preparation and characterization of an epoxy nanocomposite toughened by a combination of thermoplastic, layered and particulate nano-fillers. *Mater. Des.* **2010,** *31*, 2699-2706.

32. Bakar, M.; Kostrzewa, M.; Hausnerova, B.; Sar, K., Preparation and property evaluation of nanocomposites based on polyurethane-modified epoxy/montmorillonite systems. *Adv. Polym. Tech.* **2010,** *29*, 237-248.

33. Lee, J. H.; Jang, Y. K.; Hong, C. E.; Kim, N. H.; Li, P.; Lee, H. K., Effect of carbon fillers on properties of polymer composite bipolar plates of fuel cells. *J. Power Sources* **2009,** *193*, 523-529.

34. Papanicolaou, G.; Papaefthymiou, K.; Koutsomitopoulou, A.; Portan, D.; Zaoutsos, S., Effect of dispersion of MWCNTs on the static and dynamic mechanical behavior of epoxy matrix nanocomposites. *J. Mater. Sci.* **2012,** *47*, 350-359.

35. Amendola, E.; Scamardella, A.; Petrarca, C.; Acierno, D., Epoxy–nanocomposites with ceramic reinforcement for electrical insulation. *J. Appl. Polym. Sci.* **2011,** *122*, 3686-3693.

36. Montazeri, A.; Montazeri, N.; Pourshamsian, K.; Tcharkhtchi, A., The effect of sonication time and dispersing medium on the mechanical properties of multiwalled carbon nanotube (MWCNT)/epoxy composite. *Int. J. Polym. Anal.* **2011,** *16*, 465-476.

37. Taşdemirci, A.; Yüksel, S.; Karsu, D.; Gültürk, E.; Hall, I. W.; Güden, M., Diatom frustule-filled epoxy: Experimental and numerical study of the quasi-static and high strain rate compression behavior. *Mater. Sci. Eng., A* **2008,** *480*, 373-382.

38. Gültürk, E.; Güden, M.; Taşdemirci, A., Calcined and natural frustules filled epoxy matrices: The effect of volume fraction on the tensile and compression behavior. *Composites Part B* **2013,** *44*, 491-500.

39. Sedai, B. R.; Khatiwada, B. K.; Mortazavian, H.; Blum, F. D., Development of superhydrophobicity in fluorosilane-treated diatomaceous earth polymer coatings. *Appl. Surf. Sci.* **2016,** *386*, 178-186.

40. Wenzel, R. N., Surface roughness and contact angle. *J. Phys. Chem.* **1949,** *53*, 1466-1467.

41. Williams, D. L.; Kuhn, A. T.; Amann, M. A.; Hausinger, M. B.; Konarik, M. M.; Nesselrode, E. I., Computerised measurement of contact angles. *Galvanotechnik* **2010,** *101*, 2502-2512.

42. Jo, H.; Blum, F. D., Characterization of the interface in polymer-silica composites containing an acrylic silane coupling agent. *Chem. Mater.* **1999,** *11*, 2548-2553.

43. Zhuravlev, L., The surface chemistry of amorphous silica. Zhuravlev model. *Colloids Surf., A* **2000,** *173*, 1-38.

44. Yuan, P.; Liu, D.; Tan, D.-Y.; Liu, K.-K.; Yu, H.-G.; Zhong, Y.-H.; Yuan, A.-H.; Yu, W.-B.; He, H.-P., Surface silylation of mesoporous/macroporous diatomite (diatomaceous earth) and its function in Cu (II) adsorption: The effects of heating pretreatment. *Microporous Mesoporous Mater.* **2013,** *170*, 9-19.

45. Liang, Z.; Chen, W.; Liu, J.; Wang, S.; Zhou, Z.; Li, W.; Sun, G.; Xin, Q., FT-IR study of the microstructure of Nafion® membrane. *J. Membr. Sci.* **2004,** *233*, 39-44.

46. Heitner-Wirguin, C., Infra-red spectra of perfluorinated cation-exchanged membranes. *Polymer* **1979,** *20*, 371-374.

47. Liang, C.; Krimm, S., Infrared spectra of high polymers. III. Polytetrafluoroethylene and polychlorotrifluoroethylene. *J. Chem. Phys.* **1956,** *25*, 563-571.

48. Yuan, P.; Liu, D.; Tan, D.-Y.; Liu, K.-K.; Yu, H.-G.; Zhong, Y.-H.; Yuan, A.-H.; Yu, W.-B.; He, H.-P., Surface silylation of mesoporous/macroporous diatomite

(diatomaceous earth) and its function in Cu(II) adsorption: The effects of heating pretreatment. *Microporous Mesoporous Mater.* **2013,** *170,* 9-19.

49. Pothan, L. A.; Oommen, Z.; Thomas, S., Dynamic mechanical analysis of banana fiber reinforced polyester composites. *Compos. Sci. Technol.* **2003,** *63,* 283-293.

50. Felix, J. M.; Gatenholm, P., The nature of adhesion in composites of modified cellulose fibers and polypropylene. *J. Appl. Polym. Sci.* **1991,** *42,* 609-620.

51. Pothan, L. A.; Potschke, P.; Habler, R.; Thomas, S., The static and dynamic mechanical properties of banana and glass fiber woven fabric-reinforced polyester composite. *J. Compos. Mater.* **2005,** *39,* 1007-1025.

52. Mohanty, S.; Verma, S. K.; Nayak, S. K., Dynamic mechanical and thermal properties of MAPE treated jute/HDPE composites. *Compos. Sci. Technol.* **2006,** *66,* 538-547.

53. Moniruzzaman, M.; Winey, K. I., Polymer nanocomposites containing carbon nanotubes. *Macromolecules* **2006,** *39,* 5194-5205.

VITA

Bhishma Raj Sedai

Candidate for the Degree of

Doctor of Philosophy

Thesis: DEVELOPMENT OF SUPERHYDROPHOBICITY IN SILANE TREATED DIATOMACEOUS EARTH AND POLYMER COATINGS

Major Field: Chemistry

Biographical:

Education:

Completed the requirements for the Doctor of Philosophy in Chemistry at Oklahoma State University, Stillwater, Oklahoma in December, 2016.

Completed the requirements for the Master of Science in Chemistry at Tribhuvan University, Kirtipur, Nepal in 2003.

Completed the requirements for the Bachelor of Science in Chemistry at Tri-Chandra College, Kathmandu, Nepal in 2000.

Experience:

Teaching and research assistant, Department of Chemistry, Oklahoma State University, Stillwater, OK, USA, 2011-2016.

Teaching experience, Trinity international college (2008-2010), and DAVSKVB higher secondary school (2005-2007), Kathmandu, Nepal

Professional Memberships:

American Chemical Society (Polymer division)
Golden Key International Honor Society